FAIRCHILD

REPUBLIC DIVISION

(NASA-CR-122358) TASK 1, DESIGN ANALYSIS REPORT: PULSED PLASMA SOLID PROPELLANT MICROTHRUSTER FOR THE SYNCHRONOUS METEOROLOGICAL W.J. Guman (Fairchild Hiller Corp.) Dec. 1971 133 p CSCL 21C G3/28

N72-18776

Unclas 18877

FACILITY (NASA CR OR TMX OR AD NUMBER) (CATEGORY)

Reproduced by NATIONAL TECHNICAL INFORMATION SERVICE Springfield, Va. 22151

FAIRCHILD
REPUBLIC DIVISION

PCD-TR-71-7
PC145R8000
FRD 4070

TASK I - DESIGN ANALYSIS REPORT

Pulsed Plasma Solid Propellant Microthruster for the Synchronous Meteorological Satellite

Interim Report for Period July-November 1971

FAIRCHILD
REPUBLIC DIVISION

PCD-TR-71-7
PC145R8000
FRD 4070

TASK I - DESIGN ANALYSIS REPORT

Pulsed Plasma Solid Propellant Microthruster for the Synchronous Meteorological Satellite

Edited by William J. Guman
Fairchild Industries
Fairchild Republic Division
Farmingdale, New York 11735

December, 1971

Interim Report for Period July - November 1971

Prepared for
GODDARD SPACE FLIGHT CENTER
Greenbelt, Maryland 20771

TECHNICAL REPORT STANDARD TITLE PAGE

1. Report No.	2. Government Accession No.	3. Recipient's Catalog No.

4. Title and Subtitle	5. Report Date
Task I -Design Analysis Report, Pulsed Plasma Solid Propellant Microthruster for the Synchronous Meteorological Satellite	Dec. 1971
	6. Performing Organization Code
7. Author(s)	8. Performing Organization Report No.
Edited by W. J. Guman	PCD-TR-71-7, FRD 4070
9. Performing Organization Name and Address	10. Work Unit No.
Fairchild Industries Fairchild Republic Division Farmingdale, New York 11735	11. Contract or Grant No. NAS 5-11494
	13. Type of Report and Period Covered
12. Sponsoring Agency Name and Address	Interim Task Report July 1971-Nov. 1971
Goddard Space Flight Center Greenbelt, Maryland 20771 Mr. T. E. Williams	14. Sponsoring Agency Code

15. Supplementary Notes

16. Abstract

The propulsive system performance for the SMS mission can be met and thermal vacuum design supporting thruster tests indicate no problems under worst case conditions of sink temperature and spin rate. The reliability of the system was calculated to be 0.92 for a five year mission. Minus the main energy storage capacitor it is 0.98. Structural integrity in meeting launch environment has been ensured. The spin-rate accommodating converter-charger subsystem will perform as proposed and thus significantly extend pulse capacitor life. Only by using Beryllium instead of Aluminum as a structural material and an alternate energy-storage capacitor will it be possible to reduce the system weight by about one pound. A substantial reduction in the number of electronic parts with a corresponding increase in reliability can be achieved by using a V-shaped propellant instead of the standard breech-fed propellant. Since either of the two latter approaches are slightly higher risk approaches, they will not be considered in the final design.

17. Key Words (Selected by Author(s))	18. Distribution Statement
Electric Propulsion Pulsed Plasma Thrusters Satellite Control Plasma Propulsion	

19. Security Classif. (of this report)	20. Security Classif. (of this page)	21. No. of Pages	22. Price*
Unclassified	Unclassified		

*For sale by the Clearinghouse for Federal Scientific and Technical Information, Springfield, Virginia 22151.

PRECEDING PAGE BLANK NOT FILMED

TABLE OF CONTENTS

TABLE OF CONTENTS (CONT'D)

LIST OF ILLUSTRATIONS

LIST OF ILLUSTRATIONS (Cont'd)

LIST OF TABLES

PREFACE

This report presents the results of the studies considered necessary to complete the Task I, "Design Analysis Effort". The results provide the basis for the final design meeting program requirements and cover the period of performance from 1 July 1971 to 1 November 1971. The contributions to this report were provided by the following individuals: G. Schweitzer (system integration and mechanical design with the support of M. Katchmar), R. Gelbman (Thruster electrical design), D. Conroe and W. Geier (Reliability), H. Switzky and J. Austin (Structural analysis), W. Guman (Capacitor and Thermal analysis), Wilmore Electronics, Inc. under the direction of Dr. E. T. Moore (charger-converter subsystem). The design supporting laboratory efforts were performed by M. Katchmar, E. Poggie, and L. Odorico. The principal investigator was Dr. W. J. Guman.

Based upon the results obtained, several conclusions can be made. The propulsive performance required can be met and thermal vacuum design supporting tests indicate no problems under worst case conditions of sink temperature and spin rate. Almost all electrical components could be selected from NASA, Goddard Space Flight Center PPL-11 with the remaining few components being screened items of the LES-6 and LES-7 programs. The reliability of the system was calculated to be 0.92 for a five year mission. Structural integrity in meeting launch environment has been ensured. The spin-rate accommodating converter-charger subsystem will perform as proposed and thus significantly extend pulse capacitor life. Only by using Beryllium instead of Aluminum as a structural material and an alternate energy-storage capacitor will it be possible to reduce the system weight by about one pound. Since either of the two latter approaches are higher risk approaches, they will not be considered in the final design. A substantial reduction in the number of electronic parts with a corresponding increase in reliability can be achieved by using a V-shaped propellant instead of the standard breech-fed propellant. The alternate approach will not be incorporated in the final design because the impulse bit amplitude exceeds 25 micropound-second and the lower specific impulse will require a longer propellant rod.

1. INTRODUCTION AND GENERAL SYSTEM DESCRIPTION

This Task 1 report summarizes the design analysis and design supporting laboratory efforts performed on the propulsion system in order to provide the detailed information and final approach to be incorporated in the final design of the system.

The solid propellant pulsed plasma electric propulsion system for the SMS application is a scaled version of the system that has functionally been performing East-West stationkeeping of the spin stabilized LES-6 communication satellite.[1,2] Differences in design from the LES-6 flight system and the laboratory prototype LES-7 propulsion system that are incorporated in the SMS system are those introduced to meet the required performance level, reliability, life, pulse rates, logic requirements and volumetric constraints of the SMS mission and those improvements that have been experimentally verified by extensive laboratory tests since the design of the LES-6 system early in 1968. The basic philosophy underlying the proposed system is to utilize designs proven reliable by long term testing instead of offering a higher performance system incorporating the most recent developments which as yet have not been extensively tested. In accordance with contract requirements all electronic parts have been selected, where possible, from GSFC PPL-11 and PPL-11A, respectively.

The propulsion system will be comprised of four major subassemblies. These subassemblies, integrated as one package, will meet the thruster envelope geometric constraints (GSFC Drawing GC 1171302) for the SMS application. The four major subassemblies are: 1) thruster module, 2) discharge initiating subassembly, 3) firing control logic subassembly, and 4) the converter-charger, respectively. A block diagram showing the inter-relationship of these subassemblies is presented as Figure 1.

The basic thruster module subassembly contains essentially the same basic features as those underlying the design of the LES-6 and LES-7 systems.[1,3] Solid teflon is used as the propellant. The addition of electric energy depolymerizes an exposed surface of the teflon propellant rod and converts the depolymerized products to plasma. This plasma is subsequently accelerated through the accelerator nozzle

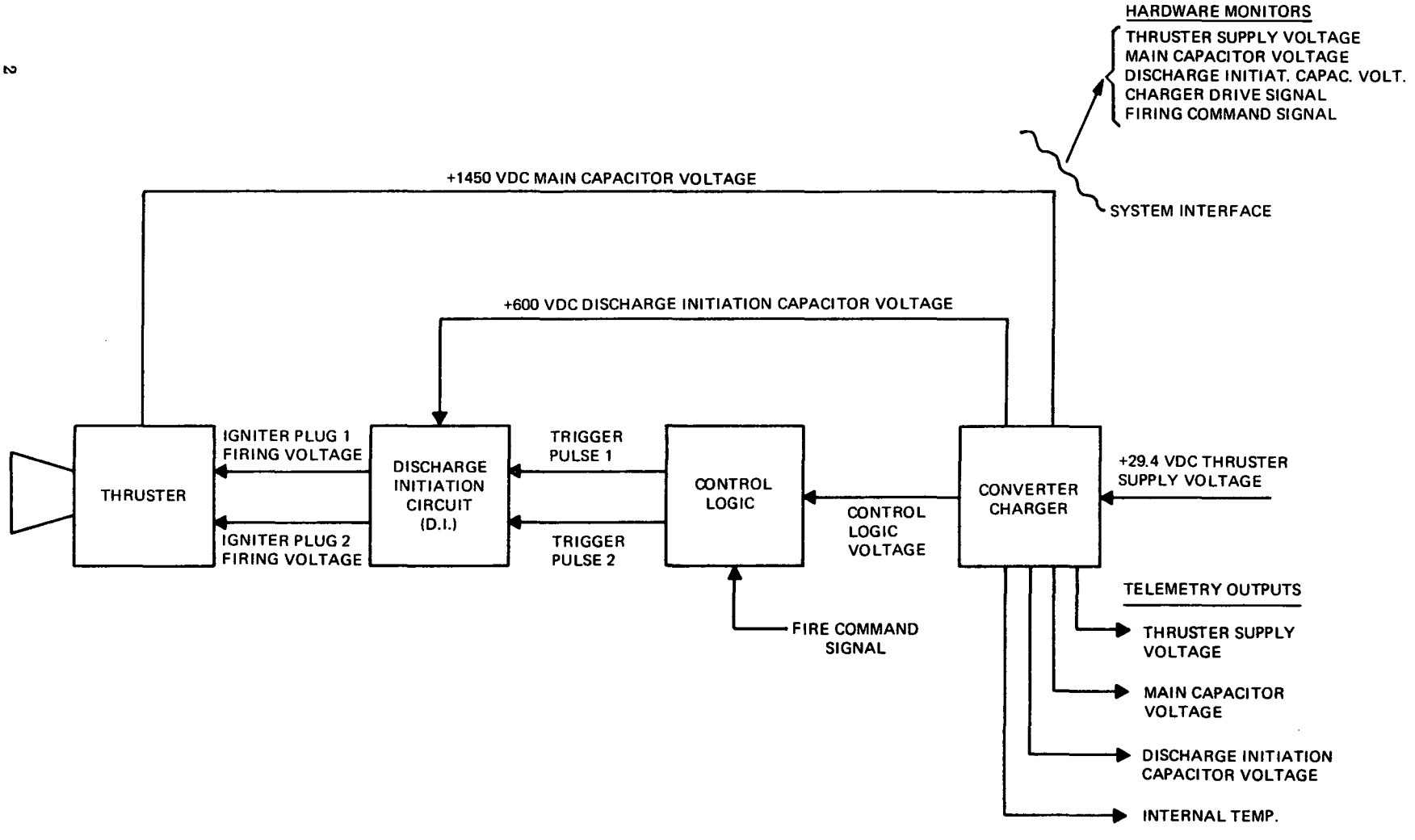

Figure 1. Functional Block Diagram of System

to deliver a sharply defined impulse bit. A schematic representation of the thruster module subassembly is shown in Figure 2.

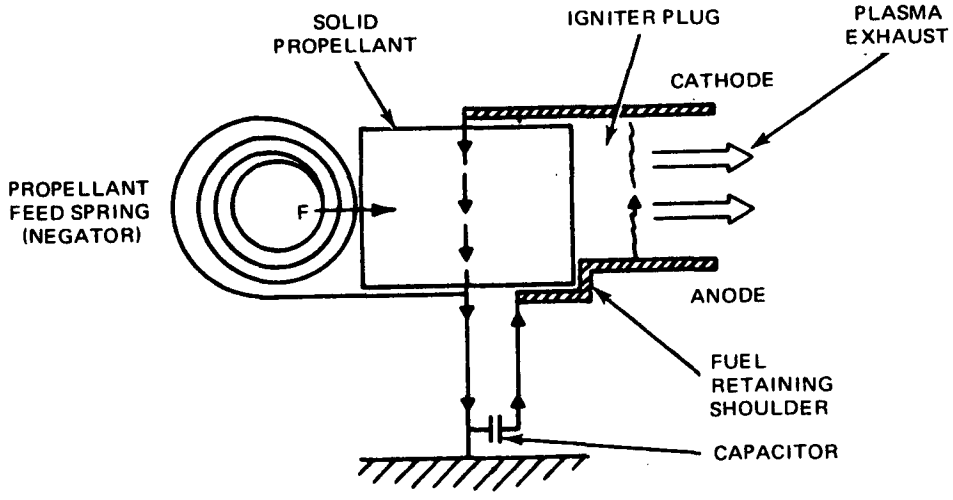

Figure 2. Thruster Module Subassembly Schematic

The terminals of the energy storage capacitor are connected by a low inductance, low resistance path to the anode and to the cathode of the thruster accelerator nozzle, respectively. A fuel retaining shoulder is machined into the anode in order to properly position the teflon propellant rod with respect to the thruster nozzle. A constant force steadily provided by a Negator spring assures that an edge of the propellant is held against the fuel retaining shoulder independent of thruster attitude, thermal environment, absence of gravity or duration of thruster operation. Since the effect of this steady force is equivalent to the effect of the centrifugal force produced by a spinning satellite no problems will arise due to the high "g" environment in the SMS application.

To generate an impulse bit, the energy storage capacitor is charged to the operating voltage of 1450 volts starting about 0.480 seconds before firing regardless of the satellite spin rate. This applied voltage appears across the two electrodes of the accelerator nozzle. Because a vacuum exists in the interelectrode spacing, the applied voltage is retained until a firing command signal from the satellite commands the firing logic subassembly to trigger the discharge initiating circuit of the thruster. The discharge initiating circuit generates a microdischarge by means of a discharge

initiating plug located in the cathode of the accelerator nozzle. This "microdischarge" bridges the two electrodes and allows the main thruster energy storage capacitor to discharge its energy into the thruster nozzle. This energy depolymerizes surface layers of teflon which become energized and ejected as a plasma through the thruster nozzle for a duration of roughly 10 microseconds. Maximum capacitor life is obtained by keeping the peak voltage stored on the capacitor just prior to firing at a fixed minimum duration independent of satellite spin rate.

Since the teflon also depolymerizes behind the fuel retaining shoulder, the Negator spring replenishes the consumed propellant by moving it into the region depleted by the previous discharge. This propellant movement is essentially imperceptible to the eye.

A flip-flop circuit in the logic control subassembly is used for alternating the firing sequence of the two igniter plugs located in each thruster-nozzle being discharged.

The pulse interval of the impulse bit is highly repeatable and can be started within microseconds after the trailing edge of the applied command pulse.

2. BACKGROUND UNDERLYING SYSTEM DESIGN APPROACH

2.1 Basic Thruster

2.1.1 Performance Demonstrated

The governing electrical and physical parameters determining the propulsive performance of the basic thruster of the design of Task I were experimentally evaluated prior to contract award. The propulsive performance was established concurrently with a life test designated as Log 126X-7 performed from December, 1970 until March, 1971. Table 1 presents a summary of the data. The test was terminated because available propellant was used up.

TABLE 1. PERFORMANCE PREVIOUSLY DEMONSTRATED
(Log 126X-7)

Thrusting Duration	2080 hours
Test Average Thrust Level	50.7 μ lb
Test Average Impulse Bit	27.62 μ lb-sec
Pulse Frequency	1.835 Hz
Total Consecutive Discharges	13,788,327
Total Impulse of Test	380.83 lb-sec
Specific Impulse of Test	405 sec
Total Length of Teflon Consumed	10.29 in.
"g" Simulation	1g
Propellant Area	1.165 $in.^2$

The performance demonstrated has verified the capability of the basic thruster underlying the design approach of Task 1 to meet the require propulsion performance requirements of the SMS mission.

2.1.2 Life Test

Section 2.1.1 has presented thruster performance data established during a life test. The life test data presented in Table 1 has shown that the 380.83 lb-sec represents 95 percent of the 400 lb-sec total impulse requirement for the five year mission. Table 2 presents the thrust and impulse bit amplitude measured during the test.

TABLE 2. THRUST LEVEL DURING LIFE TEST
(Log 126X-7)

Number of Discharges	Measured Thrust μ lb	Impulse Bit μ lb-sec	Pulse Frequency Hz
34,929	51.3	28.8	
171,568	50.3	28.2	
294,064	52.8		
602,000	51.6	28.6	1.805
991,248	53.7	29.6	1.81
1,146,492	48.3	26.8	1.805
1,305,826	61.5	33.9	1.81
3,206,038	57.7	31.5	1.83
3,362,860	46.3	25.3	1.83
3,520,690	37.6	26.6	1.82
3,550,326	44.7	24.6	
3,685,471	46.1	25.2	1.83
3,834,192	50.6	27.4	1.845
4,470,041	54.1	29.6	1.83
4,625,526	49.9	27.2	
9,383,902	48.2	26.0	1.85
9,642,524	48.7	26.0	1.87
11,543,883	49.1	26.5	1.855
13,787,926	51.1	27.35	1.87

2.1.3 Hi-g Operation

The data presented in Sections 2.1.1 and 2.1.2, respectively, were obtained for a thruster operated at 1 g condition. Since during flight, the acceleration level will nominally be at 13g's a test was also performed to check thruster performance and operational behavior at a high "g" level. Two SH16P38 Negator springs were used to provide an axial force of 21.2 pounds against a 393.4068 gr propellant rod. The initial equivalent g loading is thus (21.2) 453/393.4068 = 24.6 g. With this simulated g loading on the teflon rod the thruster was operated (prior to contract award) in a vacuum on a thrust balance. Table 3 presents the results of this test.

TABLE 3. HI-g PERFORMANCE PREVIOUSLY DEMONSTRATED
(Log 130X-1)

Date	Pulse Count	Measured Thrust, μlb	Pulse Frequency Hz	Impulse Bit μ lb-sec
4/22/71	144-300	51.5	1.84	28.0
	7,067-7,246	51.1	1.865	27.4
	21,580-21,781	50.0	1.865	26.8
	36,612-36,844	43.1	1.83	23.5
4/23/71	158.816-158,916	50.2	1.83	27.4
4/26/71	574,719-574,944	54.3	1.83	29.6
4/28/71	897,573-897,954	51.7	1.83	28.3
4/29/71	1,044,469-1,044,668	54.4	1.83	29.7
4/30/71	1,200,254	Test Terminated		

The test was terminated after 1,200,254 consecutive discharges because of vacuum pumping problems which produced some oil vapor backstreaming. A total of 0.73 inches of propellant was consumed and a visual inspection of the propellant rod showed normal depolymerization of the propellant rod. Test average performance is presented in Table 4.

TABLE 4. HI-g TEST AVERAGE PERFORMANCE
(Log 130X-1)

Thrust Duration at 24.6 g	181 hours
Test Average Thrust Level	50.78 μ lb
Test Average Impulse Bit	27.6 μ lb
Pulse Frequency	1.84 Hz
Total Consecutive Discharges	1,200,254
Specific Impulse of Test	463 sec.

The Hi-g test has established that no abnormal propellant feed or thruster performance behavior is expected at the 13 g normal SMS operational g environment. Indeed, as propellant is consumed in flight the effective force experienced by the propellant rod against the propellant retaining shoulder will decrease with time thereby providing more favorable conditions.

2.1.4 Weight

An early weight estimate of the system was made and presented in our proposal (PCD-Prop-71-2, Vol. 1 - Technical) using the LES-7 system as a basis. Table 5 presents the original estimates based upon existing operational (non-flight) laboratory hardware.

TABLE 5. EARLY WEIGHT ESTIMATES BASED UPON EXISTING LABORATORY HARDWARE

Capacitors	1100 gr
Capacitor-cases, lids, strip line, Negator spring	200 gr
Insulated front strip line and anode	60 gr
Propellant	404 gr
Cathode with Mykroy and plug	60 gr
D.I. and Logic subassembly	250 gr
RFI cone	70 gr
Miscellaneous insulation and Supports	50 gr
Thruster, D.I., logic Sub-total	2194 gr
Converter-charger & its housing (est)	698 gr
Housing and Lid (estimate)	410 gr
Estimated System Weight	3302 gr (7.3 lb)

The one component that contributes most significantly to the overall weight is the thruster energy storage capacitor. Two capacitor manufacturers* other than Dearborne (the supplier of the present capacitor) claim that the weight of the cpacitor for the same discharge energy can be appreciably reduced below present operational ones. Until actual alternate capacitors are available and life tested, a major weight reduction by using an alternate energy storage capacitor can only be considered a hopeful means of reducing system weight.

---

* Capacitor Specialists Incorporated, Escondido, California
Component Research Company, Inc., Santa Monica, California

2.1.5 Energy Storage Capacitor

The thruster uses two energy storage capacitors rated at 4 μfd ± 5% each which are charged to the operating voltage of 1450 volts. Since the demonstrated performance meets the required impulse bit performance level of 25 ± 5μ lb-sec the same rated capacitance and voltage level of operation will be used in the final design. The capacitors are bu ilt by Dearborn Electronics (a subsidiary of the Sprague Electric Company) and are of the same basic design as the cpacitor flying in the LES-6. They are of the extended foil type and are comprised of Mylar dielectric with aluminum foil electrodes wrapped upon a phenolic core. This latter construction is an improvement over earlier commercial Dearborn Hi-Jul capacitors tested by General Electric,[4] and Fairchild Republic. The improvements incorporated into the Hi-Jul line were recommended to Dearborn by Fairchild Republic based upon several years of experimental data.

The ESXP 405J20003 cpacitor is being built specifically for the SMS application. Prior history of this capacitor is as follows:

The basic capacitor from which the ESXP 405J20003 evolved is the Dearborn Hi-Jul capacitor as defined in Dearborn Bulletin 1050. This series of capacitors was tested at General Electric[4] and at Fairchild Industries. General Electric life tested the ESXP 505M25 up to 6.4×10^7 shots per capacitor. At Fairchild Industries we evaluated the ESXP 205M15 and ESXP 205M25 from 10/67 to 3/68. Based upon a failure mode analysis, Fairchild requested that a phenolic core be placed at the center of the capacitor to eliminate an initial fold in the capacitor winding. This new capacitor design is designated as the ESXP....J..... series. The first capacitor of this series was the ESXP 205J20001 for the LES-6 application.

The improved ESXP 205J20001 was life tested from 1/68 to the present at Fairchild and also selected and used on the LES-6 satellite. (Four capcitors are aboard the LES-6 satellite since its launch in September of 1968.) None of the four capacitors aboard the LES-6 satellite have experienced a failure after three years in space. Table 6 presents laboratory data of the ESXP 205J20001 capacitors.

TABLE 6. LABORATORY TEST DATA OF LES-6 TYPE CAPACITORS

Testing Period	*** Total No. of Pulses	Failures
1/16/68 - 2/23/68	14,665,281	1
2/21/68 - 5/09/68	8,744,277	0
5/08/69 - 6/26/69*	7,449,545	0
1/23/70 - 4/13/70**	11,766,194	0
Total	42,625,297	1

*Tests performed after delivery of LES-6 flight system
**Test performed at 1580 volts instead of 1360 volt design voltage
***Total pulse actually delivered

The success of the ESXP 205J20001 design of the LES-6 was used as a basis for the ESXP 405J capacitor series intended for use on the LES-7 and now for the SMS. The ESXP 405J series is a 4 μfd version of the 2 μfd ESXP 205J20001 capacitor described above. The first design, ESXP 405J20001, was procured in June of 1969. No life tests were performed with the ESXP 405J20001. Upon review of the LES-7 requirements, the ESXP 405J20001 was modified by reducing the design stress (volts/mil.) and fabricated as the ESXP 405J20002. Two of these capacitors were tested at the new SMS thruster performance level (25 micro-lb-sec impulse bit level). The test data obtained is:

#1 15,041,800 discharges before failure
#2 14,703,251 discharges before failure

In addition to this pulse life, each capacitor has accumulated about 1300 d.c. hours of life at full voltage during the test. The latter set of data has shown that even the life test of the ESXP 405J20002 capacitor would meet the SMS mission requirements. The ESXP 405J20003 capacitor to be used in the thruster will be further derated to provide an additional margin of life. The design will be discussed in more detail in Section 3.3.

2.2 Power Conditioner

The power conditioner must perform two functions. It has to accept a low d.c. voltage (typically 16 to 30 volts) and convert it to a high voltage (typically 1000 to 1500 volts) and it must also transfer energy as efficiently as possible into the thruster energy storage capacitor. Ordinary d.c.-d.c. converters are readily available which have a conversion efficiency of about 50%. If ordinary RC charging is used, then the capacitor charging efficiency will be limited to about

50%. Hence by unsophisticated techniques one arrives at an overall power conditioning efficiency of only about 25%. Obviously a 25% efficiency is unacceptable. For this reason considerable analytic and laboratory evaluation studies were carried out at Fairchild Republic for about a decade for the purpose of improving this efficiency and also for meeting long life mission requirements. A highly successful power conditioner for meeting all requirements has been developed by Wilmore Electronics, Inc. The conversion-charging techniques used by Wilmore have been discussed in some detail in References 5 and 6. Basically, small energy bits are switched at a rate of from 5 Kc to 20 Kc into the primary of a transformer. The secondary winding of this energy storage transformer, the "flyback" circuit, appears as a current source rather than a voltage source, thus enabling it to deliver energy efficiently to the thruster energy storage capacitor. Since the source and the load are never directly coupled to each other, the primary circuit becomes protected from load short circuits such as occur during pulsed operation of the thruster.

Results of laboratory life tests of breadboard Wilmore power conditioners were reported in 1968 in Reference 7. Table 7 presents a copy of the latter results, which provide sufficient confidence to develope a power conditioner for the LES-6 spacecraft. Wilmore Electronics designed and built the LES-6 power conditioner to Fairchild Repbulic's specifications. The power condtioner aboard the LES-6 is fully functional after three years in space.

Wilmore Electronics was also selected in the present program to provide the power conditioner for the SMS mission. The requirements for the SMS missions are more severe and introduce new features which will advance the state-of-the-art of power conditioner for pulsed plasma thrusters.

More details of Wilmore design approach for the SMS mission are presented in Section 3.8.

3. DESIGN APPROACH OF PROGRAM

Three different design approaches for the basic thruster to be used for the SMS mission were possible. The three design approaches are:

a) The use of a breech fed thruster
b) The use of a V-shaped propellant
c) The use of a slanted fuel propellant

TABLE 7. BREADBOARD POWER CONDITIONER LIFE TEST STUDIES
UNITL 1968 (Reference 7)

Description	Model	Serial No.	Simulated Discharges		Thruster Discharges		Total on Unit
			PC in Air	PC in Vacuum	PC in Air	PC in Vacuum	
5 j Breadboard	1032	10/13/66	19,423,714	24,033,042	3,496,659	0	46,953,415*
5 j Breadboard	B032-1	BO 32-1	23,700,016	0	11,784,933	0	35,484,949
20 j Breadboard	1035	1035BB-2	516	0	8,052,840	815,529	8,868,885***
20 j Breadboard	1035	1035BB-3	1,334,097	442,700	3,115,060+	567	4,892,424*
20 j Breadboard	1035	1035BB-4	617	0	1,743,366	0	1,743,983****
20 j Breadboard	1035	1035BB-5	7,547	3,085,509	1,247,464	0	4,341,020
20 j Breadboard	1035	1035BB-6	2,688,555	0	360,997	0	3,049,052**
20 j Breadboard	1035	1035BB-7	1,988	0	703,569	0	705,557

* 4.26×10^7 discharges were carried out before unit was repaired due to accidental damage
** Returned to manufacturer for repair after 2,688,555 discharges
*** Damaged due to vacuum failure (has been repaired)
**** Damaged during test
\+ Plus discharges accumulated at A.F.A.P.L.

The three approaches differ fundamentally in the end configuration of the solid teflon propellant. The three approaches will be briefly described as well as reasons for selecting the breech fed design being adapted.

3.1 Descriptions

3.1.1 Breech Fed Thruster

The breech fed thruster is the design that has been extensively studied at Fairchild Republic since 1966, used on the LES-6 and considered for the LES-7. The solid teflon propellant is fed into an electrode accelerator nozzle from the breech end of the nozzle in the same direction as the thrust axis. The end plane of the propellant rod is planar and normal to the thrust axis. Figure 3 presents a schematic representation of the design approach, which presents a balanced compromise between the ratio impulse bit amplitude/discharge energy, (i.e., thrust/power ratio) and propellant specific impulse. Depending upon specific details of the design, the thrust/power ratio of a typical breech fed thruster can be

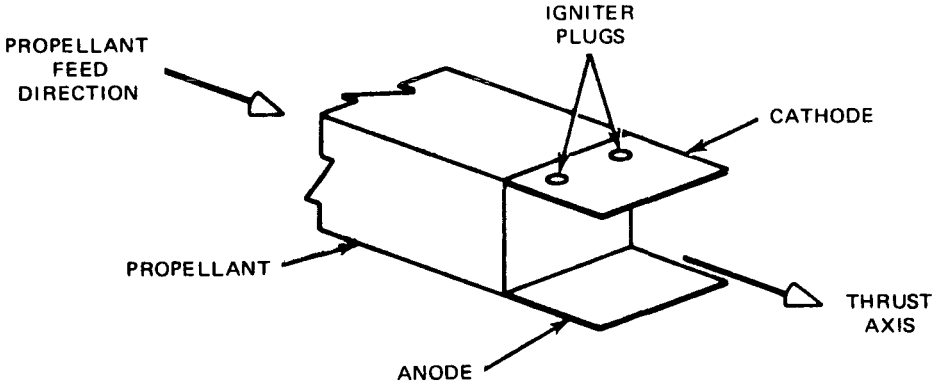

Figure 3. Schematic Representation of a Breech-Fed Thruster

designed to be in the range from about 3.3 to 4.5 μlb/watt.[8] The propellant specific impulse is a function of the energy/area ratio and typical data is presented in Figure 5.

Since the maximum pulse frequency (110 ppm) is defined by the SMS spin rate, and the corresponding maximum power (20 watts) is specified, one can immediately establish the maximum capacitor discharge energy. A meaningful calculation must also reflect power conditioning efficiency. Table 8 presents capacitor energy as a function of conversion efficiency.

TABLE 8. CAPACITOR ENERGY AS A FUNCTION OF CONVERSION EFFICIENCY

Efficiency, %	Energy, Joules
75	8.18
77	8.40
78	8.51
80	8.73

Using a conversion efficiency of 77% one finds a capacitor energy of 8.40 joules. Thus two 4 μfd capacitors connected in parallel charged to 1450 volts will provide this discharge energy. Using the lower impulse bit/energy ratio of 3μlb-sec/joule, one finds the impulse bit amplitude to be about 27.7 μlb-sec. This value is in the desired range of 25 ± 5μlb sec.

Having the discharge energy and approximate impulse bit amplitude, one can obtain the approximate propellant specific impulse. This latter quantity is evaluated from the data[8] presented in Figures 4 and 5 respectively. For a discharge energy of 8.4 joules one finds the product $I \times I_{sp}$ to be about 13,000(μ lb-sec) sec. Hence the specific impulse will be about (13,000/27.7) = 470 sec. The approximate propellant area is then found from Figure 5 which presents specific impulse as a function of the energy/area ratio. For the calculated values of specific impulse and discharge energy one finds a propellant area A=8.4/7.3=1.15 in^2. The calculated characteristics of the breech-fed thruster are summarized in Table 9.

TABLE 9. CALCULATED CHARACTERISTICS OF BASIC THRUSTER

Discharge Energy	8.4 joules
Impulse Bit	27.7 μ lb-sec
Specific Impulse	470 sec
Propellant Frontal Area	1.15 in^2

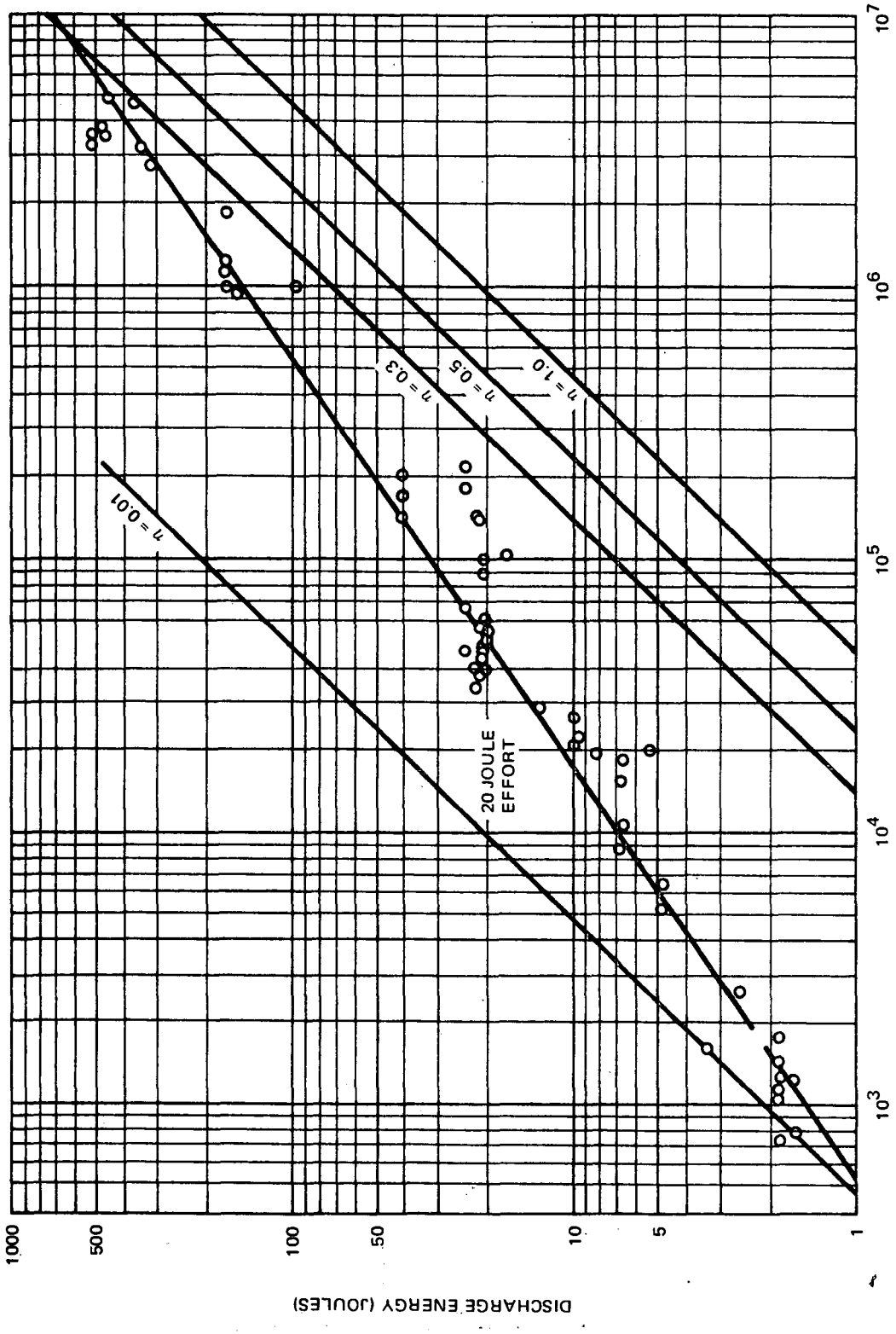

Figure 4. Discharge Energy as a Function of Impulse Bit x Specific Impulse

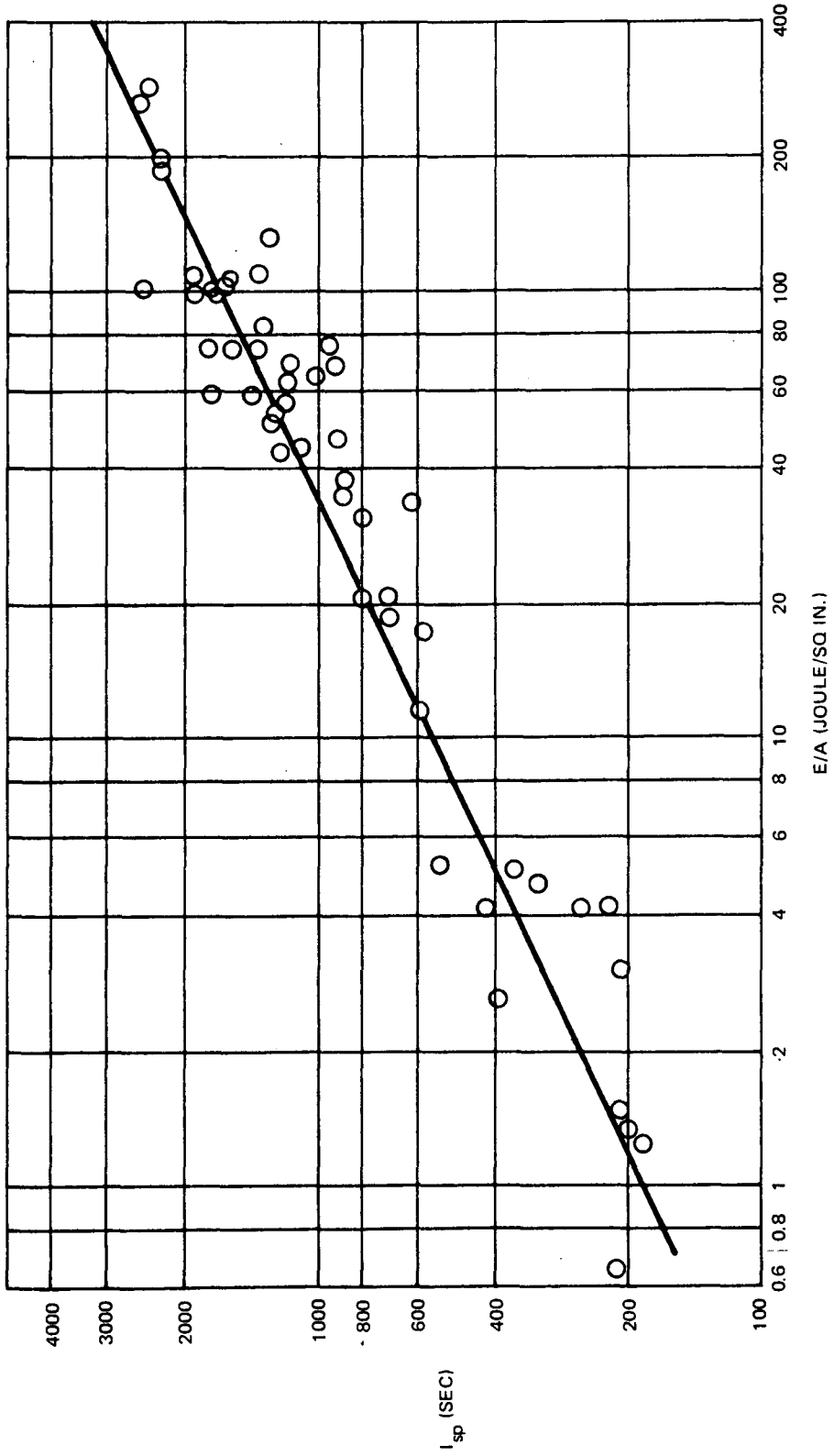

Figure 5. Specific Impulse as a Function of Energy/Area Ratio

A comparison of the calculated performance presented in Table 9 with the performance actually demonstrated (see Table 1) shows good agreement between calculated and measured parameters. This agreement suggests a confidence that the data presented in Table 1 represents the level of performance that was expected based upon all empirical data of the breech fed thruster. The design approach of the thruster during Task 1 was therefore based upon the laboratory thruster, the results of which are presented in Tables 1 and 2, respectively.

3.1.2 Alternate Design Approaches

The breech fed thruster described above represents one of three possible thruster design approaches that could have been adapted in this program. The two alternate thrust designs that were considered are briefly presented below.

3.1.2.1 V-Fuel

Instead of a breech fuel thruster with the propellant configured as shown in Figure 3, it is possible to use a V-shaped propellant such as depicted in Figure 6.

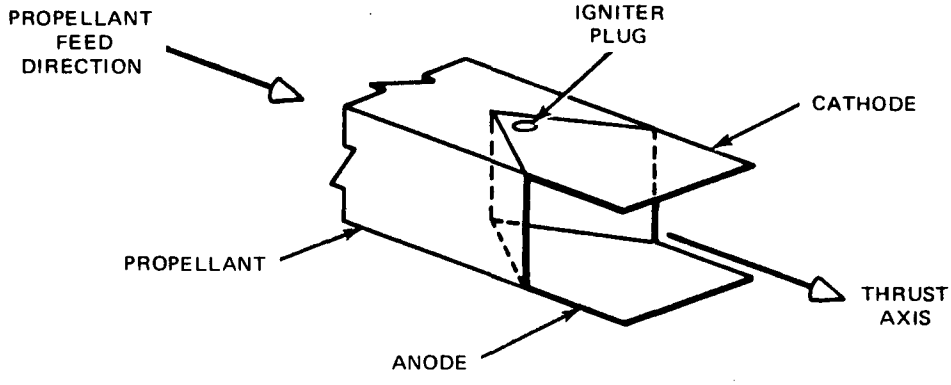

Figure 6. Schematic Representation of a V-Shaped Propellant Thruster

The V-shaped propellant geometry provides a higher thrust/power ratio at a lower specific impulse compared to a breech fed thruster operated at the same discharge energy. Since the V-shaped thruster uses only one igniter plug per nozzle the electronic part count is significantly reduced. In particular, since only one igniter plug is used per nozzle, the control logic flip-flop circuit is eliminated and only half the components are required in the discharge initiating circuit. These simplifications in the electronic circuitry are illustrated by Figures 7, 8, and 9, respectively. The circuit components grayed out in the figures are deleted for a V-shaped thruster. The parts count is seen to be significantly reduced by the V-shaped propellant approach.

The practicality of the V-shaped propellant for the SMS application was experimentally demonstrated by a life test performed by an in-house supported program. The same capacitors and general thruster geometry as the breech fed SMS thruster was tested. The results of the test are presented in Table 10.

TABLE 10. PERFORMANCE OF A V-SHAPED PROPELLANT THRUSTER
(Log 129-3)

Thrusting Duration	1440 hours
Test Average Thrust Level	74.2 μ lb
Test Average Impulse Bit	40.2 μ lb-sec
Pulse Frequency	1.84 Hz
Total Consecutive Discharges	9,590,163
Total Impulse of Test	385.5 lb-sec
Specific Impulse of Test	342 sec
Total Length of Teflon Consumed	12.28 in.
"g" Simulation	1 g

Even though the mission total impulse has been demonstrated by the V-propellant and a significant reduction in electronic part count can be realized the V-shaped propellant will not be adapted for use in the final design. The lower specific impulse of this latter approach requires an additional two inches of propellant. The overall propellant rod length would thus protrude about two inches beyond the allowable length as defined by NASA, Goddard Space Flight drawing GC1171302. Furthermore, for the same power level, the impulse bit amplitude would be about 40μlb-sec instead of 25μlb-sec as per paragraph 1.2.2.1 of the Schedule. It is important to note however that the breech fed thruster can easily

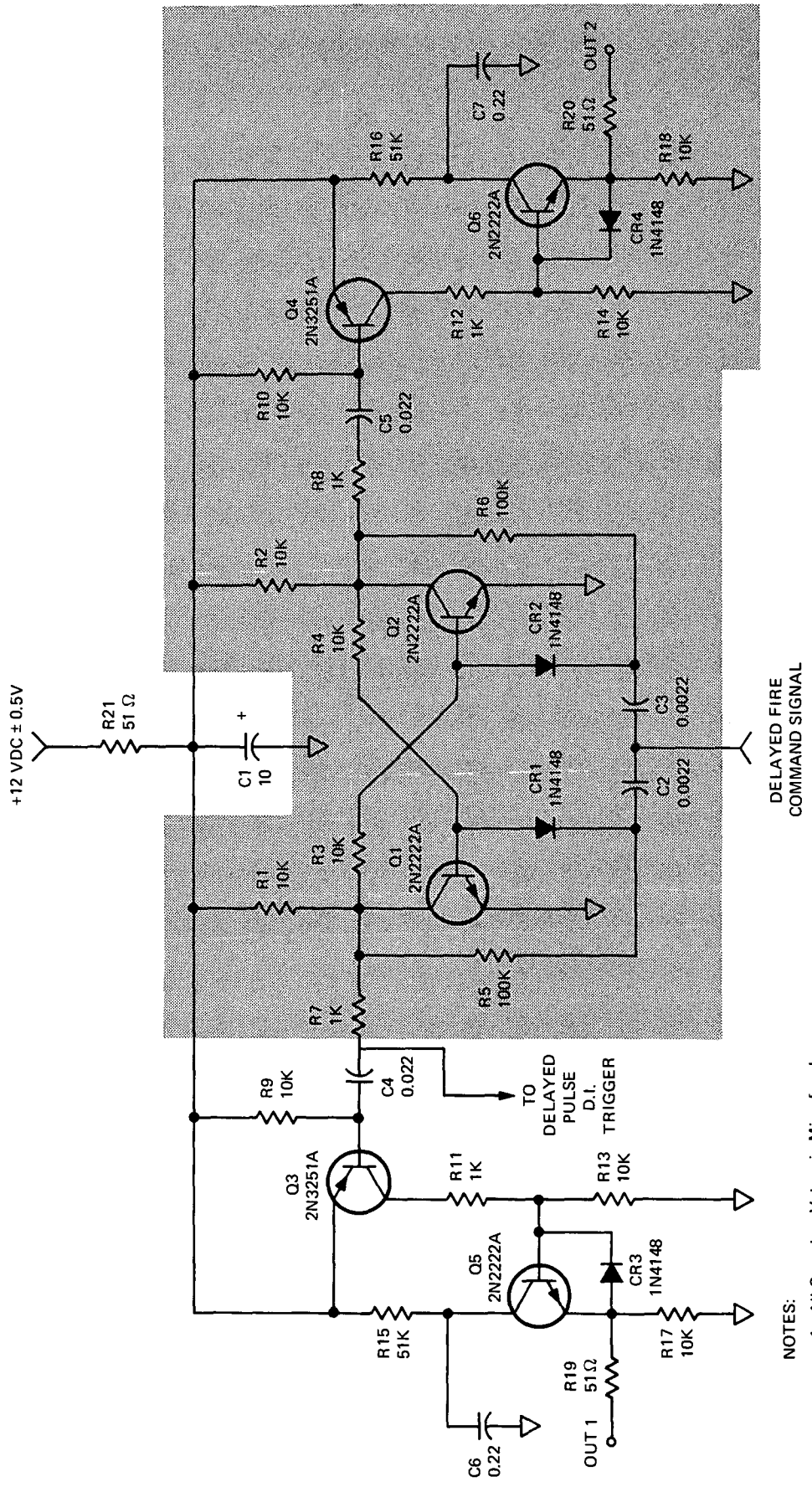

NOTES:

1. All Capacitor Values in Microfarads
2. All Semiconductors are TX
3. Greyed Out Components not Required for Single Igniter Plug Circuit

Figure 7. Control Logic Flip-Flop and SCR Pulse Driver Circuit for V-Shaped Propellant

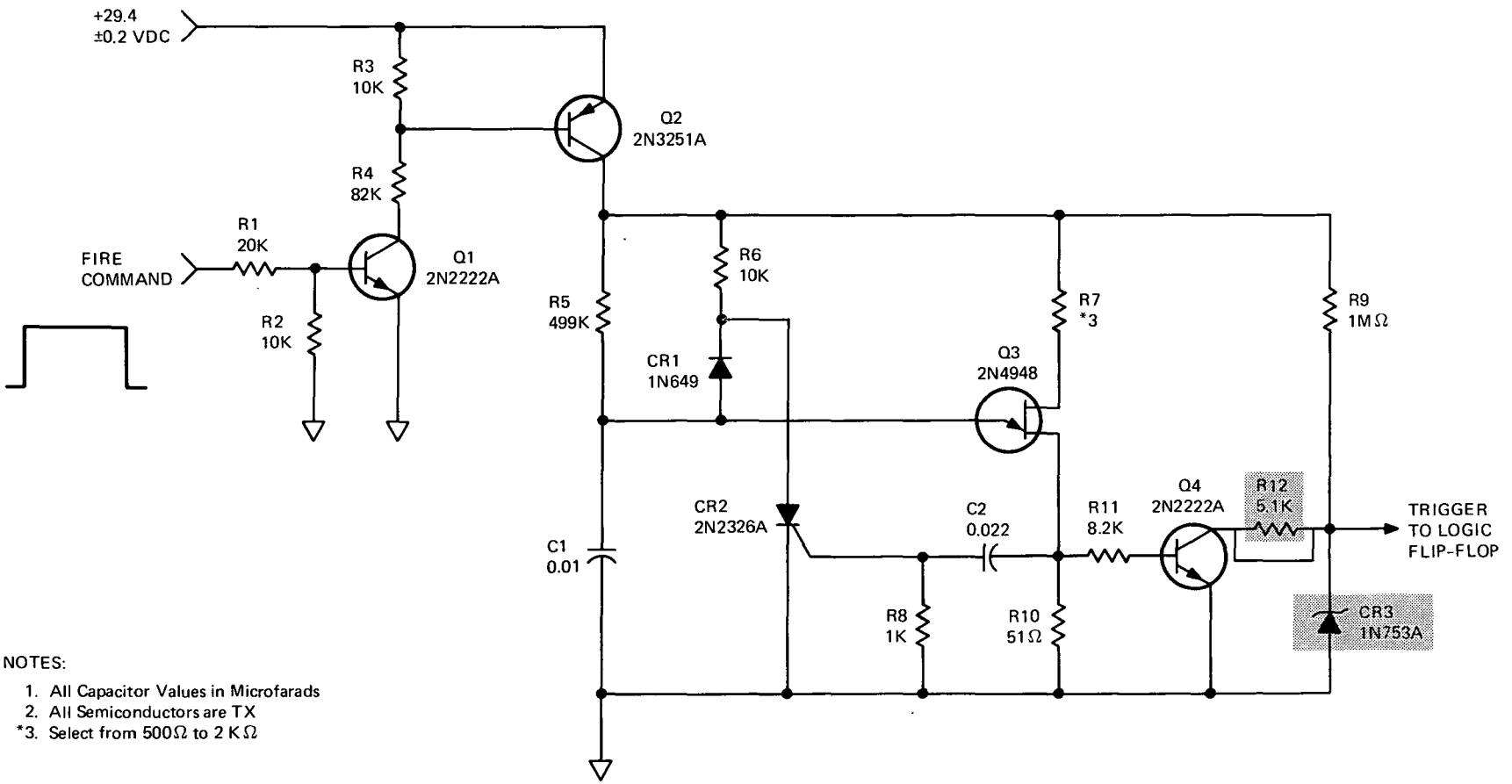

Figure 8. Delayed Pulse D.I. Trigger Circuit for V-Shaped Propellant

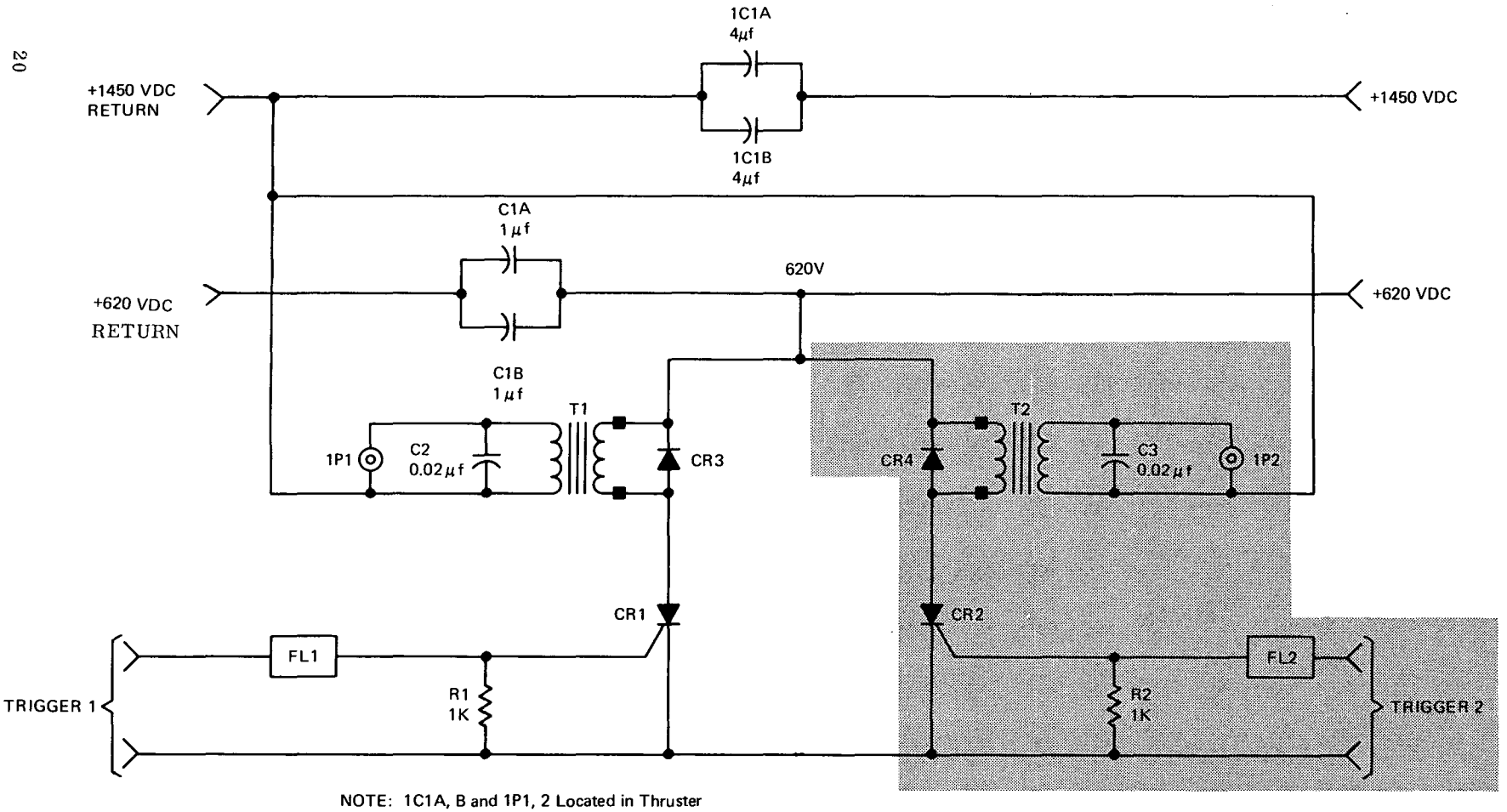

Figure 9. Discharge Initiation Circuit for V-Shaped Propellant

be modified into a V-shaped configuration at a later date if so desired.

3.1.2.2 Slanted Fuel Configuration

The slanted propellant configuration[3] is obtained by cutting one end of the propellant rod at an angle θ with respect to its longitudinal axis and providing a set of accelerator nozzles normal to the slanted end plane. Figure 10 shows a schematic presentation of the approach. The primary purpose for including this configuration is to include a configuration which reduces the stress of the teflon at the fuel retaining shoulder. Figure 11 shows one possible orientation of the slanted propellant rod in the spinning satellite. Another possible orientation is obtained by

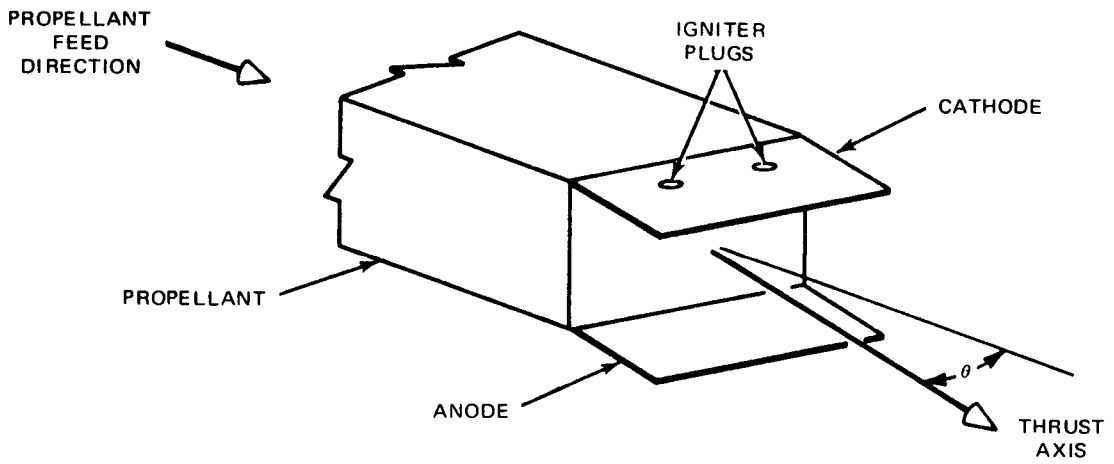

Figure 10. Schematic Presentation of a Slanted Fuel Configuration

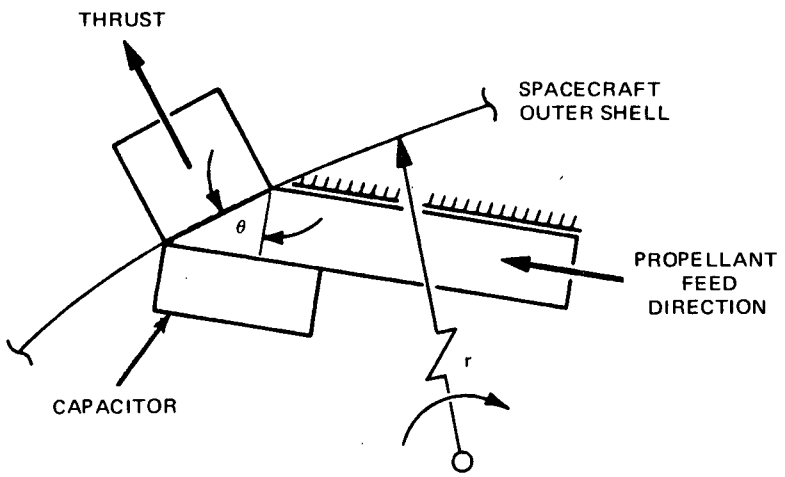

Figure 11. Slanted Fuel Approach

rotating the propulsion system by 90°. To maintain the same performance as the breech-fed thruster, the frontal propellant area must be preserved, i.e., the slanted area of the slanged propellant configuration must equal the normal area of the breech fed thruster. Thus, it is seen that the propellant rod length of the slanted configuration will be larger than that of the breech fed configuration by the factor $(1/\cos\theta)$. Since the slanted propellant configuration has only been tested at a 20 joule level, and because of the extra propellant length required, it was not considered for the final configuration to be used.

3.2 THRUSTER ELECTRONICS

3.2.1 Discharge Initiating Circuit

The design of the solid state discharge initiating (D.I.) circuit (see Figure 12) is the same as that used in the LES-6 satellite. Its function is to energize a surface igniter plug located in the cathode of the thruster nozzle. The energy input to the igniter plug from the D.I. circuit creates a microdischarge in the electrode spacing of the thruster nozzle. This microdischarge acts like a "switch" in that it closes the thruster discharge circuit (by means of a microplasma), thereby producing an impulse bit.

3.2.1.1 Implementation of Principle

The surface igniter plug is energized (see Figure 12) by the discharge of capacitor C_1 which is charged to 620 volts by the converter-charger at the same time the main thruster capacitor is charged to 1450 volts. Capacitor C_1 is discharged through an SCR into the primary of a pulse transformer.

The secondary of the transformer energizes the igniter plug and causes the main thruster capacitor to discharge across the interelectrode spacing of the thruster nozzle. Since there are two igniter plugs in the thruster nozzle, two igniter plug energizing circuits are used. These two igniter plugs are fired alternately from signals generated in the control logic assembly.

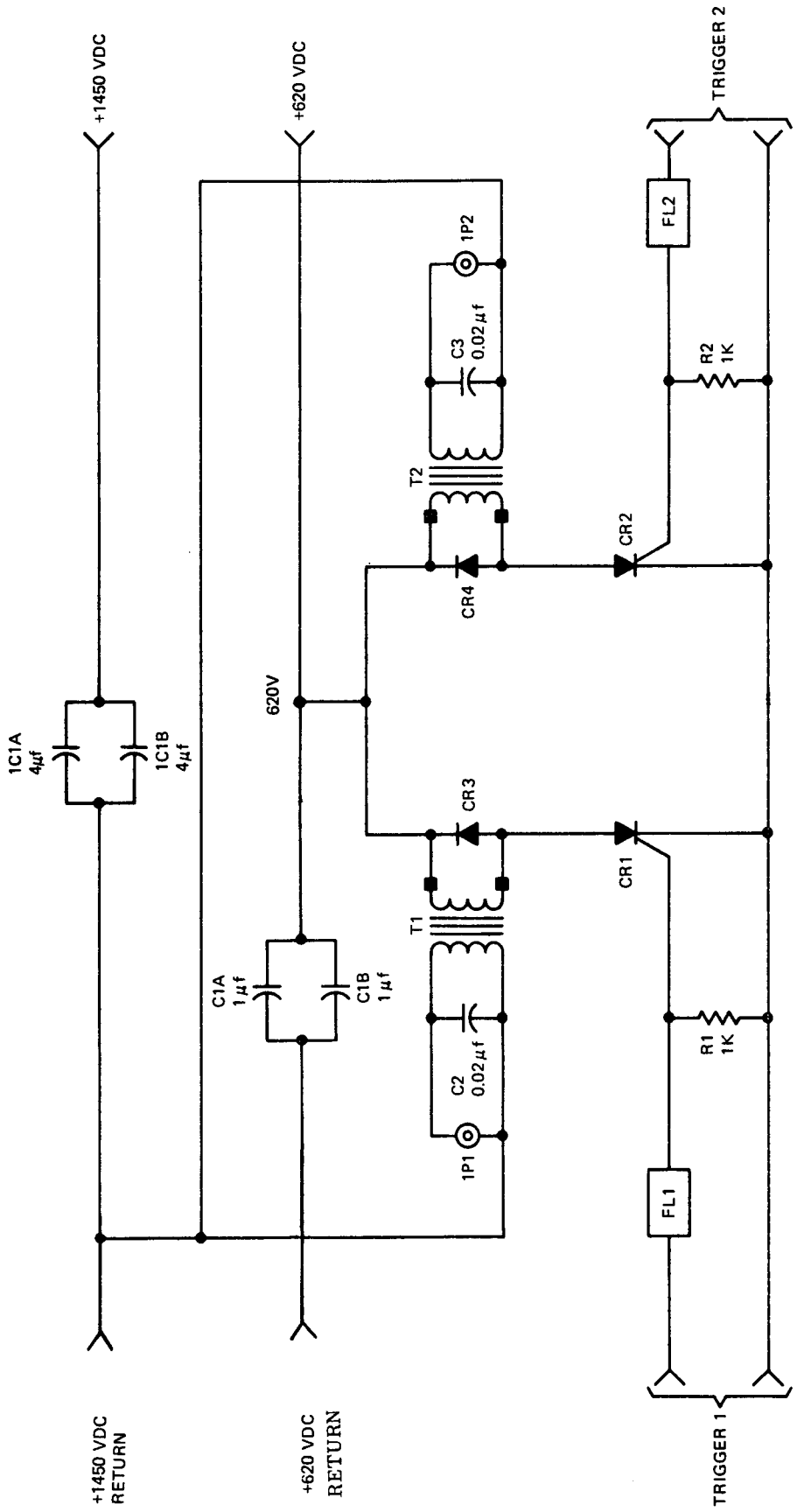

Figure 12. Discharge Initiation Circuit

3.2.1.2 Final Design

Silicon controlled rectifiers CR_1 and CR_2 in the discharge initiating circuit are alternately triggered by the control logic flip-flop circuit. Capacitor C_1 is charged to + 620 VDC through L_1 which attenuates any high frequency transient feedback into the power converter/charger circuitry while capacitor C_4 charges to +1450 VDC through L_2. When the SCR CR_1 is triggered, capacitor C_1 is discharged into transformer T_1. Capacitor C_2 is used to increase the energy transfer from the secondary of tranformer T_1 and causes igniter plug $1P_1$ to fire which in turn causes the main engine capacitor C_4 to discharge and produce an impulse bit. All non-standard components will be high reliability components such as used in the LES-6 design. They will be secured to specifications written specifically for this program

3.2.2 Logic Flip-Flop

The logic flip-flop (see Figure 13) is required to alternately provide a trigger pulse to one of the two SCR's in the D.I. circuits. The flip-flop output pulse is amplified and buffered to provide the proper SCR gate drive signal.

3.2.2.1 Implementation of Principle

The control logic shown in Figure 13 consists of a time-constant limited trailing-edge flip-flop (Q_1, Q_2). This flip-flop requires that the Fire Command signal be present for at least 3 milliseconds before it can be triggered by the delay trigger generator. When the proper signal causes the flip-flop to change states, the flip-flop drives a pulse into either of two pulse amplifiers (Q_3, Q_5 or $Q_4 Q_6$). These pulse amplifiers supply high current fast rise time pulses to the D.I. circuit. The power requirements of the pulse amplifiers is minimal since all of the pulse output current is supplied by capacitors C_6 and C_7. A long recharging time constant (10 millisec.) is used to keep the peak power requirements at a minimum.

At the present time no report on unijunction transistor radiation resistance was obtainable, however, we have been advised that Motorola will have a report available shortly.

The flip-flop design also incorporates overdrive of the "ON" transistor so that β degradations due to aging and radiation effects will not cause circuit failure. This flip-flop circuit will operate even if the β of the transistor drops to unity.

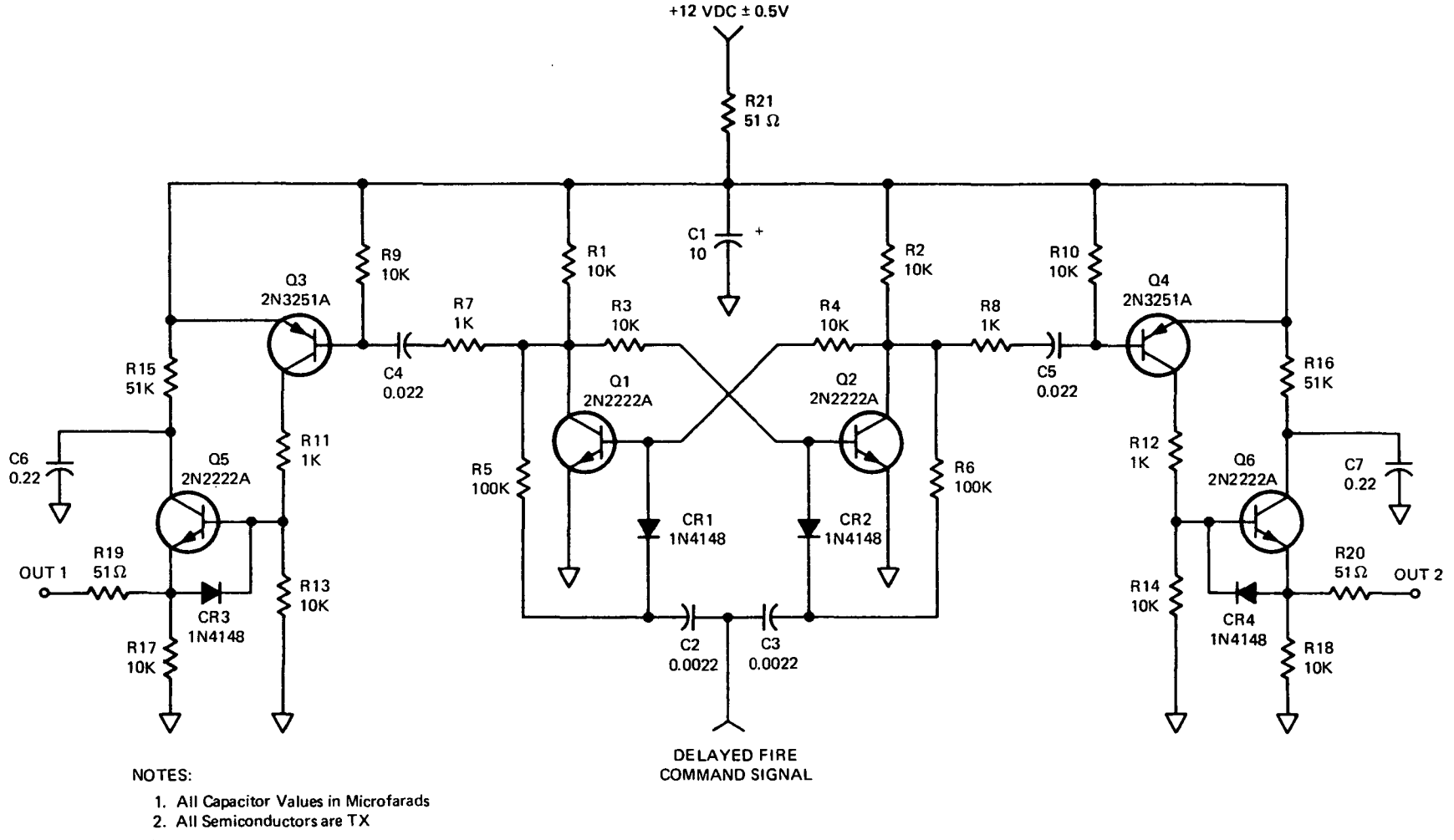

Figure 13. Control Logic Flip-Flop and SCR Pulse Driver Circuit

3.2.2.2 Final Design

Transistors Q_1 and Q_2 and resistors R_1, R_2, R_3, and R_4 form a cross coupled flip-flop. Resistors R_5 and R_6, diodes CR_1 and CR_2 and capacitors C_2 and C_3 form the steering network to allow changes of flip-flop state on each input trigger pulse. When the flip-flop change of state does occur, the negative going collector transition is coupled to Q_3 (Q_4) through R_7 (R_8) and C_4 (C_5). Resistor R_9 (R_{10}) is used for d.c. stability of Q_3 (Q_4). When Q_3 (Q_4) is turned on by this transition of the flip-flop, it causes Q_5(Q_6) to turn on and drive a pulse into the gate of the SCR in the D.I. circuit. This SCR drive current is stored in C_6 (C_7) until the Fire Command causes SCR triggering. Resistor R_{15} (R_{16}) allows the storage capacitors C_6 (C_7) to recharge slowly to keep the peak current requirements at a minimum. Diode CR_3 (CR_4) and R_{19} (R_{20}) are used to protect the base to emitter junction of Q_5 (Q_6) against reverse voltage transients from the D.I. circuit.

3.2.3 Delayed Pulse Generator

The delayed pulse generator shown in Figure 14 is used to provide a precise delay from the leading edge of the Fire Command pulse. This delay allows the circuit to accept the Fire Command pulse and reject shorter spurious noise pulses.

3.2.3.1 Implementation of Principle

Transistor Q_1 operates as an input buffer and level shifter for the Fire Command pulse. The Fire Command pulse turns on Q_1 which in turn switches Q_2 on starting the delay timing circuitry. Resistor R_5 and capacitor C_1 provide the precision RC time constant. When the voltage on C_1 reaches the trigger voltage of unijunction transistor Q_3, the latter conducts and pulses transistor Q_4 and SCR CR_2. SCR CR_2 clamps the capacitor voltage through CR_1 and prevents Q_3 from oscillating while Q_4 causes the logic flip-flop to change state since it discharges one of the input capacitors of the flip-flop through R_{12}. Additional noise immunity is provided by R_9 which slowly charges the flip-flop input capacitors so that premature spikes at the flip-flop input do not cause triggering.

3.2.3.2 Final Design

Resistor R_1 is required to meet the requirement for the minimum circuit input impedance while resistor R_2 is used for the d.c. stability of transistor Q_1.

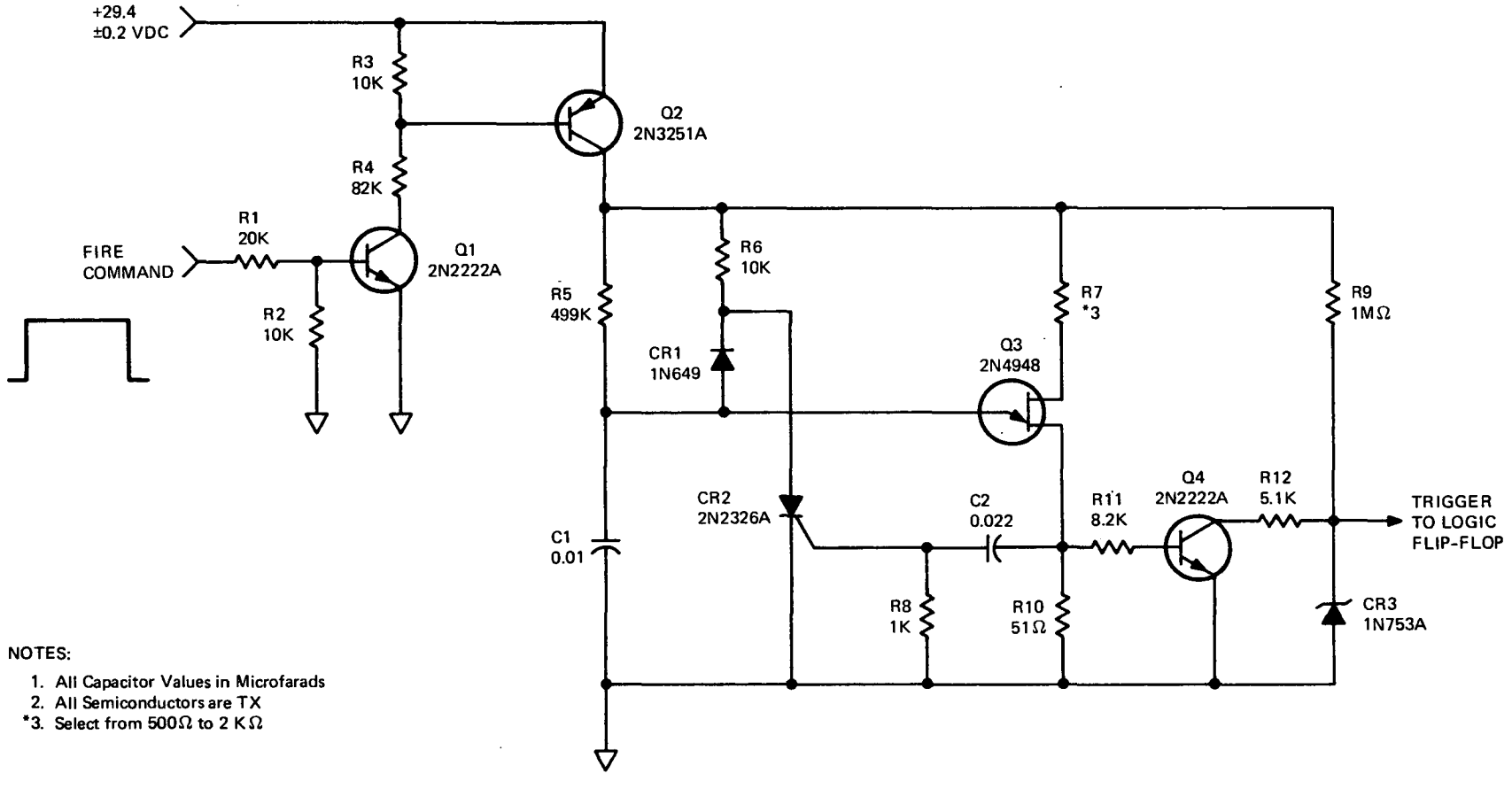

Figure 14. Delayed Pulse D.I. Trigger Circuit

Resistor R_4 limits the base current of Q_2, while R_3 provides d.c. stability. When the Fire Command pulse turns Q_1 and Q_2 on, capacitor C_1 charges through resistor R_5. When the voltage across C_1 reaches the firing voltage necessary to turn Q_3 on, Q_3 discharges C_1 through R_{10}. This voltage across R_{10} turns on Q_4 and triggers SCR CR_2 into conduction through capacitor C_2. While SCR CR_2 is on, C_1 cannot recharge since it is clamped to the SCR anode voltage through diode CR_1 while resistor R_6 supplies SCR CR_2 with its holding current. Resistor R_8 provides a low impedance gate to the cathode path to prevent CR_2 "turn-on" with increasing junctional temperatures. Resistor R_9 provides a high resistance charging path for the flip-flop input capacitors C_2 and C_3, while CR_3 limits the capacitor voltage at 6.2 volts. Resistor R_3 increases the noise threshold of the flip-flop, since the capacitor voltage must be 3 volts or greater before the triggering of Q_4 can cause the flip-flop to change states.

3.2.3.3 Noise Immunity Tests of the Breadboard Circuit

The upper trace of Figure 15 shows the normal 50 millisecond Fire Command pulse at a sweep speed of 200 milliseconds/cm, while the lower trace shows the collector of transistor Q_1 in the logic flip-flop. Each Fire Command pulse causes a flip-flop transition. Figure 16 shows the same waveforms at 10 milliseconds/cm so that the delay in the flip-flop transition can be seen. Figure 17 shows that a Fire Command pulse, 11 milliseconds long, will still cause the flip-flop to trigger, while Figure 18 shows that when the Fire Command pulse is shorter than the delay pulse time, no change of state occurs in the flip-flop. The upper trace of Figure 19 shows a noisy Fire Command line input at a sweep speed of 20 microsecond/cm, while the lower trace shows that no change of state occurs at the flip-flop.

3.3 THRUSTER CAPACITOR

3.3.1 Design Considerations

Some background information pertaining to thruster energy storage capacitors was presented in Section 2.2.3. One of the most important questions that arises in the selection of the energy storage capacitor is its life for the proposed mission. Since an energy storage capacitor is not used in the same manner as a d.c. capacitor, many criteria used to assess the life of a capacitor are not of primary importance when applied to an energy storage capacitor. To assess the life of an energy storage capacitor for the pulsed plasma thruster, the parameters noted in Table 11 become of primary importance.

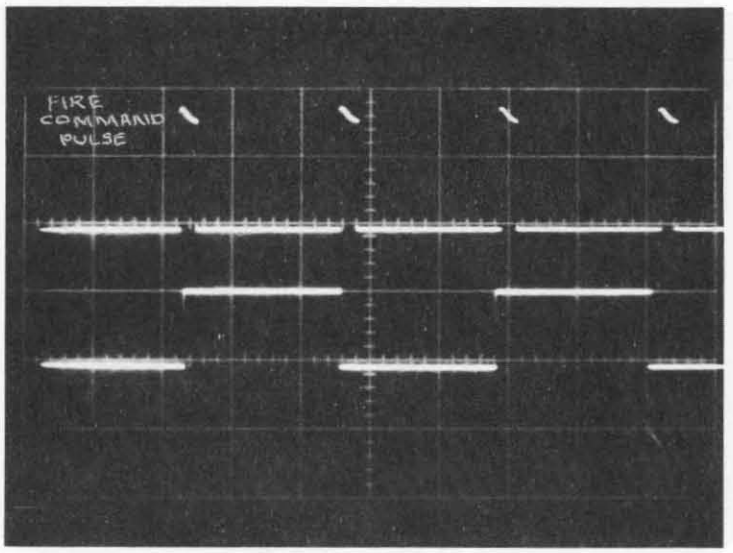

Figure 15. Normal 50μ sec Fire Command Pulse @ 200μ sec/cm Sweep Speed

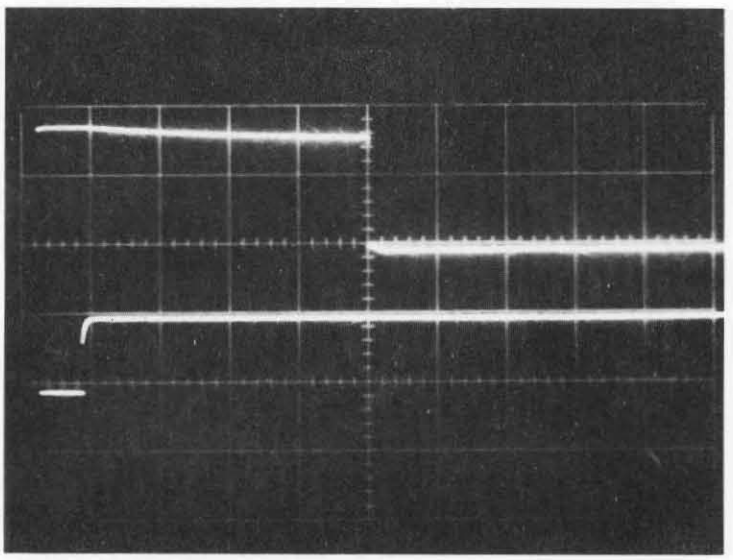

Figure 16. Normal 50 Millisecond Fire Command Pulse
@ 10 Millisecond/cm Sweep Speed

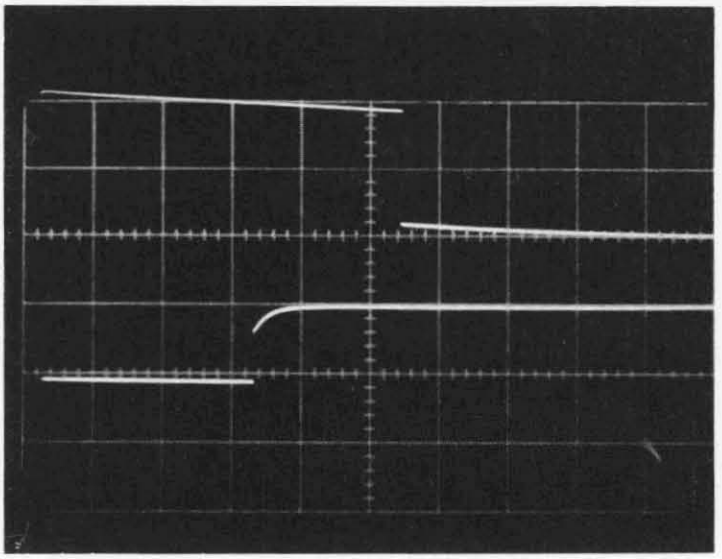

Figure 17. Abnormally Shortened Millisec Fire Command Pulse @ 2 Millisecond/cm Sweep Speed

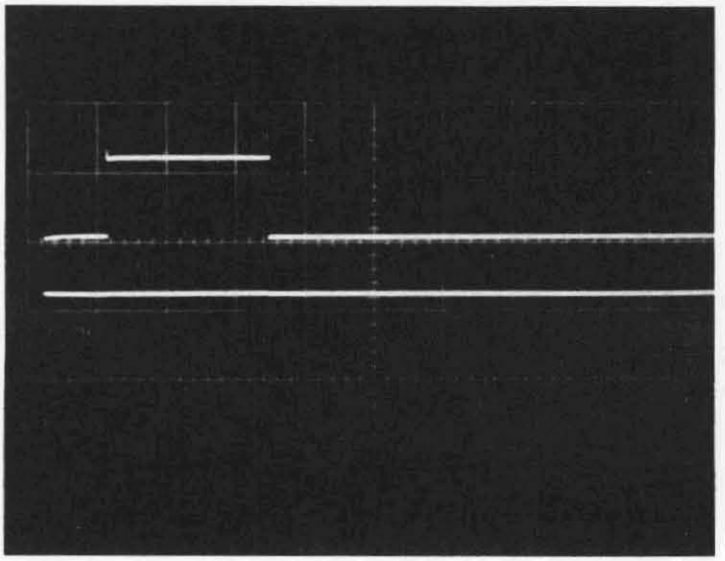

Figure 18. Longest Noise Pulse Duration which will not Cause Flip-Flop to Change State @ 0.5 Millisecond/cm Sweep Speed

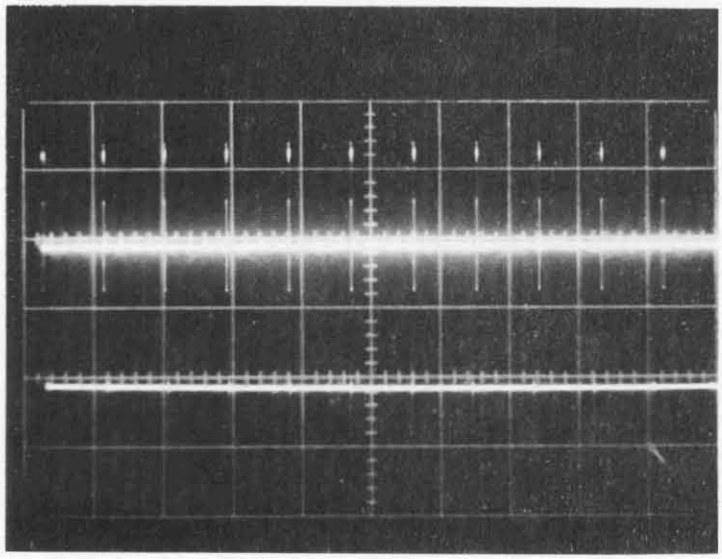

Figure 19. Random Noise Pulses on the Fire Command Line @ 20 μ sec Sweep Speed

TABLE 11. IMPORTANT ENERGY STORAGE CAPACITOR PARAMETERS

Total number of discharges desired with at least 99.5% survival probability
Charge Voltage
Capacitance
Percent Voltage Reversal
Pulse Rate
Operational temperature and the nature of cooling (radiation, conduction)
Ambient environmental pressure
D.C. hours accumulated at peak voltage during pulsed operation
Load Impedance
Peak Discharge Current
di/dt Under load Conditions

About ten years of experience at Republic Division has shown that capacitor manufacturers' data can generally be used only as a tentative guide in the selection of a capacitor. For example, manufacturers never obtain their data in a vacuum environment. Pressure differentials across the case and limiting effective cooling to that of radiation alone generally invalidate most of the data. Furthermore, the impedance of the load for which manufacturers' data is presented is typically of the order of 0.1 to 1 ohm. The actual impedance of the plasma thruster is roughly 10 milliohms. The significantly higher current densities existing in the capacitor in the latter case also generally invalidate most manufacturers' data. Generally, it has been found that one must work closely with a given manufacturer evaluating and upgrading his product to a level of performance compatible with the requirements of a pulsed plasma propulsion system. Such a level of confidence has been established with the Dearborn capacitor proposed for the SMS mission.

Suppose one now looks at some of the requirements of the SMS mission:

The number of discharges which the capacitor must produce during the five year mission is:

$$\text{number of required discharges} = \frac{\text{total impulse}}{\text{impulse bit amplitude}}$$

This expression can be evaluated for a 400 lb-sec total impulse requirement and an impulse bit amplitude of 25 ± 5μ lb-sec. Table 12 presents the results of such a calculation.

TABLE 12. PULSE LIFE REQUIREMENTS FOR A 25 ± 5μ lb-sec IMPULSE BIT LEVEL

Impulse Bit Amplitude μ lb-sec	Number of Discharges
20	20×10^6
25	16×10^6
27	14.8×10^6
30	13.3×10^6

The results show that small changes in the impulse bit level change required capacitor life significantly.

Besides the above calculation, it is important to perform another calculation before one can truly assess capacitor life requirements. The second calculation concerns itself with d.c. hours accumulated at peak voltage during pulsed operation. Typical manufacturers' data shows that besides discharge life, an energy storage capacitor also has a d.c. life. It is imperative that the d.c. hours at peak voltage imposed upon the capacitor during the life be kept at an absolute minimum. This requirement was presented by Fairchild Republic to MIT Lincoln Laboratory in the design of the highly successful LES-6 system and resulted in a minor redesign in the satellite firing command logic. In the LES-6 system, d.c. life was reduced to an absolute minimum by charging the capacitor firing voltage with a maximum hold time at peak voltage of no more than 300 millisec. Even then about 890 hours of d.c. life will be impressed upon the capacitor over and above the pulse life during the LES-6 mission.

Suppose one now examines the SMS requirement in more detail. Since the satellite spin rate can vary from 50 to 110 rpm it will be necessary to charge the capacitor in a time compatible with the higher spin rate. At 110 rpm the period between thruster firings is 0.5454 seconds while at 50 rpm it increases to 1.2 second. If the capacitor is charged to the operating voltage of 1450 volts in 0.50 second* the capacitor will accumulate 45×10^{-3} seconds and 700×10^{-3} second per discharge at the 110 rpm and 50 rpm spin rate, respectively. From the data in

---

* Note, the leading edge of the 50 millisecond long firing command signal will have already been applied 5 milliseconds before peak voltage is reached.

Table 11 one can see that the capacitor will accumulate for a 25μ lb-sec impulse bit, a life degrading 200 d.c. hours and 3120 d.c. hours, respectively. By referencing a typical manufacturers' life test data, one can see that a 3120 hour d.c. life generally requires additional derating of a given capacitor. Such a derating would be required to provide the requirements of an unnecessarily long "hold-time". Physically, the capacitor becomes bigger and heavier than necessary. Figure 20 shows typical d.c. hours accumulated as a function of satellite spin rate for several values of impulse bit and "hold-time" for a maximum fixed charge time of 0.500 second

TABLE 13. DEFINITIONS

Charge time = 0.500 second (fixed)
Hold-time = spin period - charge time
Impressed d.c. life = (number of pulses) (hold-time).

Also shown in Figure 20 are the d.c. hours accumulated for a charging scheme which impresses a fixed hold time of 50 millisec** independent of satellite spin rate (in this latter case the d.c. hours are found from the pulse number presented in Table 12 and the 50 millisec hold-time). A comparison of the results for the case of rpm dependent versus rpm independent hold-time clearly shows the superiority of the rpm independent hold-time capacitor charging technique for minimizing life-degrading d.c. hours accumulated on the capacitor.

An alternate technique to reduce d.c. hours impressed upon the capacitor is to use an rpm dependent charging time. In this latter case the charging time of the converter-charger will match the varying spin period of the satellite. This latter case draws the least average current from the power bus line. A schematic comparison of these three charging techniques is presented in Figure 21. Implementation of the latter two techniques is carried out by constantly monitoring the period of the 50 millisecond long Fire Command which is continuously impressed upon the CLPC.

** Corresponding to the case when the capacitor is fully charged as the leading edge of the 50 millisec long satellite firing command signal is impressed upon the propulsion system.

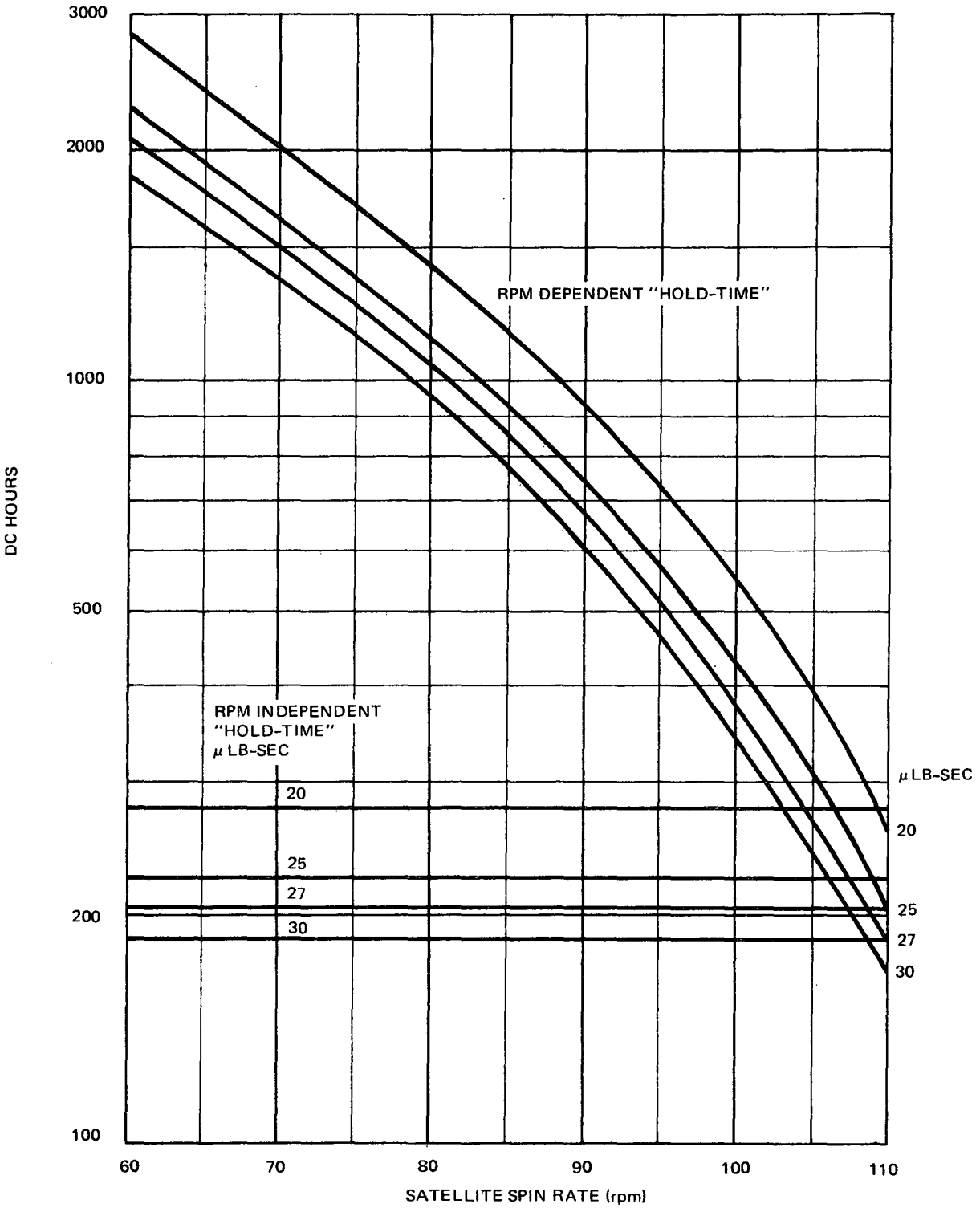

Figure 20. Approximate D.C. Hours Impressed Upon Capacitor

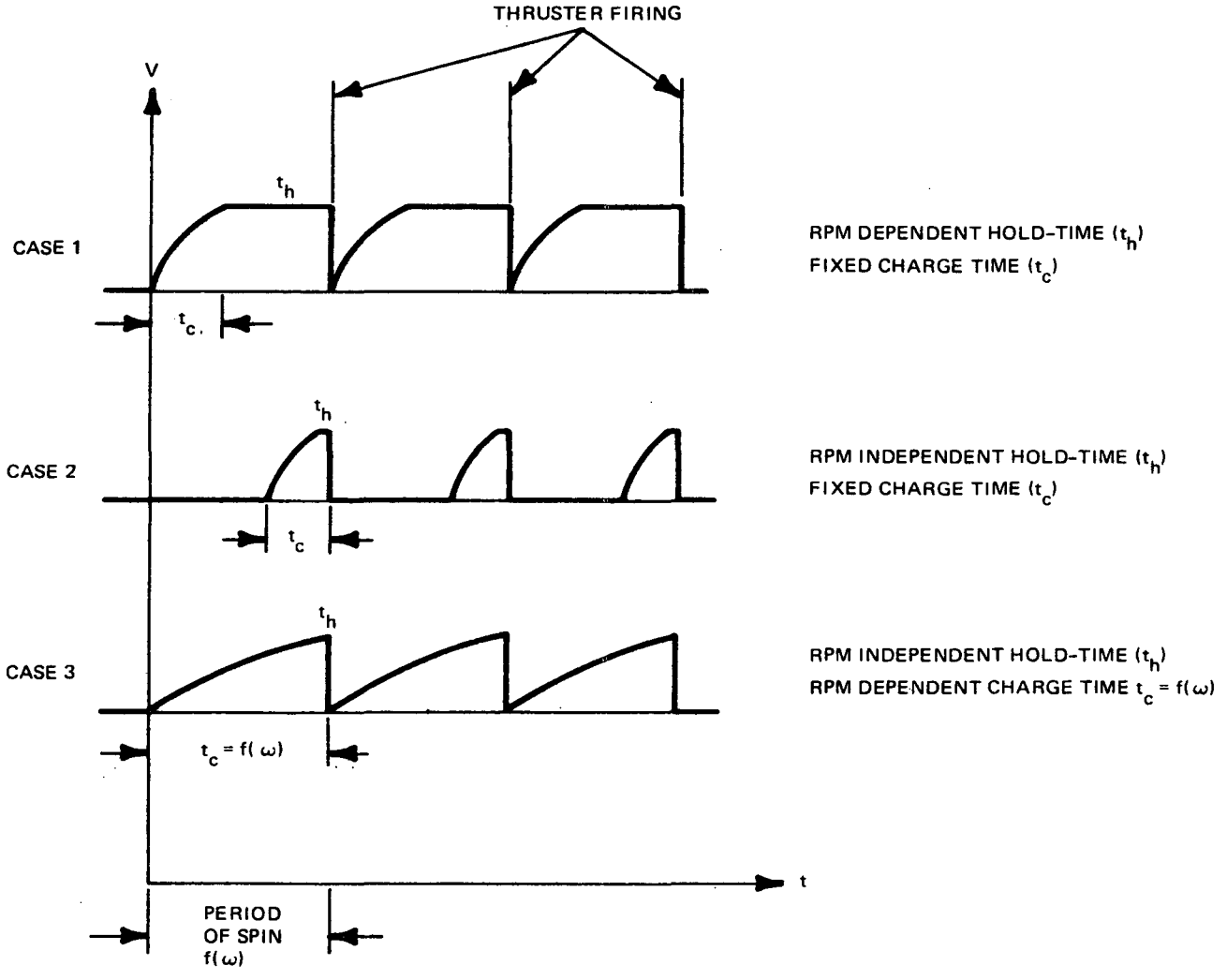

Figure 21. Comparison of Charging Techniques

Case 2, in Figure 21, represents the best of the two choices to reduce d.c. hours impressed upon the capacitor and it is being incorporated in the final design of the converter-charger (see Section 3.8).

A practical example of Case 1 above can be presented during RC charging of an available off-the-shelf capacitor that was tested* prior to the present program. The capacitor was a 4μfd capacitor and charged to 1450 volts. The RC charge time was about 0.234 second with a hold time of about 0.311 second. Of two capacitors tested (Dearborne ESXPJ20002) one operated continuously for 15,041,800 discharges whereas the second survived 14,703,251 discharges. Over and above the pulse life, each capacitor accumulated about 1300 hours of unnecessary d.c. life.

It is important for the proposed effort to note that even though the capacitor was not designed for the SMS application the demonstrated pulse life at the 27.7μ lb-sec impulse bit level would have met the requirements of the five year SMS mission with the satellite spinning at a rate of 73 rpm throughout the five year mission and if charging were performed even in the manner of Case 1.

In order to provide an additional margin of life for the SMS application, the ESXP 405J20002 discussed above will be derated from a working stress of 1115 volts/mil. (1450 volts) (3 layers 0.35 mil + 1 layer 0.25 mil) to 1035 volts/mil (1450 volts/(4 layers 0.35 mil). With capacitor pulse life inversely proportional to the 5th power of stress, this reduction in voltage stress will significantly extend the ESXP 405J20003 capacitor life beyond SMS requirements. Furthermore, with the SMS thruster power conditioner design minimizing impressed d.c. hours on charge, an additional life factor is assured. Besides the latter electrical improvements, the ESXP 405J20003 will be provided with an integral shoulder bushing assembly to assist the rate of heat transfer from the capacitor to the capacitor case.

---

* The capacitor design was for laboratory performance studies of early LES-7 type thruster. The design and construction follow that of the capacitor flying in the LES-6.

3.3.2 Alternate Capacitor Designs

While the existing capacitor designs are highly reliable for meeting the mission life, they are one of the heaviest components in the propulsion system. For example, the comparative weight of the 4 μfd energy storage capacitors developed for the ESXP 405J20001 are presented in Table 14.

TABLE 14. CAPACITOR WEIGHT OF THE ESXP 405J SERIES

Model	Weight (grams)	Life (pulses)
ESXP405J20001	458	Not Evaluated
ESXP405J20002	522	15×10^6
ESXP405J20003	598 (estimated)	To be Evaluated

An alternate capacitor using polypropylene instead of Mylar was obtained from Component Research Company, Inc. This capacitor (20PP405K403) weighs 355 gr. The basic pulse life must be evaluated and two units have been placed under test using the engineering thermal model described in Section 3.5. To date each of the two capacitors has undergone 897,619 discharges without failure. Testing on these capacitors will be carried out for as long as possible within program constraints.

Besides the polypropylene dielectric system two other potential dielectric systems that could possibly provide a lighter weight high reliability capacitor are Kapton and Kureha polyvinylidene fluoride.[9] An experimental evaluation of the reliability of these latter two dielectric systems is beyond the scope of the present effort. It is essential, however, to be aware of the fact that alternate capacitors, for a significant reduction in system weight, could be obtained and that at least two capacitor manufacturers have expressed an interest in building such units.

3.4 SYSTEM INTEGRATION

This section describes the mechanical approach of the Solid Propellant Pulsed Plasma Microthruster used in the Synchronous Meteorological Satellite.

3.4.1 General Requirement

The mechanical assembly, which finalizes the overall shape of the microthruster, provides the structural integrity to transmit thrust forces into the

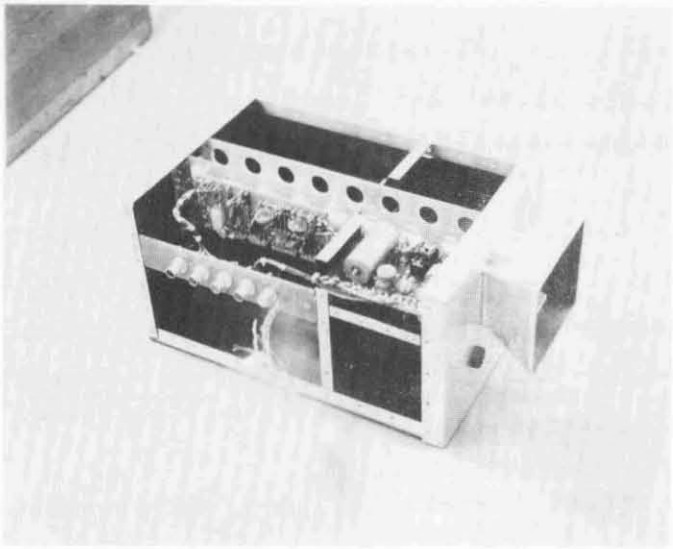

Figure 22. Center-Beam Approach

SMS and support all the essential components required to permit the unit to function and also to provide the required electrical isolation.

3.4.2 Center-Beam Approach

The first structural design approach examined was a unified assembly whose main structural support is dependent upon a center-beam or box-like spar configuration. (See Figure 22).

The center-beam is a structural member and propellant guide. This beam, although electrically isolated from the positive and negative strip line collector plates, at the thruster end, accurately positions the fuel propellant bar with respect to the anode and cathode accelerator electrodes.

A bulkhead is secured to the beam approximately at mid-length. The lower face of the bulkhead secures the cathode end of the cases that contain the thruster energy storage capacitors. These cases are electrically isolated from the bulkhead and thermally connected to the bulkhead by the use of eight beryllium oxide disk shaped shoulder washers.

The remainder of the beam, that which extends beyond the bulkhead at its lower surface, positions and secures the power conditioning package developed by Wilmore Electronics, Inc. as an integral part of the propulsion package.

The final intent of the beam is to accurately guide the fuel propellant bar by means of an inner track provision.

3.4.3 Monocoque Housing

A complete peripheral thruster enclosure with R.F. integrity is now being considered for the final design. (This is shown isometrically in Figure 23). This enclosure extends from the positive and negative strip line collector plate support structure to the mid-point bulkhead.

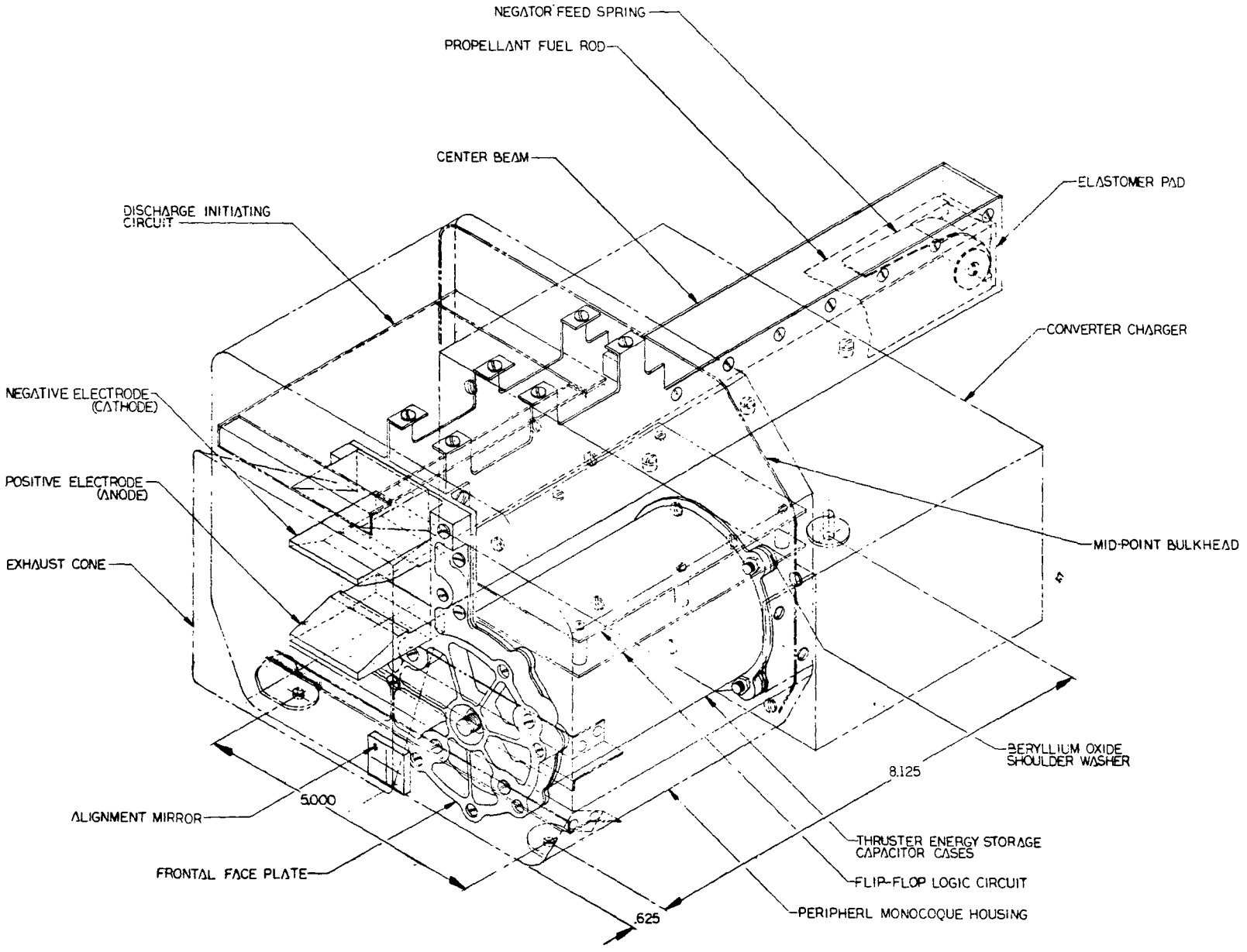

Figure 23. S.M.S. ARRANGEMENT

3.4.3.1 Housing Description

The RFI monocoque housing is a thin wall peripheral enclosure stiffened by the use of beads depressed into its surface. These beads act as fore and aft compression members and provide rigidity of their individual surfaces. Twisting or a parallelogram effect is restricted by a reinforced cover plate at the thruster end and the aforementioned mid-point bulkhead at the opposite end. The usefulness of the mid-point bulkhead to prevent twisting becomes effective only when the assembled components are entered into the housing and the already attached bulkhead is received by the housing and subassembly - secured in place by threaded fasteners.

3.4.3.2 Thruster Electrical Isolation

The mechanical structure responsible for the support and electrical isolation of the positive and negative electrodes, i.e., discharge circuit, is comprised of a ribbed and flanged frontal face plate fabricated from NEMA G-10 fiberglass sheets (see Figure 23). This faceplate is recessed on the aft surface. Its purpose is to cradle the entire positive strip line collector plate. Insulating material (two thicknesses of Teflon sheet) is added to the exposed surface of the positive plate and this subassembly is then fastened to the holes provided in the flanges around the periphery of the thruster energy storage capacitor cases. The mounting is also strengthened by the upper frame of the negative strip line collector plate which is backed up by an additional support, fabricated from NEMA G-10 fiberglass. This additional support, while providing rigidity to the upper frame of the negative strip line collector plate, also electrically isolates and supports the forward end of the aforementioned centerbeam.

3.4.3.3 Thruster Electronics Package

Two printed circuit boards will contain the initial logic flip-flop (Figure 13) and the delayed pulse discharge initiation logic circuit (Figure 14). Another board will contain the components for the discharge initiating subassembly (see Figure 12). This board is located above the thruster energy storage capacitor cases and to the left of the center-beam (see Figure 23).

Structural support will be obtained by a flange fabricated onto the side of the center-beam, a flange fabricated onto the forward face of the mid-point bulkhead and angular clips mounted on the outer and forward edges of the

printed circuit board which in turn, will be fastened to the side and forward plate of the R.F. housing.

The second printed circuit board, as mentioned above, will contain the components for the flip-flop logic circuit. This second board is located above the thruster energy storage capacitor cases and to the right of the center-beam. Supports for this second board will be fabricated in the same manner as that previously described for the discharge initiating subassembly.

A bridge will support all cross wiring between the two boards. This bridge will occupy one of the upper interruptions of the center-beam propellant tank.

3.4.4 Electrical Interfacing

Electrically isolated, feed-through, solder pin type connectors will be installed in the left hand web of the mid-point bulkhead at a location directly above the D.I. printed circuit board. These connections, at the aft side of the mid-point bulkhead, will be positioned directly above the mating connections located on the upper surface of the Wilmore power conditioning package. Hard wiring and conformal coating will complete the electrical interfacing between the two units, thereby eliminating electrical connectors between the thruster and power conditioner (see Figure 24).

R.F. shielding will be accomplished by the addition of a tunnel closure, secured to the upper face of the power conditioner and the upper aft face of the mid-point bulkhead web.

3.4.5 Propellant Subsystem

A step, total depth of .050-inch, is fabricated into the positive electrode. This step restrains the propellant fuel rod and ensures its outward positioning with respect to the igniter plugs mounted in the upper negative electrode. The propellant rod is held firmly against this step by two means: (1) centrifugal force due to the spinning of the spacecraft, and (2) a constant force low tension Negator spring (captured by a bushing assembly) to the opposite end of the propellant rod. This feed spring ensures positive contact of the propellant rod with the step

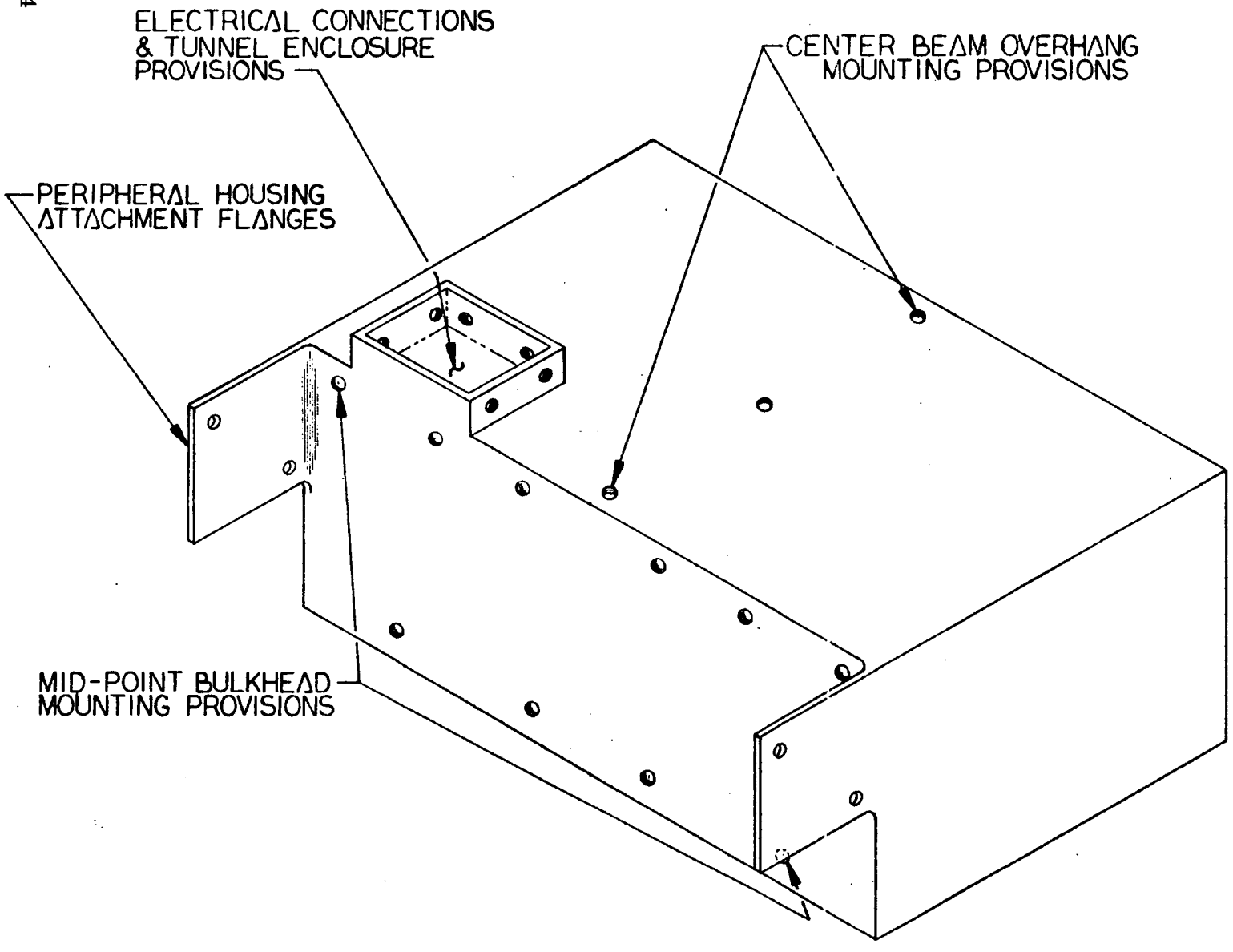

Figure 24. Converter-Charger Envelope

in the positive electrode during launch of the space vehicle. The force of the spring is negligible when the vehicle is subjected to high spin rotation in the beginning of the life of the vehicle and because of its constant force, positive feed of the propellant rod is assured when its weight has been depleted through usage.

The length of the propellant rod will occupy all but a fraction of the total length of the center-beam propellant track. At the closure end of the center-beam, an elastomer pad is permanently attached to the inside of the end cover. The thickness of this pad will be controlled so that a depression caused by the aft end of the propellant rod will prevent any form of oscillation or erratic movement of the propellant rod due to the vibration of the space vehicle during launch.

3.4.6 Converter-Charger Integration

Interfacing of the converter-charger (see Figure 24) with the microthruster unit is obtained at two places. One place was mentioned previously and that was the underside of the center-beam propellant track. The second place is the lower web area of the mid-point bulkhead. These two surfaces are at right angles to each other, therefore eliminating the possibility of a cantilever mounting of the converter-charger.

3.4.7 Spacecraft Mechanical Interface

Extensive consideration has been given towards the interfacing of the microthruster unit to the spacecraft platform. Alignment of the bottom surfaces of the monocoque housing and the converter-charger will be held to close tolerance. These two surfaces must act as one continuous flat plane to enhance the mounting and alignment and avoid excessive stresses, shock and vibration of the complete microthruster package.

Attachment points are located within the limits depicted on the NASA, Goddard Space Flight Center Drawing GC1171302. They are located at a distance by design which will reduce the probability of excessive bending moments that can be induced into the length of the microthruster package during launch of the space vehicle, (See Figure 23).

3.4.8 Alignment Mirror

A surface coated, square shaped alignment mirror will be mounted onto the forward face of the microthruster housing for the purpose of aligning the thruster with respect to the spacecraft. The mirror's vertical crosshair will be centrally located about the vertical centerline of the positive and negative electrodes and its upper edge placed at a distance adequately below the extremeties of the thruster cone. Mounting will be accomplished by using epoxy EPON #828 with an EPON V-40 curing agent. (see Figure 23).

3.4.9 Material Consideration

Aluminum alloy 6061, temper designation T6, which is a solution heat treated and then artificially aged material, is considered to be the most acceptable material for the fabrication of the main support members of the microthruster package - with the following two exceptions: where electrical isolation is required, a structural forward face plate will be fabricated from fiberglass sheet NEMA G-10. This laminated material combines important properties such as high physical strength, high impact resistance, excellent dielectric strength and moisture resistance. This material too, will be utilized with a copper-clad surface for the discharge initiating circuit and flip-flop logic printed circuit boards

The second exception is the necessity of thermal conduction with electrical isolation. Here again in the structural sense Beryllium oxide washers are used to provide a heat path from the thruster energy storage capacitor cases to the web of the mid-point bulkhead (see Figure 23). Beryllium oxide is a technical ceramic with an unequaled combination of high thermal conductivity, high electrical resistivity and excellent dielectric properties (see Table 16).

While the aforementioned materials are beneficial to the structural integrity, there are additional materials used in the microthruster package and their identification and usage will be described hereon.

Stainless steel, designation 17-7Ph is a special ultra high strength type material that has good formability and excellent fabricating characteristics. This stainless steel is used for the positive and negative accelerator electrodes. These electrodes must withstand the heat generated due to thruster firing.

Several years of testing have shown this material to exhibit relatively low electrode errosion.

An additional stainless steel, designation 301, 302, is used in the manufacture of pressed in type fasteners. This stainless steel has high corrosion resistance qualities and high strength.

3.4.10 Tentative Weight Considerations

Every effort is being made to keep the final weight of the micro-thruster unit to the absolute minimum and still maintain a structure that will meet all design constraints with sufficient margin. The tentative estimated weight of 7.3 pounds expressed in the Technical Proposal, Volume I, dated 19 March 1971, is more realistic than the 6 pound weight sought in RFP42070/144.

Only by using Beryllium (instead of 6061 Aluminum) extensively as a structural material, and a lighter thruster energy storage capacitor, will it be possible to approach the 6 pound overall weight figure. Since no experience exists with either of these approaches, they are tentatively considered as high risk alternatives. A separate effort beyond the scope of the present effort is required to assess their feasibility for the SMS application.

3.5 DESIGN SUPPORTING THERMAL MODEL ANALYSIS AND TEST

3.5.1 General Consideration

Estimates can be made on the quantity of heat rejected by the propulsion system to the SMS spacecraft when the system is enclosed as per NASA, Goddard Space Flight Center Drawing GC1171303. Even though the thrust efficiency will be only about 5%, this does not mean that 95% of the input electrical energy is dissipated as thermal energy in the thruster! Previous measurements performed with thrusters similar to the one of this program shows that roughly 25% of the energy stored in the thruster capacitor is lost thermally. Essentially, all of the 75% of the electric energy entering the thruster nozzle is ejected from the nozzle as thermal

energy and kinetic energy (some energy is absorbed by the electrode). The efficiency of the converter-charger will be roughly 80%. Since the design discharge energy is about 8.4 joules/discharge, at a maximum pulse rate of 1.83 Hz (i.e., 110 rpm), one has 15.35 watts entering the capacitor and thus about 19.2 watts (max) entering the converter-charger. Thus the maximum heat rejected will be about 3.84 watts by the thruster capacitor and 3.84 watts by the converter-charger. Tentatively, a maximum of about 7.68 watts of thermal energy will be rejected to the satellite by conduction and radiation at the 110 rpm spin rate (at 50 rpm the value reduces to 3.49 watts).

The maximum equilibrium temperature of the thruster system will depend upon the sink temperature surrounding the thruster. This sink temperature has a maximum value of 120°F (paragraph 2.8.2 of the work statement). The only two methods of cooling the thruster capacitor and other components of the propulsion system are by radiation and conduction. Since the thruster capacitor is the most critical item with regard to environmental temperature, some idealized calculations can be carried out for the purpose of assessing the equilibrium temperature attained at the worst case condition of 120°F sink temperature and 110 rpm. This simplified analysis is presented below.

3.5.2 Idealized Thermal Analysis

The only critical thermal component is the thruster energy storage capacitor. To meet the mission design life it should not operate above 150°F under worst conditions. Consider the idealized case of the two thruster capacitors losing heat by radiation only - in reality we are also going to conduct some heat out of the capacitor through the 0.75-inch diameter disk at either end of the capacitor. The worst condition is at 110 rpm with a sink temperature of 120°F.

Figure 25 schematically depicts the geometry examined in the idealized analysis. Typically, about 25% of the input power to the capacitor is lost thermally (no data exists on the ESXPJ20003 since it has not yet been built). Thus at 110 rpm,

$$P_t = (0.25)\, f\, 1/2\, cv^2 = (0.25)\,(1.83)\,(\tfrac{2}{2})\,4\,(1.45)^2 = 3.84 \text{ watt}$$

$$= 13.1 \text{ BTU/Hr.}$$

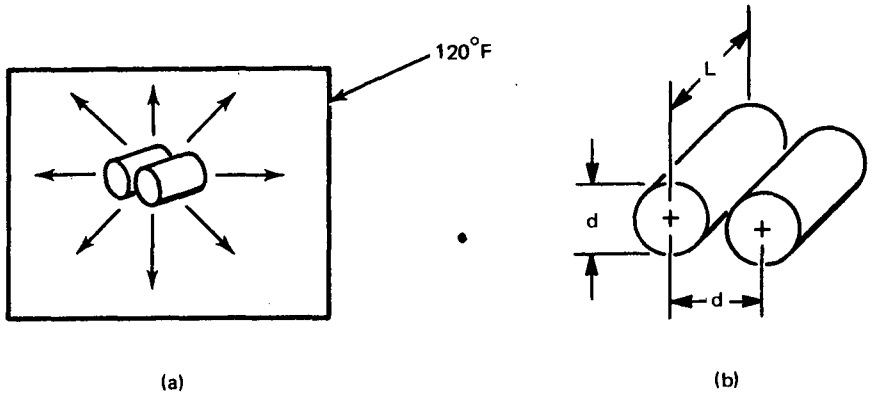

Figure 25. Idealized Thermal Analysis (Capacitor)

It will be assumed that the effective area for radiation is given by the geometry shown in Figure 26.

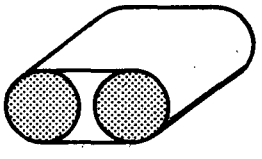

Figure 26. Idealized Capacitor Geometry

or, Aeff = (4) $\frac{d^2\pi}{4}$ + 2dL + d π L.

The heat transfer equation $Q = A\sigma\epsilon (T^4_{cap} - T^4_{sink})$ can then be solved for the equilibrium capacitor tempterature (T_{cap}) if one knows the capacitor emissivity ϵ. Since no thermal test data exists on the emissivity of the Mylar-epoxy construction of the ESXP405J20003, simple calculations of the capacitor temperature can be made for various values of ϵ varying from 0.06 for polished aluminum to 0.9 for paper

for the idealized geometry of Figure 26. Table 15 presents the result of this calculation.

TABLE 15. 120° F SINK TEMPERATURE, 110 RPM

ε	T(°F)
0.06	294.9
0.2	188.2
0.5	150.
0.7	141.9
0.9	137.

The results presented in Table 15 show that the emissivity of the capacitor must be greater than 0.5 if cooling is to be by radiation alone.

The above idealized analysis assumed no intervening surface between the capacitor and heat sink (spacecraft). In reality the capacitor is surrounded by the capacitor can structure, which in turn is surrounded by the general thruster structural housing. To reduce the temperature gradient across these latter two surfaces to the smallest possible value,the ratio of absorptivity to emissivity for each surface must be as close to unity as possible.

The effect of these intervening surfaces can also be considered analytically. However, even then the number of uncertainties in the analysis requires that design supporting vacuum thermal tests be carried out to provide accurate input design data for the mechanical design. Figure 27 shows the laboratory thruster located in an isolated heated enclosure simulating as reasonably as can be determined at this time,the ther mal environment to be encountered in the satellite. By maintaining a constant sink temperature of 120°F surrounding the thruster and operating the laboratory thruster at a pulse rate of 110 rpm in a vacuum it was possible to establish the capacitor equilibrium temperature under conditions more reasonably approximating the final design.

In addition to the radiation cooled thruster configuration, it is further possible to reduce capaci' or temperature by providing electrically insulating but thermally conducting disks between the thruster and its surrounding structural housing (i.e., RFI-EMI suppressing housing). Some idealized calculation of the

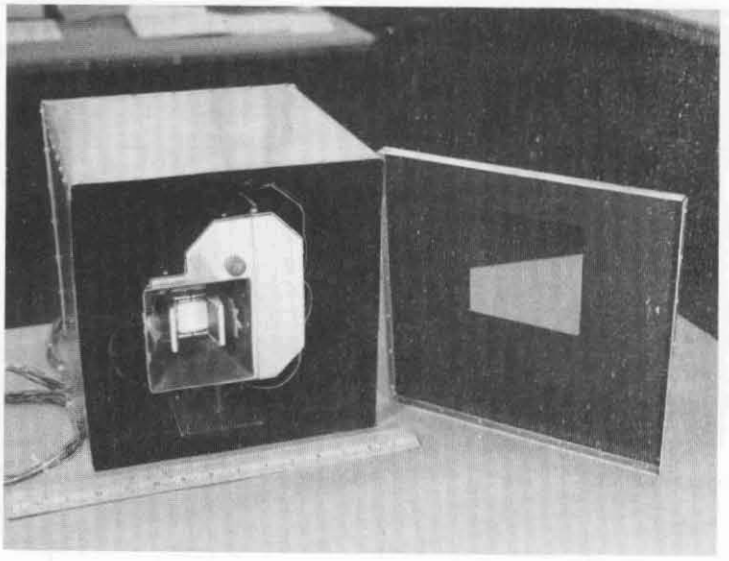

Figure 27. Isolated Laboratory Thruster in Isolated Heated Enclosure

temperature differential between capacitor case and thruster housing can be made by using the conduction equation $Q = KA\ \Delta T/\Delta X$, valid for a single wall and neglecting thermal contact resistance. Suitable material for the disks are Beryllium oxide and Boron Nitride. Their physical properties are presented in Table 16. The thermal conductivity of Boron Nitride is comparable to stainless steel whereas Beryllium oxide is comparable to aluminum. Though the final design will use Beryllium oxide, Boron Nitride was used since a simple calculation indicated that the gradient in temperature between capacitor case and structural housing can be measurably reduced by the use of eight one-half inch diameter disks of Boron Nitride. The laboratory thruster with the eight Boron Nitride disks at the rear face of the capacitor housing, connecting the capacitor housing to the thruster housing, is shown in Figure 28.

TABLE 16. PHYSICAL PROPERTIES OF MATERIAL FOR HEAT TRANSFER DISKS

	Beryllium Oxide	Boron Nitride
Density	2.52 - 2.96	2.0
Thermal Conduct. BTU/hr ft°F	135 - 145	~ 20
Specific Heat BTU/lb	0.30	----
Dielectric Constant 1 KMC	6.1	----
Dielectric Constant 1 MHz	6.4	~4.4 - 4.5
Dielectric Constant 10 GHz	6.1	----
Dielectric strength volts/mil	~700	500
Dissipation Factor 25°C	0.0001	0.00055
Modulus of Rupture (flex strength) psi	34,000 typ	14,000 - 16,000
Youngs Mod. of Elasticity 10^6 psi	50	9 to 11
Shear Modulus 10^6	20	----
Poisson Ratio	0.26	----
Tensile Strength	20,700	6,500- 8,000
Compressive Strength	225,000	26,800 - 27,500
Thermal Expansion in/in/°F	4.1×10^{-6} °F	1×10^{-6}/°C
Thermal shock Resistance	Excellent	Excellent
Electrical Resistance ohm-cm	$\sim 10^{15}$	10^{13}
Other	(toxic dust)	(non-toxic)
Vendor	Brush Beryllium Company	Union Carbide

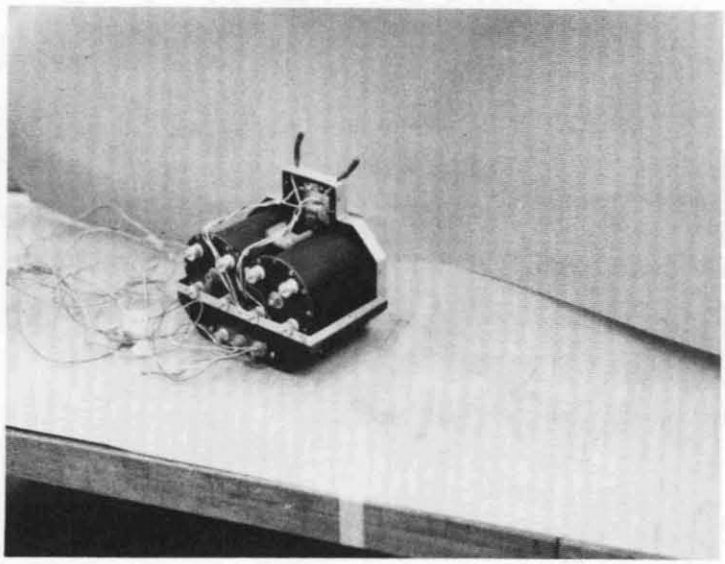

Figure 28. Laboratory Thruster with Electrically Insulating Thermally Conducting Disks

3.5.3 Design Supporting Thermal Tests

The thermal model test assembly shown in Figure 27 was suspended in a vacuum chamber providing essentially no heat conduction to the chamber except by radiation. Figure 29 shows the model assembly in the vacuum chamber with power leads and thermocouple wires from the sink and laboratory thruster emerging from the rear of the enclosure simulating the spacecraft as a heat sink. Figure 30 shows the assembly rotated to show the thruster protruding the opening in the enclosure.

Three tests were performed with the laboratory thruster and Dearborne ESXP405J20002 capacitors:

Test 1: "Radiation Cooled" thruster at 120°F sink temperature and 110 ppm

Test 2: "Supplementary Conduction Cooled" thruster at 120°F sink temperature and 110 ppm

Test 3: "Supplementary Conduction Cooled" thruster at 76°F and 110 ppm.

Test 1 represents the case of either a LES-6 or LES-7 design but operated at worst case SMS environmental conditions. Tests 2 and 3, respectively utilize electrically insulating but thermally conducting disks to transfer heat from the thruster to the thruster structural housing as discussed in Section 3.5.2.

In performing thermal vacuum Tests 1 and 2, the heat sink was brought to "120°F" equilibrium temperature with the thruster inactive. The thrusters were operated from the moment the 120°F sink temperature was reached until equilibrium temperature was reached on the thruster capacitors. For test 3, the thrusters were started immediately. Figures 31, 32, and 33 present the data of tests 1, 2, and 3, respectively. Thermocouples were attached to the heat sink, RFI housing (thruster housing) capacitor case and the two thruster-capacitors. About two hours of heating were required to bring the sink temperature to 120°F before the thruster was operated. Thermal equilibrium was reached after about five hours. For test 1 (Figure 31), the capacitor equilibrium temperature was 151°F. Since the idealized thermal analysis presented above neglected intervening surfaces between the capacitor and heat sink, it is seen that for the 151°F capacitor equilibrium temperature the effective emissivity with the intervening surfaces is about 0.5. While the 151°F temperature is considered just acceptable for maximum

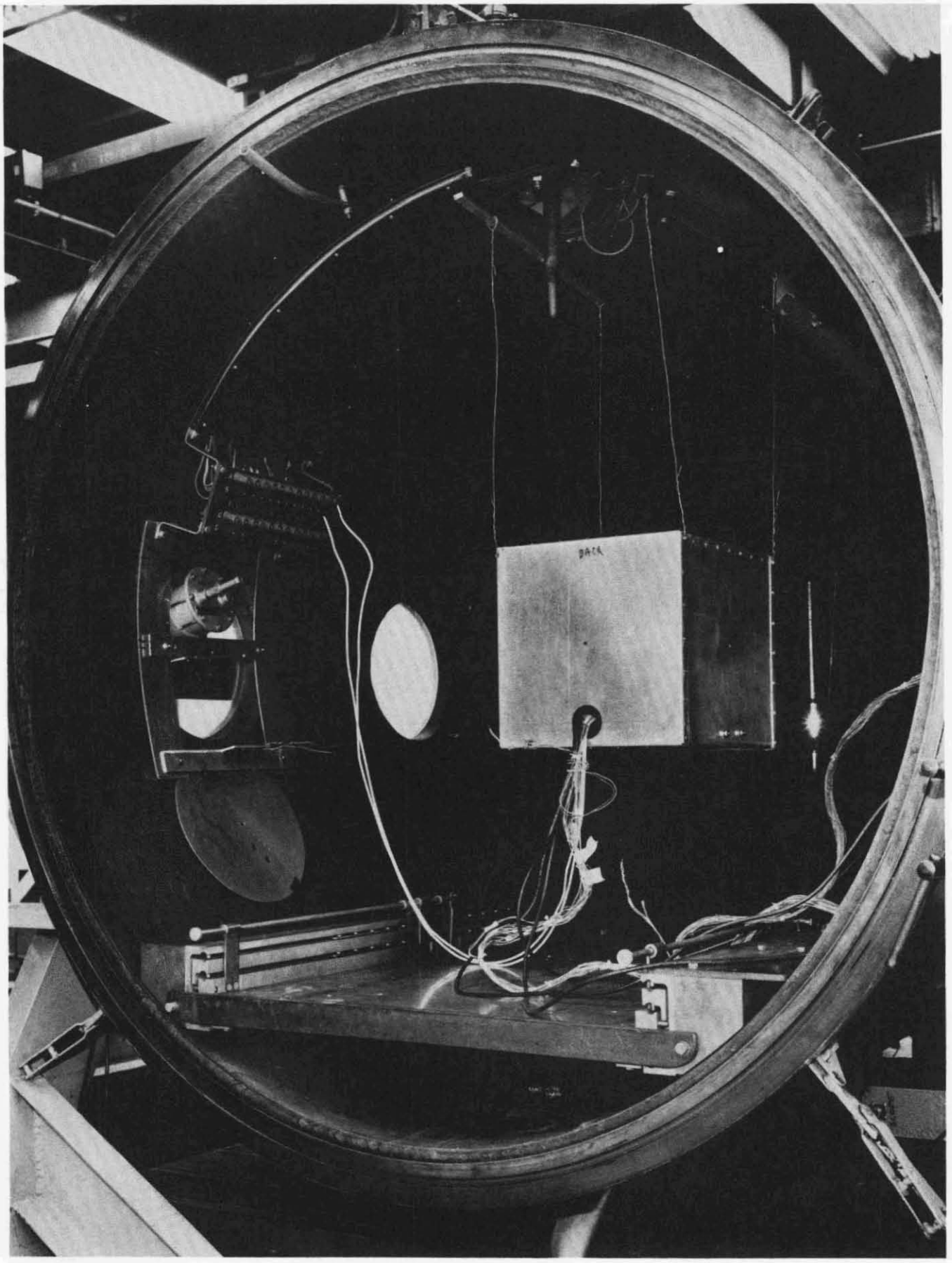

Figure 29. Thermal Model in Vacuum Chamber

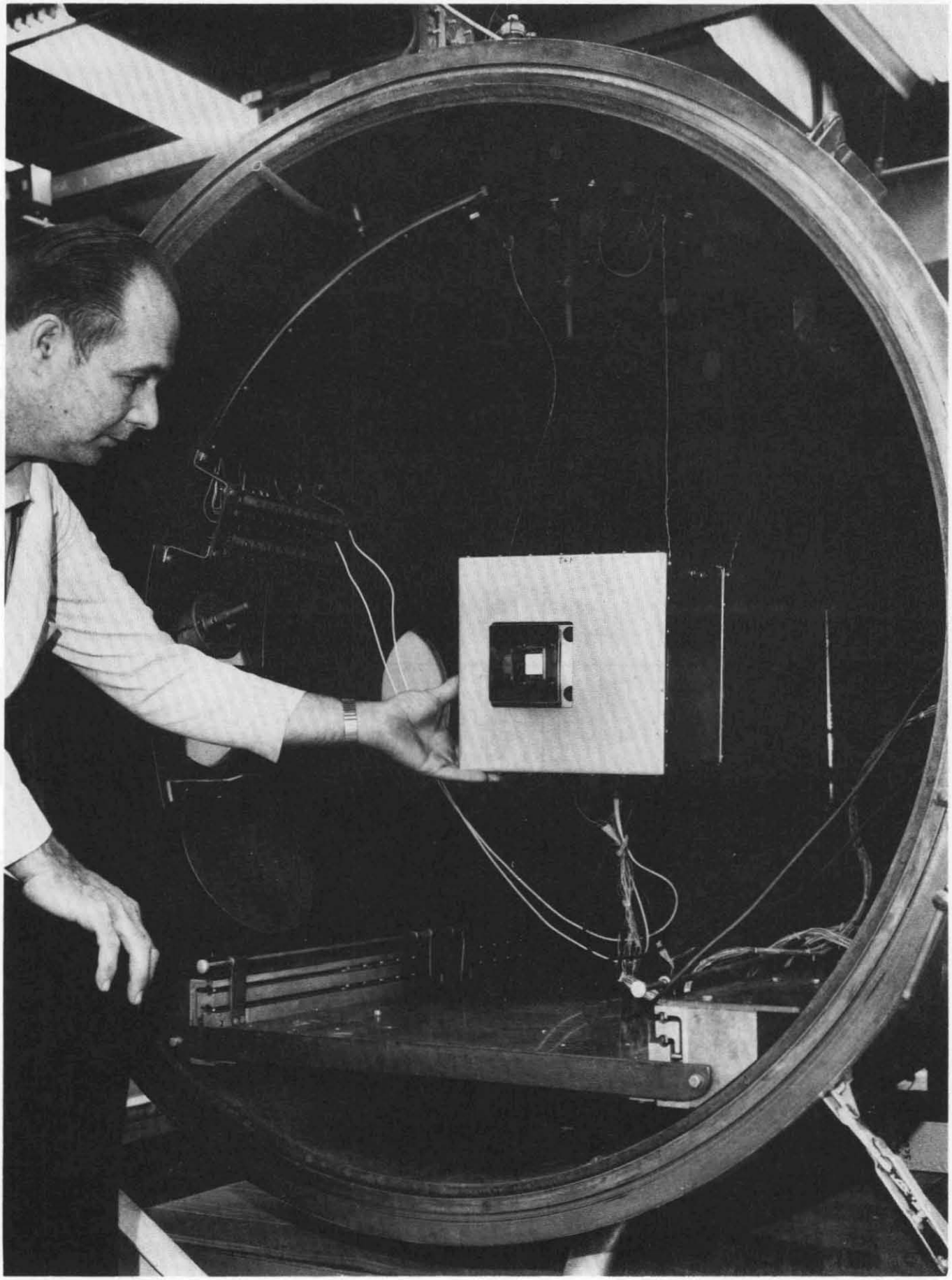

Figure 30. Thermal Model in Vacuum Chamber-Rotated

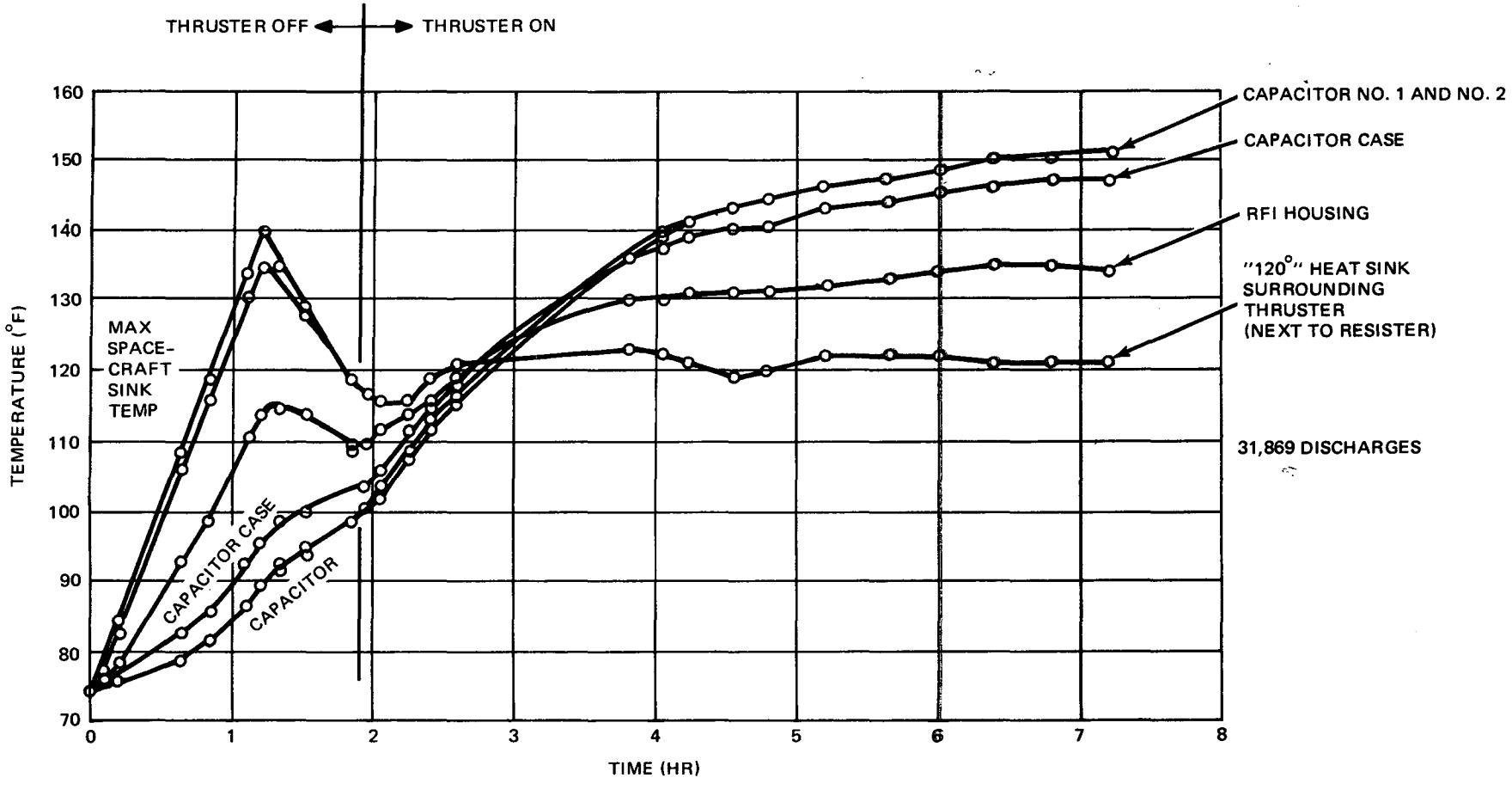

Figure 31. "Radiation Cooled" Thruster (Engineering Thermal Model Test)
(120°F Ambient)

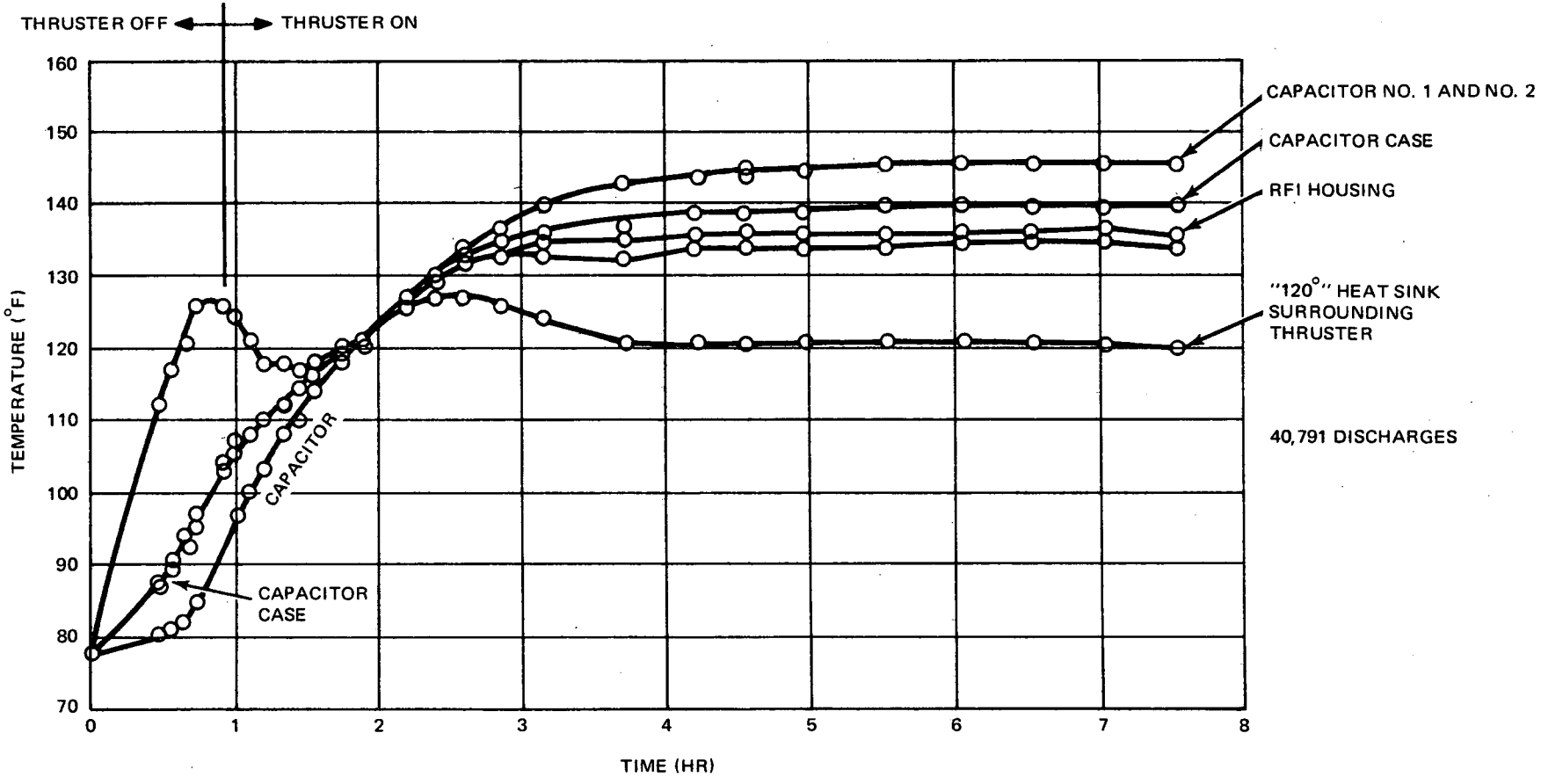

Figure 32. BN Disk Cooled Thruster (Engineering Thermal Model Test) (120°F Ambient)

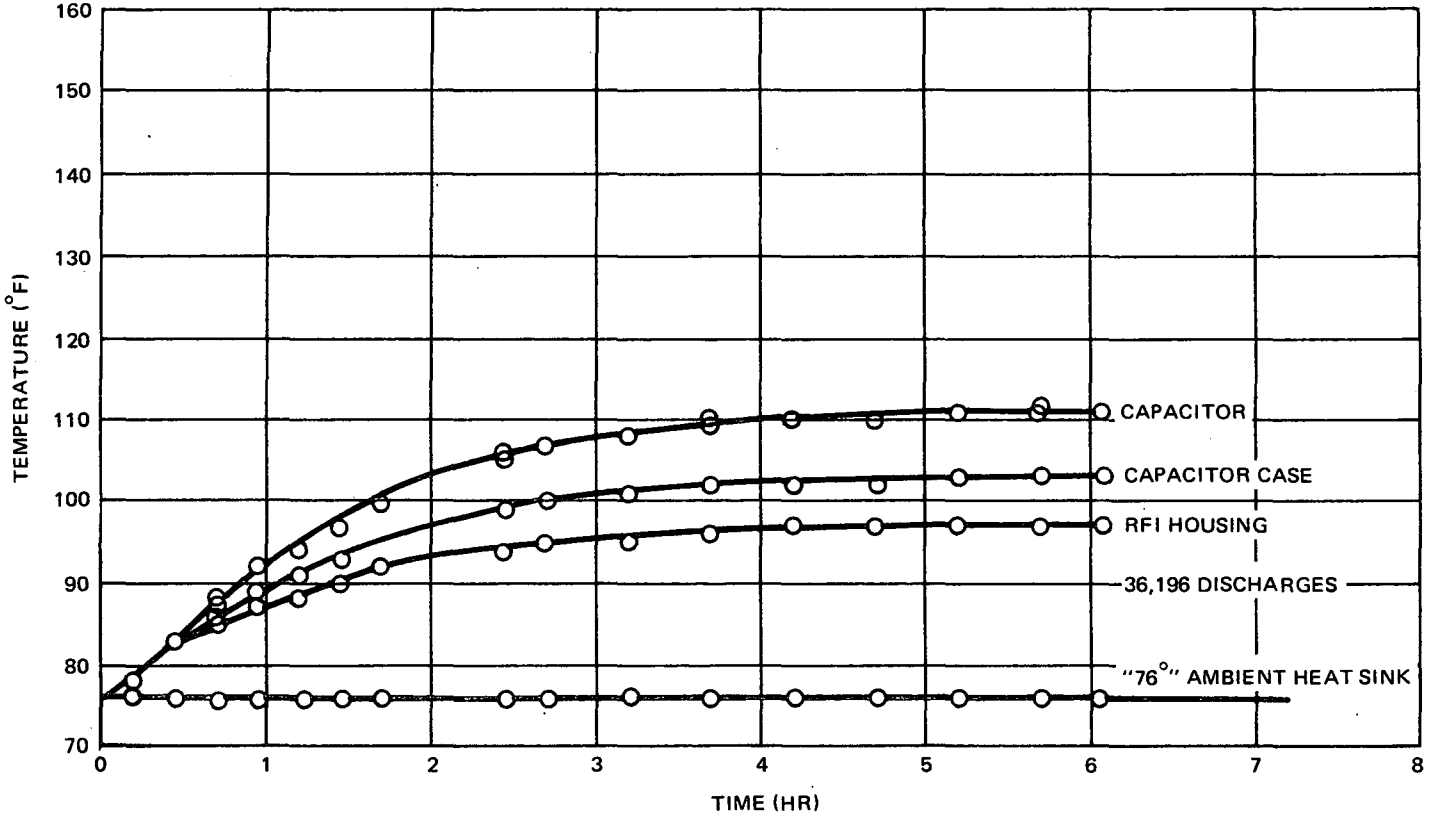

Figure 33. BN Conductive Disk Cooled Thruster (Engineering Thermal Model Test) (76°F Ambient)

capacitor life, it would be desirable in the final design to reduce this temperature. The experimental data shows roughly a 12°F gradient between the capacitor case and the RFI thruster housing. If instead of only depending upon radiation cooling, one provides some conduction cooling between these two components, one can lower the capacitor temperature. The simplified analysis performed above showed a reduction in the temperature gradient between the capacitor case and RFI housing. Data of the modified laboratory thruster (Figure 28) with the eight boron nitride disks between the RFI housing and capacitor case (all thermal interfacings were left dry - no grease was used) are presented in Figure 32. A comparison of Figures 31 and 32 reveals that the capacitor equilibrium temperature under worst conditions can be lowered by about 5°F. The reduction in temperature gradient between the capacitor case and the RFI housing is clearly demonstrated. The final test, test 3, (Figure 33) was performed at 110 ppm, using the boron nitride conducting disk scheme with a sink temperature of about 76°F ambient. In this latter case the capacitor equilibrium temperature was only about 110°F.

The thermal data presented shows that by incorporating eight Beryllium disks as electrically insulating and thermally conducting paths, the capacitor temperature will be kept below the maximum capacitor temperature even in the simultaneous occurrence of maximum spin rate and maximum sink temperature.

Based upon the latter thermal design data, it was decided to provide an electrically insulating but thermally conducting path between the capacitor case and the RFI housing in the final design. In the final design Beryllium oxide will be used instead of boron nitride and special care will be exercised with regard to surface finish to minimize interface contact resistance. Unless advised otherwise only dry interfaces (i.e., no grease or compounds) will be used in the final design.

3.5.4 EMI Aspects of the Thermal Design

Since the heat conducting disks, could in principle, capacitively couple the thruster ground circuit to the thruster housing (i.e., spacecraft ground), calculations were made of the electrical isolation maintained. In the limit of an infinite frequency, the impedance of the heat conducting disks vanishes. Calculations presented below, show effective isolation to be maintained for the frequency range of interest and for disk geometries to be used. Each heat conducting disk represents a pure capacitance ($C = K\epsilon A/d$) and resistance (R) in parallel. The impedance of each disk is $|Z| = R/\left[1 + (R/X_c)^2\right]^{1/2} \approx X_c$. The dielectric coefficient K is 6.1 for Beryllium oxide and 4.4 for Boron nitride. Using Beryllium oxide disks, one finds the capacitance of each disk of area 9.51×10^{-5} m^2 and thickness 1.59×10^{-3} m to be 3.22×10^{-12} fd. The impedance of each disk as a function of frequency is shown in Figure 34. At the thruster ringing frequency ($\sim$ 100 KC) one finds $|Z| \approx X_c = 4.45 \times 10^5$ ohms. Since $X_c \propto f^{-1}$ one finds that for each decimal order of magnitude increase in frequency the impedance of each disk decreases by an order of magnitude. The effective impedance of the eight heat conducting disks in parallel is then $1/8\,|Z|$. Whether or not this order of isolation represents sufficient isolation should be established experimentally.

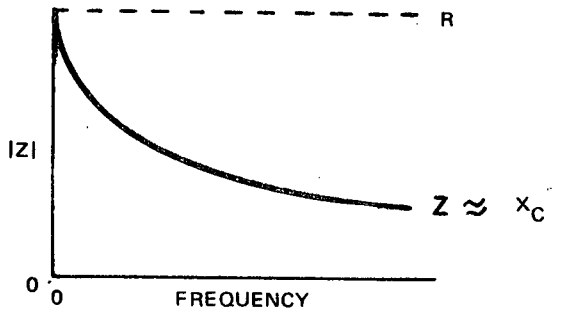

Figure 34. Impedance Variation with Frequency

3.5.5 Flat Black Thermal Control

An evaluation was also made of black paint for thermal control. Since Hughson Chemglaze Z-306 flat black paint (α = 0.96, ϵ = 0.91) was approved by Goddard Space Flight Center for the ATS spacecraft, samples were obtained from Hughson for evaluation. According to Mr. A Patterson of Hughson, adherence of Chemglaze Z-306 without a primer to an aluminum substrate was not considered too strong. Samples of aluminum were sandblasted, cleaned and painted directly with Chemglaze Z-306. Tear tests* were subsequently performed and satisfactory results were achieved within periods of 24 and even 48 hours (see Figure 35), of applying the paint. The paint is now being further evaluated as part of the vacuum thermal model tests described above. Unless these latter results should indicate poor vacuum adherence during thruster thermal cycling, we intend to use the Chemglaze Z-306 as a flat black thermal control material.

3.6 STRUCTURAL CONSIDERATIONS IN DESIGN

A primary consideration in designing the engine is to achieve a minimum weight structure which has the strength and siffness to remain functional after undergoing severe static and dynamic loading. The sinusoidal vibration test schedule, Table 17 (reference 10) indicates that the base of the engine will be subjected to maximum vibration levels of 25 g's in the lateral direction and 14 g's in the engine thrust direction for a frequency range below 80 Hz. For frequencies of 80 to 2000 Hz the maximum level in any direction will be 5 g's. At a resonant mode involving motion of significant masses in the engine the overall response to the input g levels may be amplified by a factor as high as 10. Thus 25 g's acceleration at the shaker may give as high as 250 g response and 5 g's may give as much as 50 g response. An engine designed to have no natural frequencies below 80 Hz would therefore have its maximum possible response reduced by a factor of 5 from 250 to 50 g's. Therefore the design approach has been to fabricate a structure capable of taking

---

* An X-shaped line was cut through the coating down to the aluminum substrate tape tacked to the surface and wider than the scribe mesh was rapidly pulled from the surface.

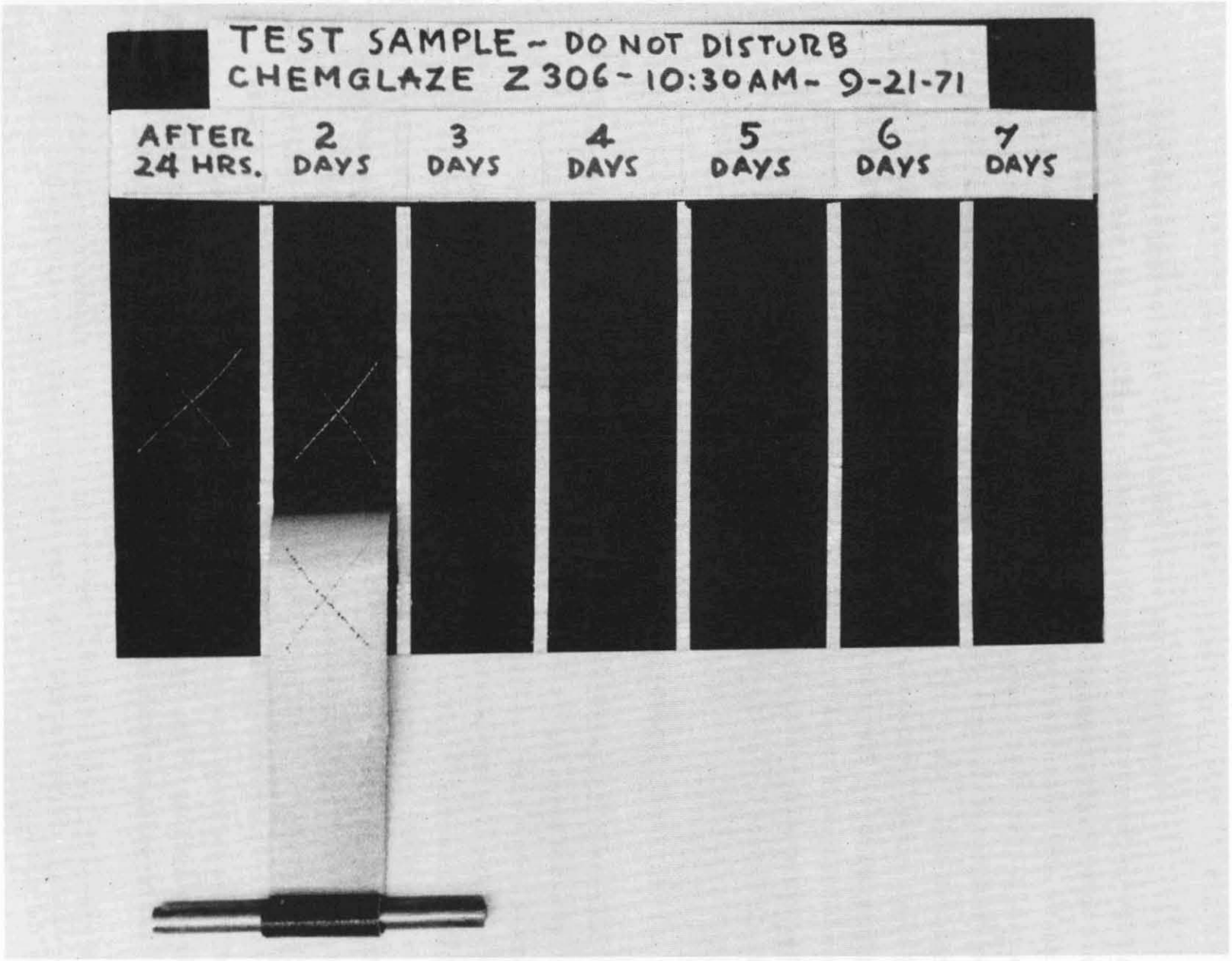

Figure 35. Paint Tear Test

TABLE 17. SMS DESIGN SINUSOIDAL VIBRATION LEVELS
FOR OUTBOARD MOUNTED EQUIPMENT
(LATERAL AXIS, THRUST AXIS)

	Frequency (Hz)	Level (g, 0 to peak)	
Lateral	5 - 10	0.5" DA	(double amplitude)
	10 - 20	14.0	
	20 - 100	4.0	
	100 - 200	2.0	
	200 - 2000	5.0	
Thrust	5 - 11	0.5" DA	(double amplitude)
	11 - 17	3.0	
	17 - 23	7.0	
	23 - 30	12.5	
	30 - 60	25.0	
	60 - 80	8.0	
	80 - 200	3.0	
	200 - 2000	5.0	
NOTE: Sweep rate is 2 octaves/minute for all spectra			

50 g loading with direct load paths of adequate stiffness, so that all primary structure resonances are above 80 Hz. A 50 g loading in any direction is much higher then would be experienced by the engine during its service lifetime. Certain features have been incorporated in the mechanical design to ensure that the condition exists. Figure 23, a general view of the engine, shows some detail of these features. The housing between the front and rear bulkhead has been beaded to obtain stiffness for in-plane compression and shear as well as tension. In that way, it is possible to stabilize the .020-inch sheets and provide an efficient link in the load paths from the fuel bar and capacitor masses to the system supports. The bulkheads represent another link in the load path. As shown in Figure 23, two Z sections have been attached at the front face of the thruster housing to carry the loads to the sides. In general, as in the above example, beam-like elements have been employed to resist the loads normal to skins. The reactions at the ends of the beams are then introduced into the supporting structure as in-plane loads. Use of the above design principles results in load paths of high stiffness from the mass load points to the supports. Additional stiffness in each direction has been gained by securely attaching the capacitor housing, the fuel bar supporting beams and the power conditioner housing to one another.

The acceleration at any point on the engine in response to random or sinusoidal excitation from the mounting points may be calculated. To do this the engine is modeled as a set of discrete masses connected by structural elements such as beams or plates. A set of flexibility coefficients is then derived, based on this model. From these "influence coefficients" and the mass data, natural frequencies and mode shapes are calculated. Response in these modes to 1 g sinusoidal excitation at the engine base may then be derived. These responses, as a function of frequency for each mass, are "transfer functions" which are the basis for obtaining the response to random excitation. Existing computer programs may be used in this analysis.

The effort required to take the complete analytical approach outlined above would not be justified for this phase of the engine development if simplified desk calculations establish an upper bound for the response to the random or sinusoidal excitations and if this response is within the capability of the structure to carry. Accordingly the latter approach was taken as follows. The engine was overviewed for the purpose of roughly establishing all the possible primary structure vibration modes, e.g., bending or twisting of the entire engine as a beam,

fore and aft motion of the capacitors etc. Simplified structural models were then used to estimate the frequency of these modes. The models were set up in such a way as to provide frequencies lower than those that would exist in the actual structure. For instance, concentrated loads replaced uniform loads on beams and no contribution to stiffness of backup structure was included.

These simplified calculations established a lowest frequency boundary of 111 Hz for a mode involving motion of 111 Hz of the two capacitors and the fuel bar in the engine thrust direction. Therefore, according to the vibration schedule,no engine resonances should be excited sinusoidally at more than 5g.

In any of the primary modes,the damping ratio should be .05 or greater,which limits the overall amplification of the input forces to a factor of 10. The engine supporting structure should therefore feel 50 g or less peak forces under sinusoidal vibration. Overall response to the 9.2 g rms random excitation would be less than 50 g's. On the basis of these results it is not considered necessary to do a more complete analysis for this phase of the engine development.

The engine structure has been designed to carry much more than 50 g's. Therefore since under vibration the loads should not exceed 50 g, the engine should have satisfactory structural integrity for the vibration test and the service life.

3.7 RELIABILITY

3.7.1 Principle of Approach

The reliability analysis for the SMS pulsed plasma microthruster consisted of component stress analysis, failure rate predictions, and system reliability computations.

The stress analysis was performed to ensure compliance with the Fairchild Republic SMS microthruster derating criteria (Section 3.7.5) and to provide necessary inputs in deriving part failure rates used in the SMS reliability prediction. The steps followed in performing the reliability analyses are listed below:

a) System Definition

b) Definition of operating environmental stress, duty cycle and operating time

c) Definition of system failure

d) Development of applicable reliability equations

e) Compilation of parts list

f) Performance of a piece-part stress analysis

g) Determination of environmental-applied failure rates

h) Computation of reliability

Items b, e, and f are discussed further in the following sections.

3.7.1.1 Definition of Environmental Stress, Duty Cycle and Operating Time

Environmental stresses experienced by the SMS microthruster include launch vibration, shock, space vacuum, radiation, thermal and high g. The design and testing approach discussed elsewhere in the report provides the requisite confidence in the ability of the Fairchild Republic microthruster to withstand these environmental stresses except for the thermal environment of the microthruster circuitry which is the primary obstacle to a successful five-year mission.

Recent thermal model testing confirms about a 10°C temperature rise for the microthruster components over the SMS ambient. Since the maximum SMS temperature is 50°C, the worst case microthruster electrical component environment will be 60°C. Therefore, 60°C was the temperature chosen for the stress analysis as well as the reliability prediction.

The greatest electrical stress (dissipated power) that could be imposed on the microthruster circuitry was determined as continuous microthruster operation at 110 pulses per minute.

Total continuous operating time (T) at 110 ppm during a five-year mission is computed as follows:

$$T = \frac{\text{number of required discharges}}{\text{discharge rate}} = \frac{\text{total impulse}}{\text{impulse bit amplitude}} \times \frac{1}{\text{discharge rate}}$$

With a 400 lb-sec total impulse requirement and the impulse bit amplitude limits of 20 micropound second and 30 micropound second, a T of 3030 hours and 2020 hours respectively are obtained. The value of 3030 operating hours has been used in the SMS microthruster reliability computation for conservative analysis.

3.7.1.2 Parts List

Parts have been selected from the "flight" category of the NASA, Goddard Space Flight Center PPL-11 and PP-11A preferred parts list, as much as possible. Columns 1 through 3 of Table 20, provide identification of all electronic parts include controlling specifications and non-standard screening specifications as applicable.

The full type designation for established reliability (E.R.) resistors and capacitors includes the lowest failure rate available for each individual part. This was determined after review of the applicable military qualified product list (QPL) for each part.

3.7.1.3 Stress Analysis

The results of the stress analysis performed are given in Columns 4 through 8 of Table 20. The applied stress ratios under the worst case conditions of microthruster operation (T_A = 60°C and thruster operation at 110 ppm) are listed in Column 8. These values of worst case stress were compared to the corresponding values set forth in the Fairchild Republic SMS microthruster derating criteria provided in Section 3.7.5. All parts were found to be used within the limitations specified in the derating criteria.

3.7.1.4 Stress Analysis Example

Analysis of the control logic flip-flop circuit of Figure 36 is used to illustrate the manner in which each microthruster circuit was analyzed.

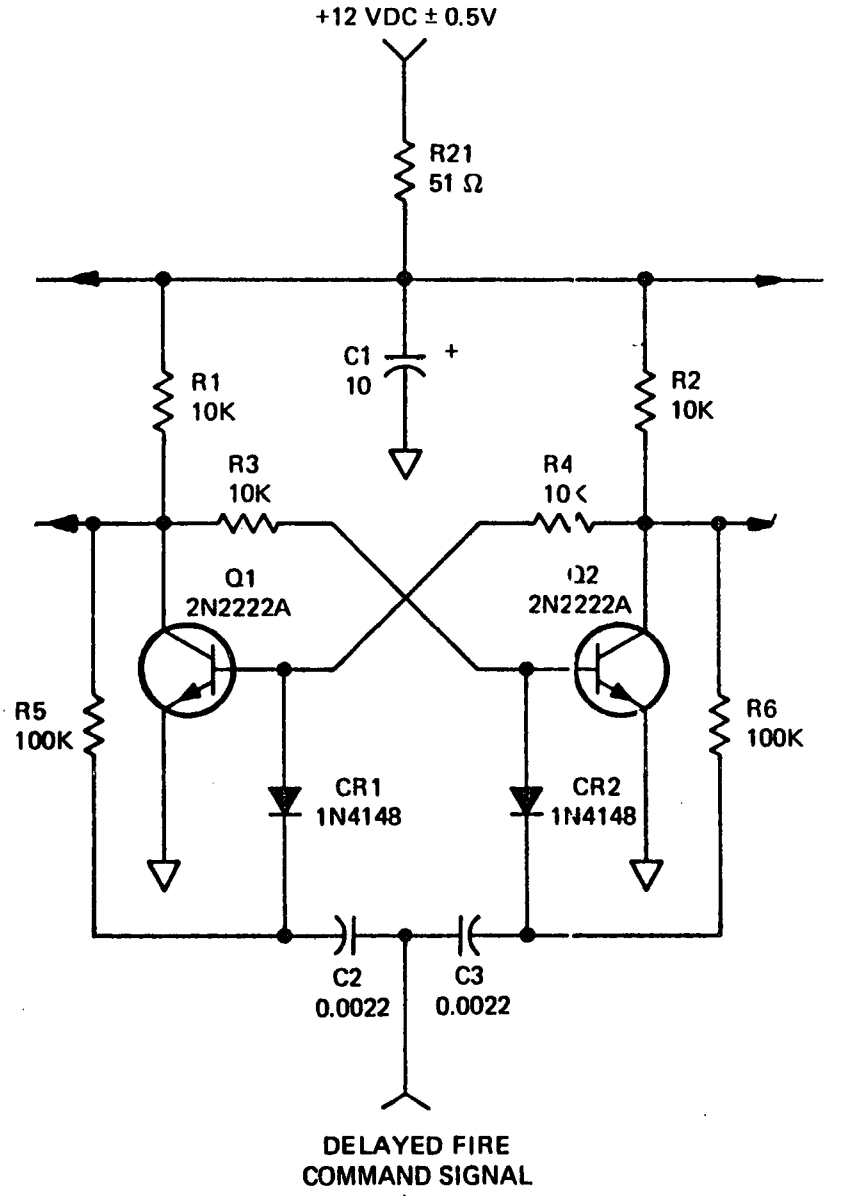

Figure 36. Logic Flip-Flop

Component C1:

The voltage experienced by capacitor C1 is 12.5 VDC in the worst case. This voltage is present 100% of the time that the SMS microthruster is "ON" (enable signal present). Therefore, the following relevant data is calculated for inclusion in the stress analysis.

Rated Voltage = 20 V

Rated Voltage at 60°C = 20 V Voltage derating of CSR 13 capacitors begin at 85°C per MIL-C-39003.

$$\text{Stress Ratio} = \frac{\text{Applied Voltage}}{\text{Rated Voltage (at 60°C)}} = \frac{12.5}{20} = .625$$

Component R3:

Resistors R1 and R3 act as a voltage divider when transistor Q2 is "ON". The voltage across R3 is computed as follows:

$$V_{R3} = (12.4 - V_{BEQ2}) \frac{R_3}{R_1 + R_3}$$

With transistor Q2 in saturation, $V_{BE(sat)} = 1V$

$$V_{R3} = 11.4 \times \frac{10 \times 10^3}{20 \times 10^3} = 5.7\,V$$

$$\text{Power Dissipated} = \frac{V^2}{R} \times \text{Duty Cycle (D.C.)}$$

Duty Cycle = 50% for the flip-flop

Rounding V_{R3} from 5.7 to 6 volts to be conservative.

$$\text{Power Dissipated} = \frac{6^2}{10 \times 10^3} \times .5 = 1.8 \text{ milliwatt (mw)}$$

Rated Power at 60°C, obtained from MIL-R-39008/2C is 500 mw as power derating does not begin until the temperature reaches 70°C. As the voltage rating of this part is 350 volts, the voltage stress is insignificant.

$$\text{Stress Ratio} = \frac{\text{Applied Power}}{\text{Rated Power (at 60°C)}} = \frac{1.8 \times 10^{-3}}{500 \times 10^{-3}} = .0036$$

Component C2:

The voltage across capacitor C2 is a function of the state of the flip-flop. With Q1 initially "OFF", the voltage across C2 is zero. The fire command generates a delayed fire command signal input to C2 and C3. The input to C2 is a 5 millisecond pulse of 6.51 volts (BV_{max} of the 1N753A obtained from the mil. spec) worst case. The voltage across C2 then returns to zero for 545 milliseconds (at 110 ppm) when the flip-flop again receives a command signal input and changes state. At this time the voltage across C2 is a pulse of 6.51 volts for 45 milliseconds. Thus we compute:

$$\text{Stress Ratio} = \frac{\text{Applied Voltage}}{\text{Rated Voltage (at 60°C)}} = \frac{6.51}{200} = .033$$

$$\text{Duty Cycle} = \frac{5 \text{ ms} + 45 \text{ ms}}{545 \text{ ms} + 545 \text{ ms}} = \frac{50 \text{ ms}}{1090 \text{ ms}} = .04587$$

Component Q1:

The total power dissipated by Q1 is computed as follows:

$$P_T = (V_{CE}I_C + V_{BE}I_B) \text{ (D.C.)}$$

With Q1 in saturation, $V_{CE} = .6V$ and $V_{BE} = 1V$

The collector current $(I_C) = \frac{12.4 - .6}{10 \times 10^3} = 1.8$ ma

The base current $(I_B) = \frac{6 - V_{BE(sat)}}{10 \times 10^3} = .5$ ma

The flip-flop duty cycle (D.C.) is 50%,

$$\therefore P_T = (.6 \times 1.18 + .5)(.5 \times 10^{-3})$$

$$= .604 \text{ mw}$$

Rated Power (at 60°C) is computed from the derating value of 3.33 mw/°C above T_A = 25°C found in MIL-S-19500/255E and is 383 mw.

$$\text{Stress Ratio} = \frac{\text{Applied Power}}{\text{Rated Power (at 60°C)}} = \frac{.6 \text{ mw}}{383 \text{ mw}} = .0016$$

Transistor Junction Temperature (T_j)

$$T_j = T_A + \theta_{JA} P_T = 60 + \left(\frac{.3°C}{mw} \right) \quad (.6 \text{ mw}) \approx 60°C$$

Normalized Junction Temperature (T_n)

$$T_n = \frac{T_J - T_S}{T_{J_{max}} - T_S} = \frac{60 - 25}{200 - 25} = .2$$

3.7.2 Reliability Analysis

Reliability analysis data is presented in Table 3 for all SMS microthruster electronic piece parts. Discussion of salient points regarding each of the microthruster circuits and components is given in Sections 3.7.2.2 through 3.7.2.6.

3.7.2.1 Reliability Stress Analysis Form

A description of the form by column number and heading is given as follows:

a) Reference Symbol - The part identification symbol and number corresponding to the electrical schematics of Figures 12-14 and 39 -44, is listed.

b) Part Number - The full type designation for each part is provided.

c) Applicable Specification - The controlling military or supplier specification is identified.

d) Nominal Device Rating - The applicable device rating(s) as specified in the Fairchild Republic derating criteria is listed (usually at T_A = 25°C).

e) Device Rating at 60°C - The applicable military/supplier specification for each part was reviewed to determine the device rating at 60°C.

f) Duty Cycle - The "ON" or stress time of a part expressed as a percentage of total operating time.

g) Applied Circuit Usage - The actual power voltage or current stress applied. In accordance with MIL-HDBK-217A methodology the dissipated power entries for resistors and semiconductors are average dissipated powers. These values are computed as the peak power times the duty cycle entry in Column 6. Capacitor voltages are the peak voltages to which the capacitor charges regardless of duty cycle.

h) Stress Ratio - The ratio of applied circuit usage to the device rating at 60°C.

i) T_n - MIL-HDBK-217A defines the normalized junction temperature (T_n) of semiconductors as:

$$T_n = \frac{T_J - T_S}{T_{J(max)} - T_S}$$

where: T_J = junction temperature (ambient of 60° + internal rise)

T_S = temperature at which power derating begins

$T_{J(max)}$ = maximum junction temperature of the device

Junction temperatures were calculated by the following equation:

$$T_J = T_A + Q_{JA} P_S$$

Where T_A was assumed 60°C, worst case

Q_{JA} the thermal resistance values which were the maximum values listed in the applicable military specifications

P_J is the average dissipated power of semiconductors obtained from Column 7.

j) Failure Rate Source - MIL-HDBK-217A was used for semiconductors and for the other devices in which a failure rate deviation was not covered in MIL-STD-198 and MIL-STD-199.

k) Basic Failure Rate - The failure rate obtained from the Column 10 source, expressed in failure/10^6 hours.

l) K_E - The environmental factor is a failure rate modifier used in a MIL-HDBK-217A failure rate derivation. The "ground" factor is used in all cases as the closest approximation to the SMS orbital spacecraft environment. The failure rates of established reliability parts does not require a K_E modifier as the reliability level applies to a ground environment.

m) K_S - The screening application factor accounts for the reduction of base failure rates resulting from semiconductor TX (testing extra) screening as well as non-standard part screening.

n) Application Failure Rate - This failure rate is the product of the base failure rate x K_E x K_S and is expressed in failures/10^6 hours.

3.7.2.2 Thruster Capacitor

The most critical and the most tested component in the pulsed plasma microthruster is the main thruster capacitor. The following sections on capacitor stress, reliability design features and failure rates derivation summarizes the detail analysis of Section

Stress Analysis: As discussed in Section 3.3 of this report, the main energy storage capacitor dielectric is subjected to voltage stress during charging from 0 to 1450 volts in 500 milliseconds followed by a hold time of 45 milliseconds. This This stress exists for satellite spin rates between 50 and 110 rpm. Since the capacitor is rated at 2000 volts, the voltage stress varies between 0 and .725. However, the percentage of total operating time that the capacitor experiences the peak stress is small;

$\frac{45 \text{ ms}}{545 \text{ ms}}$ = 8.3% at 110 rpm and $\frac{45 \text{ ms}}{1200 \text{ ms}}$ = 3.8% at 50 rpm.

Reliability Design Features: The PC142S1000-1 capacitor and the specific charging technique employed were designed to achieve the five year SMS life requirement. These features represent improvements in the capacitor design life (consisting of discharge life and d.c. life) over the highly successful LES-6 and LES-7 designs.

The first improvement obtained is a reduction of dielectric stress, accomplished by using four layers of 35 mil dielectric instead of three layers of 35 mil and one layer of 25 mil dielectric.

The second improvement is a thruster system design providing a fixed charge time - rpm independent hold time capacitor charging technique. This technique was chosen to minimize the life degrading d.c. hours accumulated at peak voltage during pulsed operation between 50 and 110 pulses per minute. The magnitude of this improvement is evidenced by the fact that the SMS capacitor will only sustain 250 hours of d.c. (at 20 micropound-sec/impulse) while the LES-6 will sustain 890 hours of d.c. The third improvement is reflected in higher quality standards and the 100% screening test described in Fairchild Republic specification PC142S1000.

Failure Rate Derivation: Demonstration of reliability through a test program provides an excellent method of determining reliability, especially when the test is conducted in the intended use environment. The use of this type of thruster capacitor in the LES-6 satellite, which has been on station and functioning since 1968, gives Fairchild Republic a substantial data bank for determining capacitor reliability. Backing up this data is a laboratory testing program starting in 1968 and continuing through 1970. This data is presented in Tables 18 and 19.

TABLE 18. LABORATORY DATA OF INDIVIDUAL LES-6 CAPACITORS

Testing Period	Total No. of Pulses	Failures
1/16/68 - 2/23/68	14,665,281	1
2/21/68 - 5/9/68	8,744,277	0
5/8/69 - 6/26/69*	7,449,545	0
1/23/70 - 4/13/70*	20,000,000**	0
Total	50,859,103	1

* Tests performed after delivery of LES-6 flight system

** Equivalent discharges - Capacitor design life (20×10^6 pulses) attained before failure during accelerated testing. Equivalent life L' was computed as follows:

$$L' = Lx \left(\frac{\text{accelerated voltage}}{\text{rated voltage}}\right)^5 = 11,766,194 \left(\frac{1580}{1360}\right)^5 = 24,901,579$$

where L was the actual number of pulses attained before failure

The flight data for the LES-6 satellite accumulated to January 19, 1970 is given below in Table 19.

TABLE 19. FLIGHT DATA - LES-6 SYSTEM AT SYNCHRONOUS ALTITUDE

Thruster	Pulse Frequency	Pulses	Failure
#2	10 pulses/minute	3,050,000	0
#5	10 pulses/minute	3,050,000	0
#6	10 pulses/minute	3,050,000	0
#9	10 pulses/minute	3,050,000	0
	Total	12,200,000	0

Based upon the above data the best estimate for the failure rate of the thruster capacitor is:

$$\frac{1}{63,059,103} = 1.585 \times 10^{-8} \left(\frac{\text{Failures}}{\text{Impulse}}\right).$$

The main thruster failure rate, expressed in faulures per hour (110 pulses per minute assumed) is derived as follows:

$$\lambda = 1.585 \times 10^{-8} \frac{\text{Failures}}{\text{Impulse}} \times \frac{110 \text{ Impulses}}{\text{Minute}} \times \frac{60 \text{ Minutes}}{\text{Hour}}$$

$$\lambda = 104.6 \times 10^{-6} \text{ Failures/Hour}$$

However, an adjustment factor is assumed to account for the expected reliability improvement due to the reliability design features discussed in Section 3.7.2.2. With an adustment factor of .1, the predicted application failure rate of the SMS thruster capacitor becomes 10.46×10^{-6} Failures/Hour.

3.7.2.3 Discharge Initiation Circuit

The stress analysis of this circuit indicates the selection of two electronic parts which require further explanation. Capacitors C1A, C1B, and C2, C3, are subject to peak stress of approximately 60%. However, the percentage of time the capacitors are subject to peak voltage is low. In addition, the application and reliability of these capacitors have been proven in the LES-6 and LES-7.

Auxiliary discharge capacitors C1A and C1B are charged similarly to the main thruster capacitor but to 620 volts in 500 milliseconds followed by a hold time of 45 milliseconds. Thus, the voltage stress varies from 0 to .62 with the peak voltage applied 8.3% of the total time at 110 rpm and a 3.8% at 50 rpm.

Capacitors C2 and C3 are subjected to a peak voltage of approximately 1900 volts during firing. Since the pulse time is 5 milliseconds and the surface igniter plugs fire alternately, the duty cycle is:

$$1/2 \times \frac{5 \text{ ms}}{545 \text{ ms}} = .00459 \approx .5\%$$

3.7.2.4 Logic Flip-Flop

The part types and values of the controlled logic flip-flop and SCR pulse driver circuit of Figure 13 are essentially identical to the proven LES-6 circuit. However, screened (TX) versions of the semiconductors and established reliability (ER) resistors and capacitors have been substituted in the SMS design.

The conservative design philosophy is evidenced in the stress analysis shown in Table 20. For the power dissipating resistors and semiconductors, the highest applied power is 1% of its rating at 60°C (R21). This occurs because of low current and peak power levels as well as the short duration of pulses.

3.7.2.5 Delayed Trigger Logic

The stress analysis for the delayed pulse, discharge initiation circuit of Figure 14 is shown in Table 20. The extremely low stress ratios listed indicate the conservative design of this circuit. For example, the temperature rises (above ambient) for the junctions of silicon controlled rectifier CR2 and transistor Q3 have been computed at less than 1°C and 8°C, respectively.

3.7.2.6 Converter-Charger Subsystem

The stress analysis for the converter-charger subsystem is shown in Table 20. This analysis corresponds to a worst case analysis (operation at 110 ppm) for the six converter-charger circuits shown in Figures 39 through 44. The converter-charger circuitry reflects low stress levels commensurate with the thruster module subsystem.

The application failure rate column of Table 20 lists the total failure rate when multiple parts are considered. For this case, the application failure rate of the individual part is multiplied by the quantity of parts.

3.7.3 SMS Microthruster System Reliability Prediction

The specific objective of the system reliability analysis is to predict the probability of success of a single Fairchild Republic microthruster during five years of in-orbit operation. The results obtained may be used to derive the probability of success of various modes of SMS thruster operation when multiple thrusters are installed.

The prediction is based on the following assumptions and conditions:

a) Electronic parts exhibit constant failure rates. The onset of wearout is not reached during the five year mission and infant mortality failures have been eliminated through the 100% screening tests.

b) The probability of surviving the launch and ascent into orbit is unity.

c) The reliability of the propellant feed system and surface igniter plugs is unity. LES-6 operation and extensive simulated laboratory tests support this assumption.

d) Thruster operation is at 110 ppm.

e) Operating time during the five year mission as computed in Section 3.7.1.1 is 3030 hours.

f) Operating ambient is 60°C.

TABLE 20

RELIABILITY STRESS ANALYSIS

DISCHARGE INITIATION CIRCUIT

PART IDENTIFICATION			STRESS						PREDICTION				
			Device Rating		Applied								
Ref. Symbol	Part Number	Applicable Specification	Nominal	at 60°C	Duty Cycle %	Circuit Usage	Stress Ratio	T_N	Failure Rate Source	Base F.R. x 10^6	K_E	K_S	Application Failure Rate x 10^6
R1	RCR20G102JS	MIL-R-39008/2	500mw	500mw	.005	.05 μw 1 V	< .001		MIL-STD-199 (301.2)	.000225			.000225
R2	RCR20G102JS	MIL-R-39008/2	500mw	500mw	.005	.05 μw 1 V	< .001		MIL-STD-199 (301.2)	.000225			.000225
C1A	118P105910S2	Sprague; FI/FRD Screening Spec PC145S8003	1000 V	1000 V	N/A	620 V	.62		MIL-HDBK-217A (7.6.29)	.1821	1.3	.1	.0236
C1B	118P105910S2	Sprague; FI/FRD Screening Spec PC145S8003	1000 V	1000 V	N/A	620 V	.62		MIL-HDBK-217 (7.6.29)	.1820	1.3	.1	.0236
C2	B161Y203-302K	AEROVOX; FI/ FRD Screening Spec. PC145S8002	3000 V	2550 V	.001	1900 V	.633		MIL-HDBK-217A (7.6-75)	.005	2.	.1	.0010
C3	B161Y203-302K	AEROVOX; FI/ FRD Screening Spec. PC145S8002	3000 V	2550V	.001	1900 V	.633		MIL-HDBK 217A (7.6-75)	.005	2.	.1	.0010
CR1	C137PB1200	GE; FI/FRD Screening Spec. PC145S8004	61W(Instantaneous) 22A (Average) 1200 PRV	1200 V	.001	36mw 163 μA (avg) 620 V	< .001 < .001 .517	.25	MIL-HDBK-217A (7.4-11)	.340	1.0	.1	.0340
CR2	C137PB1200	GE; FI/FRD Screening Spec. PC145S8004	61W(Instantaneous) 22A (Average) 1200 PRV	1200 V	.001	36mw 163 μA (avg) 620 V	< .001	.25	MIL-HDBK-217A (7.4-11)	.340	1.0	.1	.0340
CR3	UT2080	UNITRODE;FI/ FRD Screening Spec. PC145S8006	800 V 2 W	800 V 2 W	.001	620 V 6.2mw		.2	MIL-HDBK-217A	.280	1.0	.1	.0280
CR4	UT2080	UNITRODE; FI/ FRD Screening Spec. PC145S8006	800 V 2 W	800 V 2 W	.001	620 V 6.2 mw		.2	MIL-HDBK-217A	.280	1.0	.1	.0280
T1	PTE-5904E	Pulsetronics Eng. Co. FI/FRD Screening Spec. PC145S8007			.0000	assume @ 100° C worst			MIL-HDBK-217A (page 7.7-3 assume class C insulation, page 7.7-8-F.R. min = .2	.2	none till 140°C	.1	.02

TABLE 20

DISCHARGE INITIATION CIRCUIT (Continued)

PART IDENTIFICATION			STRESS						PREDICTION				
			Device Rating		Applied								
Ref. Symbol	Part Number	Applicable Specification	Nominal	at 60°C	Duty Cycle %	Circuit Usage	Stress Ratio	T_N	Failure Rate Source	Base F.R. x 10^6	K_E	K_S	Application Failure Rate x 10^6
T2	PTE-5904E	Pulsetronics Eng. Co., FI/FRD Screening Spec. PC145S8007			.0001	assume @ 100°C		10°C rise	MIL-HDBK-217A (page 7-7-3 assume class C installation page 7-7-8 FR min = .2)	.2	none till 100°C	.1	.02
L1, L3	PC097D0042-1	Product Spec. to be written	N/A	N/A	.001	620 VDC		10°C rise	MIL-HDBK 217A 7-7-2 and 7-7-3	.2	1.5	.1	.03
L2	PC097D0042-1	Product Spec. to be written	N/A	N/A	8.3	1450 VDC		10°C rise	MIL-HDBK-217A 7-7-2 and 7-7-3	.2	1.5	.1	.03
FL1	P-5(03)-3	GSFC Spec. 311-P-5(03)-3	35 V		.005	5 V 100 ma peak	.17		MIL-HDBK-217A 7.7-8 and 7.6-23	.36215		.1	.036215
FL2	P-5(03)-3	GSFC Spec. 311-P-5(03)-3	35 V		.005	5 V 100 ma peak	.17		MIL-HDBK 217A 7.7-8 and 7.6-23	.36215	2	.1	.036215

TABLE 20

CONTROL LOGIC FLIP FLOP AND SCR PULSE DRIVER CIRCUIT

PART IDENTIFICATION			STRESS						PREDICTION					
			Device Rating		Applied									
Ref. Symbol	Part Number	Applicable Specification	Nominal	at 60°C	Duty Cycle %	Circuit Usage	Stress Ratio	T_N	Failure Rate Source	Base F.R. x 10^6	K_E	K_S	Application Failure Rate x 10^6
R1	RCR20G103JS	MIL-R-39008/2	500mw	500mw	50	2.18mw 6.6 V	.0044		MIL-STD-199 (301.2)	.000225			.000225
R2	RCR20G103JS	MIL-R-39008/2	500mw	500mw	50	2.18mw 6.6 V	.0044		MIL-STD-199 (301.2)	.000225			.000225
R3	RCR20G103JS	MIL-R-39008/2	500mw	500mw	50	1.8mw 6 V	.0036		MIL-STD-199 (301.2)	.000225			.000225
R4	RCR20G103JS	MIL-R-39008/2	500mw	500mw	50	1.8mw 6 V	.0036		MIL-STD-199 (301.2)	.000225			.000225
R5	RCR20G104JS	MIL-R-39008/2	500mw	500mw	.002	.72uw 6 V	<.001		MIL-STD-199 (301.2)	.000225			.000225
R6	RCR20G104JS	MIL-R-39008/2	500mw	500mw	.002	.72uw 6 V	<.001		MIL-STD-199 (301.2)	.000225			.000225
R7	RCR20G102JS	MIL-R-39008/2	500mw	500mw	.001	144uw 12 V	<.001		MIL-STD-199 (301.2)	.000225			.000225
R8	RCR20G102JS	MIL-R-39008/2	500mw	500mw	.001	144uw 12 V	<.001		MIL-STD-199 (301.2)	.000225			.000225
R9	RCR20G103JS	MIL-R-39008/2	500mw	500mw	.001	.1uw 1 V	<.001		MIL-STD-199 (301.2)	.000225			.000225
R10	RCR20G103JS	MIL-R-39008/2	500mw	500mw	.001	.1uw 1 V	<.001		MIL-STD-199 (301.2)	.000225			.000225
R11	RCR20G102JS	MIL-R-39008/2	500mw	500mw	<.0001	.6uw 12 V	<.001		MIL-STD-199 (301.2)	.000225			.000225
R12	RCR20G102JS	MIL-R-39008/2	500mw	500mw	<.0001	.6uw 12 V	<.001		MIL-STD-199 (301.2)	.000225			.000225
R13	RCR20G103JS	MIL-R-39008/2	500mw	500mw	.001	15uw 12 V	<.001		MIL-STD-199 (301.2)	.000225			.000225
R14	RCR20G103JS	MIL-R-39008/2	500mw	500mw	.001	15uw 12 V	<.001		MIL-STD-199 (301.2)	.000225			.000225
R15	RCR20G513JS	MIL-R-39008/2	500mw	500mw	.02	56uw 12 V	<.001		MIL-STD-199 (301.2)	.000225			.000225

TABLE 20

CONTROL LOGIC FLIP-FLOP AND SCR PULSE DRIVER CIRCUIT (CONTINUED)

PART IDENTIFICATION			STRESS						PREDICTION				
			Device Rating		Applied								
Ref. Symbol	Part Number	Applicable Specification	Nominal	at 60°C	Duty Cycle%	Circuit Usage	Stress Ratio	T_N	Failure Rate Source	Base F.R. x 10^6	K_E	K_S	Application Failure Rate x 10^6
R16	RCR20G513JS	MIL-R-39008/2	500mw	500mw	.02	56uw 12 V	<.001		MIL-STD-199 (301.2)	.000225			.000225
R17	RCR20G104JS	MIL-R-39008/2	500mw	500mw	.001	15uw 12 V	<.001		MIL-STD-199 (301.2)	.000225			.000225
R18	RCR20G104JS	MIL-R-39008/2	500mw	500mw	.001	15uw 12 V	<.001		MIL-STD-199 (301.2)	.000225			.000225
R19	RCR20G510JS	MIL-R-39008/2	500mw	500mw	<.0001	7uw 11 V	<.001		MIL-STD-199 (301.2)	.000225			.000225
R20	RCR20G510JS	MIL-R-39008/2	500mw	500mw	<.0001	7uw 11 V	<.001		MIL-STD-199 (301.2)	.000225			.000225
R21	RCR20G510JS	MIL-R-39008/2	500mw	500mw	100	5mw .5 V	.01		MIL-STD-199 (301.2)	.000225			.000225
C1	CSR13E106KS M39003/01-3006	MIL-C-39003/1	20 V	20 V	100	12.5 V MAX	.625		MIL-STD-198 (801.5)	.0014			.0014
C2	CKR06BX222KR M39014/02-286	MIL-C-39014/2	200 V	200 V	4.6	6.5 V MAX	.033		MIL-STD-198 (1001.2)	.0005			.0005
C3	CKR06BX222KR M39014/02-286	MIL-C-39014/2	200 V	200 V	4.6	6.5 V MAX	.033		MIL-STD-198 (1001.2)	.0005			.0005
C4	CKR06BX223KR M39014/02-302	MIL-C-39014/2	100 V	100 V	.002	12V MAX	.12		MIL-STD-198 (1001.2)	.0005			.0005
C5	CKR06BX223KR M39014/02-302	MIL-C-39014/2	100 V	100 V	.002	12V MAX	.12		MIL-STD-198 (1001.2)	.0005			.0005
C6	CKR06Bx224KR M39014/02-316	MIL-C-39014/2	50 V	50 V	10	12.5 V	.25		MIL-STD-198 (1001.2)	.0005			.0005
C7	CKR06BX224KR M39014/02-316	MIL-C-39014/2	50 V	50 V	10	12.5 V	.25		MIL-STD-198 (1001.2)	.0005			.0005
CR1	TX1N4148	MIL-S-19500/116E	75 V 75mw	75 V 58mw	50	7 V Peak < 1u W	.09 <.001	.2	MIL-HDBK-217A	.195	1.5	0.1	.002925
CR2	TX1N4148	MIL-S-19500/116E	75 V 75mw	75 V 58mw	50	7 V Peak < 1u W	.09 <.001	.2	MIL-HDBK-217A	.195	1.5	0.1	.002925

TABLE 20

CONTROL LOGIC FLIP FLOP AND SCR PULSE DRIVER CIRCUIT (CONTINUED)

PART IDENTIFICATION			STRESS						PREDICTION				
			Device Rating		Applied								
Ref. Symbol	Part Number	Applicable Specification	Nominal	at 60°C	Duty Cycle%	Circuit Usage	Stress Ratio	T_N	Failure Rate Source	Base F.R. x 10^6	K_E	K_S	Application Failure Rate x 10^6
CR3	TX1N4148	MIL-S-19500/116E	75 V 75mw	75 V 58mw	.005	1V Peak	.013 <.001	.2	MIL-HDBK-217A	.195	1.5	0.1	.002925
CR4	TX1N4148	MIL-S-19500/116E	75 V 75mw	75 V 58mw	.005	1V Peak	.013 <.001	.2	MIL-HDBK-217A	.195	1.5	0.1	.002925
Q1	TX2N2222A	MIL-S-19500/255E	500mw 50 BV_{ECO} *8 BV_{EBO} 75 BV_{CBO}	383mw 50 V 8 V 75 V	50	.6mw 6.3 V 6 V 5.7 V	.002 .126 .75 .076	.2	MIL-HDBK-217A	.195	1.5	0.1	.002925
Q2	TX2N2222A	MIL-S-19500/255E	500mw 50 BV_{ECO} *8 BV_{EBO} 75 BV_{CBO}	383mw 50 V 8 V 75 V	50	.6mw 6.3 V 6 V 5.7 V	.002 .126 .75 .076	.2	MIL-HDBK-217A	.195	1.5	0.1	.002925
Q3	TX2N3251A	MIL-S-19500/323A	360mw 60 BV_{ECO} 5 BV_{EBO} 60 BV_{CBO}	288mw 60 V 5 V 60 V	.001	.01uw 12 V 0 V 12 V	<.001 .2 - .2	.2	MIL-HDBK-217A	.470	1.5	0.1	.0705
Q4	TX2N3251A	MIL-S-19500/323A	360mw 60 BV_{ECO} 5 BV_{EBO} 60 BV_{CBO}	288mw 60 V 5 V 60 V	.001	.01uw 12 V 0 V 12 V	<.001 .2 - .2	.2	MIL-HDBK-217A	.470	1.5	0.1	.0705
Q5	TX2N2222A	MIL-S-19500/255E	500mw 50 BV_{ECO} *8 BV_{EBO} 75 BV_{CBO}	383mw 50 V 8 V 75 V	.001	12mw 12 V 5 V 12 V	<.001 .24 .63 .16	.2	MIL-HDBK-217A	.195	1.5	0.1	.002925
Q6	TX2N2222A	MIL-S-19500/255E	500mw 50 BV_{ECO} *8 BV_{EBO} 75 BV_{CBO}	383mw 50 V 8 V 75 V	.001	12mw 12 V 5 V 12 V	<.001 .24 .63 .16	.2	MIL-HDBK-217A	.195	1.5	0.1	.002925

*Selected Parameters

TABLE 20

DELAYED PULSE D. I. TRIGGER CIRCUIT

PART IDENTIFICATION			STRESS						PREDICTION				
			Device Rating		Applied								
Ref. Symbol	Part Number	Applicable Specification	Nominal	at 60°C	Duty Cycle%	Circuit Usage	Stress Ratio	T_N	Failure Rate Source	Base F.R. x 10^6	K_E	K_S	Application Failure Rate x 10^6
Q1	TX2N2222A	MIL-S-19500/255E	500 mw 50 BV_{ECO} 8 BV_{EBO} 75 BV_{CBO}	383 mw 50 V 8 V 75 V	10	33 uw 30 V 0 30 V	<.001 .6 --- .4	.2	MIL-HDBK-217	.195	1.5	0.1	.002925
Q2	TX2N3251A	MIL-S-19500/323A	360 mw 60 BV_{ECO} 5 BV_{EBO} 60 BV_{CBO}	288 mw 60 V 5 V 60 V	10	1.2 mw 30 V 0 30 V	.004 .5 --- .5	.206	MIL-HDBK-217	.471	1.5	0.1	.0706
Q3	TX2N4948	MIL-S-19500/388	360 mw	276 mw	10	18 mw	.065	.243	MIL-HDBK-217	.546	1.5	0.1	.0819
Q4	TX2N2222A	MIL-S-19500/255E	500 mw 50 BV_{ECO} 8 BV_{EBO} 75 BV_{CBO}	383 mw 50 V 8 V 75 V	10	1 uw 7 V 0 7 V	<.001 .14 --- .09	.2	MIL-HDBK-217	.195	1.5	0.1	.002925
R1	RCR20G203JS	MIL-R-39008/2	500 mw	500 mw	10	.125 mw 5 V	<.001		MIL-STD-199 (301.2)	.000225			.000225
R2	RCR20G103JS	MIL-R-39008/2	500 mw	500 mw	10	.1 mw 1 V	<.001		MIL-STD-199 (301.2)	.000225			.000225
R3	RCR20G103JS	MIL-R-39008/2	500 mw	500 mw	10	.1 mw 1 V	<.001		MIL-STD-199 (301.2)	.000225			.000225
R4	RCR20G103JS	MIL-R-39008/2	500 mw	500 mw	10	1.1 mw 30 V	.002		MIL-STD-199 (301.2)	.000225			.000225
R5	RNR60E4993FS	MIL-R-55182/3E	125 mw	125 mw	10	.05 mw 30 V	<.001		MIL-STD-199 (302.2)	.0021			.0021
R6	RCR20G104JS	MIL-R-3900812	500 mw	500 mw	10	9 mw 30 V	.018		MIL-STD-199 (301.2)	.000225			.000225
R7	RNR60EXXXXFS*	MIL-R-55182/3E	125 mw	125 mw	10	1.8 mw 3 V	.014		MIL-STD-199 (302.2)	.0021			.0021
R8	RCR20G102JS	MIL-R-39008/2	500 mw	500 mw	10	.1 mw 1 V	<.001		MIL-STD-199 (301.2)	.000225			.000225
R9	RCR20G105JS	MIL-R-39008/2	500 mw	500 mw	10	.09 mw 30 V	<.001		MIL-STD-199 (301.2)	.000225			.000225
R10	RCR20G510Js	MIL-R-39008/2	500 mw	500 mw	10	.01 mw 21 V	<.001		MIL-STD-199 (301.2)	.000225			.000225

*Select from 500 Ω to 2K - Ω; Stress analyses and prediction computed for worst case (500Ω)

TABLE 20

DELAYED PULSE D. I. TRIGGER CIRCUIT (continued)

PART IDENTIFICATION			STRESS						PREDICTION				
			Device Rating		Applied								
Ref. Symbol	Part Number	Applicable Specification	Nominal	at 60°C	Duty Cycle %	Circuit Usage	Stress Ratio	T_N	Failure Rate Source	Base F. R. x 10^6	K_E	K_S	Application Failure Rate x 10^6
R11	RCR206822 JS	MIL-R-39008/S	500 mw	500 mw	10	.05 mw 20 V	< .001		MIL-STD-199 (301.2)	.000225	-	-	.000225
R12	RCR206512 JS	MIL-R-39008/2	500 mw	500 mw	10	.004 uw 6.8 V	< .001		MIL-STD-199 (301.2)	.000225	-	-	.000225
C1	CYR30C103 JM M23269/04-3036	MIL-C-23269/4	300 V	300 V	10	21 V	.07		MIL-STD-198 (701.2)	.10	-	-	.10
C2	CKRO6BX223 KR M39014/02-0302	MIL-C-39014/02	100 V	100 V	.183	21 V	.21		MIL-STD-198 (1001.2)	.0005	-	-	.0005
CR1	TXIN649	MIL-S-19500/290B	50 mw 600 V	50 mw 600 V	.22Bk 8.26 Fwd	1.5 uw 30 V	< .001 .05	.2	MIL-HDBK-217	.470	1.5	.1	.0705
CR2	TX2N2326A	MIL-S-19500/276A	1.4 w 1.6 a 200 V_{RM}	1.4 w 1.6 a 200 V_{RM}	10	.6 mw	< .001	.381	MIL-HDBK-217	.575	1.0	.1	.0575
CR3	TXIN753A	MIL-S-19500/127E	400 mw	368 mw	10	17.5 uw	<.001	.233	MIL-HDBK-217	.212	1.5	.1	.0318

TABLE 20

THRUSTER AND THERMAL SENSOR

PART IDENTIFICATION			STRESS						PREDICTION				
			Device Rating		Applied								
Ref. Symbol	Part Number	Applicable Specification	Nominal	at 60°C	Duty Cycle%	Circuit Usage	Stress Ratio	T_N	Failure Rate Source	Base F.R. x 10^6	K_E	K_S	Application Failure Rate x 10^6
C1A	ESXP405J20003	Dearborne FI/FRD Spec. PC 142S1000	2000 V	2000 V	8.3	1450 V	.725		See Paragraph 3.7.2.2	104.6		.1	10.46
C1B	ESXP405J2003	Dearborne FI/FRD Spec. PC 142S1000	2000 V	2000 V	8.3	1450 V	.725		See Paragraph 3.7.2.2	104.6		.1	10.46
P1	10-380729-1 Change A-4	Bendix	NA	NA	50	NA	NA		See Paragraph 3.7.2.2	~ 0			~ 0
P2	10-380729-1 Change A-4	Bendix	NA	NA	50	NA	NA		See Paragraph 3.7.2.2	~ 0			~ 0
	RTH06BS472	MIL-T-23648/1B	500mw	350mw	100	10mw	.035		MIL-HDBK-217A (page 7.12.3)	.30		.1	.03
	RNR55E8062FS	MIL-R-55182/1G	100mw	100mw	100	11mw	.11		MIL-STD-199 (302.2)	.0021			.0021
									Total Thruster Electronics Subsystems				21.926805
									Total Thruster Electronics Subsystems less main energy capacitors				1.006805

TABLE 20

CONVERTER CHARGER SUBSYSTEM HIGH VOLTAGE POWER CONVERTER

PART IDENTIFICATION			STRESS						PREDICTION				
			Device Rating		Applied								
Ref. Symbol	Part Number	Applicable Specification	Nominal	at 60°C	Duty Cycle%	Circuit Usage	Stress Ratio	T_N	Failure Rate Source	Base F.R. x 10^6	K_E	K_S	Application Failure Rate x 10^6
R1	RCR05G431JS	MIL-R-39008/4	125mw	125mw		21mw	.168		MIL-STD-199 (301.2)	.000225			.000225
R2	RNR55C99R9FS	MIL-R-55182/1	400mw	400mw		160mw	.40		MIL-STD-199 (302.2) (4 resistors)	.0005			.002000
R3	RCR05103JS	MIL-R-39008/4	125mw	125mw		<1mw	<.008		MIL-STD-199 (301.2)	.000225			.000225
R4	RCR05G222JS	MIL-R-39008/4	125mw	125mw		<1mw	<.008		MIL-STD-199 (301.2)	.000225			.000225
R5	RCR05G102JS	MIL-R-39008/4	125mw	125mw		9mw	.072		MIL-STD-199 (301.2)	.000225			.000225
R6	RCR05G472JS	MIL-R-39008/4	125mw	125mw		<1mw	<.008		MIL-STD-199 (301.2)	.000225			.000225
R7	RCR05G472JS	MIL-R-39008/4	125mw	125mw		8mw	.064		MIL-STD-199 (301.2)	.000225			.000225
R8	RCR05G472JS	MIL-R-39008/4	125mw	125mw		31mw	.248		MIL-STD-199 (301.2)	.00026			.000260
R9	RCR05G473JS	MIL-R-39008/4	125mw	125mw		3mw	.024		MIL-STD-199 (301.2)	.00025			.000250
R10	RCR05G203JS	MIL-R-39008/4	125mw	125mw		2mw	.016		MIL-STD-199 (301.2)	.000225			.000225
R11	RCR32G680JS	MIL-R-39008/3	1w	1w		530mw	.53		MIL-STD-199 (301.2)	.000700			.000700
R12, R13	MG721	Caddock	2w	2w		78.w	.039		MIL-STD-199 (302.3)	.003150		.1	.000630
R14	RNR55C1003FS	MIL-R-55182/1	100mw	100mw		<.1mw	.01		MIL-STD-199 (302.2)	.002250			.002250
*R15	RCR05GXXXJS	MIL-R-39008/4	125mw	125mw		<.1mw	<.008		MIL-STD-199 (301.2)	.000225			.000225
R16	RNR55C7682FS	MIL-R-55182/1	100mw	100mw		<.1mw	<.01		MIL-STD-199 (302.2)	.00225			.00225
R17	RCR05G753JS	MIL-R-39008/4	125mw	125mw		<.1mw	<.008		MIL-STD-199 (301.2)	.000225			.000225
R18	RCR07G151JS	MIL-R-39008/2	250mw	250mw		60mw	.24		MIL-STD-199 (301.2)	.000250			.000250
C1	CLR25BH231TGP	MIL-C-39006/1	50 V	50 V		30 V	.60		MIL-STD-198 (802.6)	.040000			.040000
C2	CKR06BX104KR	MIL-C-39014/2	100 V	100 V		40 V	.40		MIL-STD-198 (1001.2)	.000700			.000700
C3	CKR06BX103KR	MIL-C-39014/2	200 V	200 V		6 V	.03		MIL-STD-198 (1001.2)	.000500			.000500
R19	RCR05G132JS	MIL-R-390084	125mw	125mw		<001w	.008		MIL-STD-199 (301.2)	.000225			.000225
Q1	S 2N4003	MSFC SPEC 85M02714	100w 100BV_{CEO}	100w 100w		.665w 65 V	<.001 .65	.223	MIL-HDBK-217A	.411000	1	.1	.411000

* Select 510K to 1 MEG

TABLE 20

CONVERTER CHARGER SUBSYSTEM HIGH VOLTAGE POWER CONVERTER (CONTINUED)

PART IDENTIFICATION			STRESS						PREDICTION					
			Device Rating		Applied									
Ref. Symbol	Part Number	Applicable Specification	Nominal	at 60°C	Duty Cycle%	Circuit Usage	Stress Ratio	T_N	Failure Rate Source	Base F.R. x 10^6	K_E	K_S	Application Failure Rate x 10^6
Q2	TX2N2222A	MIL-S-19500/255E	500mw 50 BV_{CEO}	383mw 50 V		5.6mw 12 V	015 .240	.211	MIL-HDBK-217A	.196400	1.5	.1	.029400
Q3	TX2N2222A	MIL-S-19500/255E	500mw, 50 BV_{ECO}	383mw, 50V		< .1mw	< 001	.2	MIL-HDBK-217A	.195	1.5	.1	.02925
Q4	TX2N2222A	MIL-S-19500/255E	500mw 50 BV_{ECO}	383mw 50 V		.54mw 6.5 V	.001 .13	.2	MIL-HDBK-217A	.195	1.5	.1	.029250
D1, D2 D3, D4	TX1N5615	MIL-S-19500/429	1w 200 V	883mw		14mw		.223	MIL-HDBK-217A	.208	1.5	.1	.124800
D5	TX1N5615	MIL-S-19500/429	1w 200 V	883mw		10mw 65 V		.217	MIL-HDBK-217A	.207	1.5	.1	.031050
D6	TX1N5615	MIL-S-19500/429	1w 200 V	883mw		10mw 65 V		.217	MIL-HDBK-217A	.207	1.5	.1	.031050
D7	TX1N2992	MIL-S-19500/124	10w	10w		390mw	.039	.233	MIL-HDBK-217A	.3196	1.5	.1	.047940
D8	SCF5000	SEMTECH; WILMORE P/N 35A0008	PIV=7.5KV (1W)			PIV=3.5KV (16.6mw)	.466 (.017)	(.228)	MIL-HDBK-217A (12, TX1N5619)	.242	1.5	.1	.435600
D9	TX1N4148	MIL-S-19500/116	75mw 75 V	58mw		.3mw .7 V	.005 .009	.2	MIL-HDBK-217A	.195	1.5	.1	.029250
D10	TX1N5615	MIL-S-19500/429	1.2W 200 V	1.08W		1.5mw 6 V	.001 .03	.206	MIL-HDBK-217A	.28	1.5	.1	.042000
C4	CKR06BX104 KR	MIL-C-39014/2	100 V	100 V		5 V	.05		MIL-STD-198 (1001.2)	.0015			.001500
T1		WILMORE				ΔT = 5°c			MIL-HDBK-217A (7.7)	.21	1.5	.1	.315000
T2		WILMORE				ΔT = 12°c			MIL-HDBK-217A(7.7)	.21	1.5	.1	.315000

TABLE 20

CONVERTER-CHARGER SUBSYSTEM
AUXILIARY POWER SUPPLY

PART IDENTIFICATION			STRESS						PREDICTION					
			Device Rating		Applied									
Ref. Symbol	Part Number	Applicable Specification	Nominal	at 60°C	Duty Cycle %	Circuit Usage	Stress Ratio	T_N	Failure Rate Source	Base F.R. x 10^6	K_E	K_S	Application Failure Rate x 10^6
R1	RCR07G153JS	MIL-R-39008/1	250 mw	250 mw		60 mw	.24		MIL-STD-199 (301.2)	.000250			.000250
R2, 3	RCR07G131JS	MIL-R-39008/1	250 mw	250 mw		70 mw	.28		MIL-STD-199 (301.2)	.000300			.000600
R4	RCR07G623JS	MIL-R-39008/1	250 mw	250 mw		60 mw	.24		MIL-STD-199 (301.2)	.000250			.000250
R5	RCR70F1202P	MIL-R-39008/1	15 W	12.9 W		.296 W	.023		MIL-HDBK-217A	.008400			.008400
R6	RCR60F4701M	MIL-R-39009/1	5 W	4.27 W		.104 W	.024		MIL-HDBK-217A	.084000			.084000
R7	M6 680	CADDOCK	800 mw	800 mw		41 mw	.051		MIL-STD-199 (302.3)	.003150			.003150
R8	RNR55C8062FS	MIL-R-55182/1	100 mw	100 mw		< 1 mw	<.01		MIL-STD-199 (302.2)	.002100			.000225
R9	RCR05G160JS	MIL-R-39008/4	125 mw	125 mw		16 mw	.121		MIL-STD-199 (301.2)	.000225			.000225
R10	RCR05G103JS	MIL-R-39008/4	125 mw	125 mw		< 1 mw	.008		MIL-STD-199 (301.2)	.000225			.000225
R11	RCR05G474JS	MIL-R-39008/4	125 mw	125 mw		< 1 mw	.008		MIL-STD-199 (301.2)	.000225			.000225
R12	RCR05G224JS	MIL-R-39008/4	125 mw	125 mw		< 1 mw	.008		MIL-STD-199 (301.2)	.000225			.000225
R13	RCR05G274JS	MIL-R-39008/4	125 mw	125 mw		< 1 mw	.008		MIL-STD-199 (301.2)	.000225			.000225
R14	RCR05G113JS	MIL-R-39008/4	125 mw	125 mw		13 mw	.104		MIL-STD-199 (301.2)	.000225			.000225
R15	RCR05G204JS	MIL-R-39008/4	125 mw	125 mw		4.2 mw	.034		MIL-STD-199 (301.2)	.000370			.000370
R17	RCR05G302JS	MIL-R-39008/4	125 mw	125 mw		1 mw	.008		MIL-STD-199 (301.2)	.000225			.000225
R18	RCR05G273JS	MIL-R-39008/4	125 mw	125 mw		31 mw	.248		MIL-STD-199 (301.2)	.000225			.000225
C1	CKR06BX103KR	MIL-R-39014/2	200 V	200 V		60 V	.30		MIL-STD-198 (1001.2)	.0005			.0005
C2	CLR25BH100 MP	MIL-C-39006/1	50 V	50 V		30 V	.60		MIL-STD-198 (802.6)	.04			.04
C3, C4	CPV09A1KF473KR	MIL-C-14157/2	600 V	600 V		310 V	.517		MIL-C-14157E	.004			.008
C5, C6	CLR25BE700UP	MIL-C-39006/1	25 V	25 V		13 V	.52		MIL-STD-198 (802.6)	.035			.07
D1, D2	TX1N5615	MIL-S-19500/429	1 W	883 mw		.12 mw	<.004	.2	MIL-HDBK-217A	.195	1.5	.1	.0585
D3, D4	TX1N5615	MIL-S-19500/429	1 W	883 mw		1.0 mw	.001	.2	MIL-HDBK-217A	.195	1.5	.1	.0585
D5, D6	TX1N5623	MIL-S-19500/429	1 W	883 mw		5 mw	.006	.211	MIL-HDBK-217A 2 diodes ea.	.1964	1.5	.1	.11784
D7, D8	TX1N5615	MIL-S-19500/429	1 W	883 mw		25 mw	.028	.246	MIL-HDBK-217A	.220	1.5	.1	.132
D9, D10 D11 D12	TX1N4148	MIL-S-19500/116	75 mw	62.8 mw		.1 mw	.0015	.2	MIL-HDBK-217A	.195	1.5	.1	.0585

TABLE 20

CONVERTER CHARGER SUBSYSTEM
AUXILIARY POWER SUPPLY ((Continued)

PART IDENTIFICATION			STRESS						PREDICTION					
			Device Rating		Applied									
Ref. Symbol	Part Number	Applicable Specification	Nominal	at 60°C	Duty Cycle%	Circuit Usage	Stress Ratio	T_N	Failure Rate Source	Base F.R. x 10^6	K_E	K_S	Application Failure Rate x 10^6
Q1,Q2	TX2N3019	MIL-S-19500/391	800 mw 80 V_{CEO}	739 mw 80 V		50 mw 65 V	.068 .18	.263	MIL-HDBK-217A	.2307	1.5	.1	.06921
Q3	TX2N2905A	MIL-S-19500/290	600 mw 60 BV_{CBO}	480 mw 60 V		10 mw 12 V	.021 .20	.217	MIL-HDBK-217A	.970	1.5	.1	.1455
Q4	TX2N2907A	MIL-S-19500/291	400 mw 60 BV_{CBO}	321.2 mw 60 V		<.1 mw 12 V	<.001 .20	.2	MIL-HDBK-217A	.470	1.5	.1	.0705
Q5	TX2N2222A	MIL-S-19500/255E	500 mw 50 BV_{ECO}	383 mw 50 V		<.1 mw 8 V	<.001 .016	.2	MIL-HDBK-217A	.195	1.5	.1	.02925
Q6	TX2N2222A	MIL-S-19500/255E	500 mw 50 BV_{ECO}	383 mw 50 V		.5 mw 12 V	<.001 .24	.2	MIL-HDBK-217A	.195	1.5	.1	.02925
Q7	TX2N2905A	MIL-S-19500/290	600 mw 60 BV_{CBO}	480 mw 60 V		10 mw 30 V	.002 .5	.217	MIL-HDBK-217A	.970	1.5	.1	.1455
Q8	TX2N222A	MIL-S-19500/255E	500 mw 50 BV_{ECO}	383 mw 50 V		.5 mw 30 V	<.001 .6	.2	MIL-HDBK-217A	.195	1.5	.1	.62925
T1		WILMORE				ΔT = 5°C			MIL-HDBK 217A (7.7)	.21	1.5	.1	.315

TABLE 20

CONVERTER CHARGER SUBSYSTEM COMPARATOR - REGULATOR

PART IDENTIFICATION			STRESS						PREDICTION				
			Device Rating		Applied								
Ref. Symbol	Part Number	Applicable Specification	Nominal	at 60°C	Duty Cycle%	Circuit Usage	Stress Ratio	T_N	Failure Rate Source	Base F.R. x 10^6	K_E	K_S	Application Failure Rate x 10^6
R1	RCR05G824 JS	MIL-R-39008/4	125 mw	125 mw		< 1 mw	<.008		MIL-STD-199 (301.2)	.000225			.000225
R2	RCR05G914 JS	MIL-R-39008/4	125 mw	125 mw		< 1 mw	<.008		MIL-STD-199 (301.2)	.000225			.000225
R3	RCR05G434 JS	MIL-R-39008/4	125 mw	125 mw		< 1 mw	<.008		MIL-STD-199 (301.2)	.000225			.000225
R4	RNR60C3653 FS	MIL-R-55182/3	125 mw	125 mw		< 1 mw	<.008		MIL-STD-199 (302.2)	0.00210			0.00210
R5	RNR60C1213 FS	MIL-R-55182/3	125 mw	125 mw		< 1 mw	<.008		MIL-STD-199 (302.2)	0.00210			0.00210
R6	RCR05G473 JS	MIL-R-39008/4	125 mw	125 mw		<1 mw	<.008		MIL-STD-199 (301.2)	.000225			.000225
R7	RCR05G204 JS	MIL-R-39008/4	125 mw	125 mw		< 1 mw	<.008		MIL-STD-199 (301.2)	.000225			.000225
R8	RCR05G684 JS	MIL-R-39008/4	125 mw	125 mw		< 1 mw	<.008		MIL-STD-199 (301.2)	.000225			.000225
R9	RCR05G684 JS	MIL-R-39008/4	125 mw	125 mw		< 1 mw	<.008		MIL-STD-199 (301.2)	.000225			.000225
R10	RCR05G334 JS	MIL-R-39008/4	125 mw	125 mw		<1 mw	<.008		MIL-STD-199 (301.2)	.000225			.000225
R11	RCR05G204 JS	MIL-R-39008/4	125 mw	125 mw		<1 mw	<.008		MIL-STD-199 (301.2)	.000225			.000225
R12 R13 R14	RCR05G104 JS	MIL-R-39008/4	125 mw	125 mw		< 1 mw	<.008		MIL-STD-199 (301.2)	.000225			.000675
R15 R16	RCR05G103 JS	MIL-R-39008/4	125 mw	125 mw		4 mw	.032		MIL-STD-199 (301.2)	.00032			.00064
R17	RCR05G511 JS	MIL-R-39008/4	125 mw	125 mw		<1 mw	<.008		MIL-STD-199 (301.2)	.000225			.000225
R18	RCR05G102 JS	MIL-R-39008/4	125 mw	125 mw		<64 mw	.512		MIL-STD-199 (301.2)	.00067			.00067
R19	RCR05G102 JS	MIL-R-39008/4	125 mw	125 mw		20 mw	.16		MIL-STD-199 (301.2)	.000225			.000225
D1	FCT-1125	Fairchild Wilmore P/N 35A-0005-A	400 mw	368 mw		.67 mw	.002	.24	MIL-HDBK 217A	.2166	1.5	.1	.03249
Q1,Q2	TX2N930	MIL-S-19500/253	300 mw 45 BV_{CEO}	230 mw 45 V		2.5 uw 7 V	<.001 .155	.234	MIL-HDBK 217 A	.213	1.5	.1	.06390
Q3,Q4	JAN2N2605	MIL-S-19500/354	360 mw 45 BV_{CEO}	288 mw 45 V		70 uw 7 V	<.001 .1	.2	MIL-HDBK 217 A	.470	1.5	.1	.1410
Q5	TX2N930	MIL-S-19500/253	300 mw 45 BV_{CEO}	230 mw 45 V		.72 mw 6 V	.003 .133	.234	MIL-HDBK 217 A	.213	1.5	.1	.03195
Q6	JAN2N2605	MIL-S-19500/354	360 mw 45 BV_{CEO}	288 mw 45 V		.6 mw 12 V	.002 .171	.2	MIL-HDBK 217 A	.470	1.5	.1	.0705
Q7	TX2N2222A	MIL-S-19500/255	500 mw 50 BV_{ECO}	383 mw 50 V		.4 mw 12 V	.001 .24	.2	MIL-HDBK 217 A	0.195	1.5	.1	0.02925

TABLE 20

CONVERTER CHARGER SUBSYSTEM
DELAY TIME GENERATOR (CONTINUED)

PART IDENTIFICATION			STRESS						PREDICTION				
			Device Rating		Applied								
Ref. Symbol	Part Number	Applicable Specification	Nominal	at 60°C	Duty Cycle%	Circuit Usage	Stress Ratio	T_N	Failure Rate Source	Base F.R. x 10^6	K_E	K_S	Application Failure Rate x 10^6
R29	RCR05G205JS	MIL-R-39008/4	125mw	125mw		< 1mw	<.008		MIL-STD-199 (301.2)	.000225			.000225
R30	RNR55C4532FS	MIL-R-55182/4	100mw	100mw		< 1mw	<.01		MIL-STD-199 (302.2)	.0021			.0021
R31	RNR55C6982FS	MIL-R-55182/1	100mw	100mw		< 1mw	<.01		MIL-STD-199 (302.2)	.0021			.0021
R33	RCR05G334JS	MIL-R-39008/4	125mw	125mw		< 1mw	<.008		MIL-STD-199 (301.2)	.000225			.000225
R35	RCR05G155JS	MIL-R-39008/4	125mw	125mw		< 1mw	<.008		MIL-STD-199 (301.2)	.000225			.000225
R41	RNR60C2493FS	MIL-R-55182/3	125mw	125mw		< 1mw	<.008		MIL-STD-199 (302.2)	.0021			.0021
R42	RNR55C6982FS	MIL-R-55182/1	100mw	100mw		< 1mw	<.01		MIL-STD-199 (302.2)	.0021			.0021
R43	RCR05G621JS	MIL-R-39008/4	125mw	125mw		40mw	.32		MIL-STD-199 (301.2)	.000225			.000225
R44	RCR05G104JS	MIL-R-39008/4	125mw	125mw		< 2mw	<.016		MIL-STD-199 (301.2)	.000225			.000225
R45	RCR05G104JS	MIL-R-39008/4	125mw	125mw		< 2mw	<.016		MIL-STD-199 (301.2)	.000225			.000225
R47	RCR05G474JS	MIL-R-39008/4	125mw	125mw		1.4 mw	<.01		MIL-STD-199 (301.2)	.000225			.000225
R48	RNR55C4532FS	MIL-R-55182/1	100mw	100mw		< 1mw	<.01		MIL-STD-199 (302.2)	.0021			.0021
R49	RCR05G154JS	MIL-R-39008/4	125mw	125mw		< 1mw	<.008		MIL-STD-199 (301.2)	.000225			.000225
R51	RCR05103JS	MIL-R-39008/4	125mw	125mw		10 mw	.08		MIL-STD-199 (301.2)	.000225			.000225
R52	RCR05G154JS	MIL-R-39008/4	125mw	125mw		< 1mw	<.008		MIL-STD-199 (301.2)	.000225			.000225
R53	RCR05G104JS	MIL-R-39008/4	125mw	125mw		< 2mw	<.016		MIL-STD-199 (301.2)	.000225			.000225
R54	RCR05G274JS	MIL-R-39008/4	125mw	125mw		< 1mw	<.008		MIL-STD-199 (301.2)	.000225			.000225
R55	RCR05G104JS	MIL-R-39008/4	125mw	125mw		< 2mw	<.016		MIL-STD-199 (301.2)	.000225			.000225
R50	RCR05G243JS	MIL-R-39008/4	125mw	125mw		6mw	.048		MIL-STD-199 (301.2)	.000225			.000225
C1	CKR06BX104KR	MIL-C-39014/2	100 V	100 V		13 V	.13		MIL-STD-198 (1001.2)	.00005			.00005
C2	CKR06BX103KR	MIL-C-39014/2	200 V	200 V		.7 V	.0035		MIL-STD-198 (1001.2)	.00005			.00005
C3	CKR06BX104KR	MIL-C-39014/2	100 V	100 V		13 V	.13		MIL-STD-198 (1001.2)	.00005			.00005
C4	CKR06BX104KR	MIL-C-39014/2	100 V	100 V		5 Vp	.05		MIL-STD-198 (1001.2)	.00005			.00005

TABLE 20

CONVERTER CHARGER SUBSYSTEM
DELAY TIME GENERATOR (CONTINUED)

PART IDENTIFICATION			STRESS						PREDICTION				
			Device Rating		Applied								
Ref. Symbol	Part Number	Applicable Specification	Nominal	at 60°C	Duty Cycle %	Circuit Usage	Stress Ratio	T_N	Failure Rate Source	Base F.R. x 10^6	K_E	K_S	Application Failure Rate x 10^6
C6	CKR06BX104KR	MIL-C-39014/2	100 V	100 V		12 V	.12		MIL-STD-198 (1001.2)	.00005			.00005
C7	CKR06BX474KR	MIL-C-39014/2	100 V	100 V		5 V	.05		MIL-STD-198 (1001.2) (6, .47 uf capacitors)	.00005			.00030
C8	CKR06BX474KR	MIL-C-39014/2	100 V	100 V		5 V	.05		MIL-Std-198 (1001.2) (4, .47uf capacitors)	.00005			.00020
C10	CKR06BX103KR	MIL-C-39014/2	200 V	200 V		.7 V	.0035		MIL-STD-198 (1001.2)	.00005			.00005

TABLE 20

CONVERTER CHARGER SUBSYSTEM DELAY TIME GENERATOR (Continued)

PART IDENTIFICATION			STRESS						PREDICTION				
			Device Rating		Applied								
Ref. Symbol	Part Number	Applicable Specification	Nominal	at 60°C	Duty Cycle%	Circuit Usage	Stress Ratio	T_N	Failure Rate Source	Base F.R. x 10^6	K_E	K_S	Application Failure Rate x 10^6
D1	TX1N4148	MIL-S-19500/116E	75mw	58mw		.25mw	.004	.2	MIL-HDBK-217A	.195	1.5	.1	.02925
D2	TX1N4148	MIL-S-19500/116E	75mw 75V	58mw 75V		10uw 5V	<.001 .067	.2	MIL-HDBK-217A	.195	1.5	.1	.02925
D3	FCT-1125	Fairchild	400mw	368mw		.67mw	.002	.24	MIL-HDBK-217A	.2166	1.5	.1	.03249
D4	TX1N4148	MIL-S-19500/116E	75mw 75V	58mw 75V		10uw 6.7V	<.001 .089	.2	MIL-HDBK-217A	.195	1.5	.1	.02925
D5	TX1N4148	MIL-S 19500/116E	75mw 75V	58mw 75V		40uw 13V	<.001 .173	.2	MIL-HDBK-217A	.195	1.5	.1	.02925
D8	TX1N4148	MIL-S-19500/116E	75mw 75V	58mw 75V		2.5uw 5V	<.001 .067	.2	MIL-HDBK-217A	.195	1.5	.1	.02925
D9	TX1N4148	MIL-S-19500/116E	75mw	58mw		.1mw	.002	.2	MIL-HDBK-217A	.195	1.5	.1	.02925
D10	TX1N4148	MIL-S-19500/116E	75mw 75V	58mw 75V		1mw 13V	.017 .173	.2	MIL-HDBK-217A	.195	1.5	.1	.02925

TABLE 20

CONVERTER-CHARGER SUBSYSTEM
DELAY TIME GENERATOR (Continued)

PART IDENTIFICATION			STRESS						PREDICTION				
			Device Rating		Applied								
Ref. Symbol	Part Number	Applicable Specification	Nominal	at 60°C	Duty Cycle%	Circuit Usage	Stress Ratio	T_N	Failure Rate Source	Base F.R. x 10^6	K_E	K_S	Application Failure Rate x 10^6
Q1	TX2N2222A	MIL-S-19500/255E	500 mw 50 BV_{CEO}	383 mw 50 V		.8 mw	.002	.2	MIL-HDBK-217A	.195	1.5	.1	.02925
Q2	JAN2N2605	MIL-S-19500/354	360 mw 70 BV_{CBO}	288 mw 70 V		.14 mw 7 V	<.001 .1	.24	MIL-HDBK-217A	.542	1.5	.1	.0813
Q3	TX2N930	MIL-S-19500/253	300 mw 45 BV_{CEO}	230 mw 45 V		.14 mw 14 V	<.001 .311	.2	MIL-HDBK-217A	.195	1.5	.1	.02925
Q4	TX2N930	MIL-S-19500/253	300 mw 45 BV_{CEO}	230 mw 45 V		.12 mw 12 V	<.001 .267	.234	MIL-HDBK-217A	.213	1.5	.1	.03195
Q5	TX2N930	MIL-S-19500/253	300 mw 45 BV_{CEO}	230 mw		.12 mw 12 V	<.001 .267	.234	MIL-HDBK-217A	.213	1.5	.1	.03195
Q6	JAN2N2605	MIL-S-19500/354	360 mw 45 BV_{CEO}	288 mw		.375 mw 25 V	.001 .56	.20	MIL-HDBK-217A	.470000	1.5	.1	.070500
Q7	TX2N930	MIL-S-19500/253	300 mw 45 BV_{CEO}	230 mw		.925 mw 25 V	.004 .56	.24	MIL-HDBK-217A	.217000	1.5	.1	.032550
Q8	TX2N930	MIL-S-19500/253	300 mw 45 BV_{CEO}	230 mw		1.2 mw 12 V	.005 .267	.24	MIL-HDBK-217A	.217000	1.5	.1	.032550
Q10	JAN2N2605	MIL-S-19500/354	360 mw 45 BV_{CEO}	288 mw		.324 mw 12 V	001 .267	.20	MIL-HDBK-217A	.470000	1.5	.1	.070500
Q11	TX2N930	MIL-S-19500/253	300 mw 45 BV_{CEO}	230 mw		.153 mw 17 V	<.001 .378	.234	MIL-HDBK-217A	.531000	1.5	.1	.079500
Q12	TX2N930	MIL-S-19500/253	300 mw 45 BV_{CEO}	230 mw		.12 mw 12 V	<.001 .267	.234	MIL-HDBK-217A	.213000	1.5	.1	.031950
Q13	TX2N930	MIL-S-19500/253	300 mw 45 BV_{CEO}	230 mw 45 V		.12 mw 12 V	<.001 .267	.234	MIL-HDBK-217A	.213	1.5	0.1	.03195
Q14	JAN2N2605	MIL-S-19500/354	360 mw 70 BV_{CBO}	288 mw 70 V		60 μ w 12 V	<.001 .171	.2	MIL-HDBK-217A	.470	1.5	0.1	.0705

TABLE 20

CONVERTER-CHARGER SUBSYSTEM
DELAY TIME GENERATOR (Continued)

PART IDENTIFICATION			STRESS						PREDICTION				
			Device Rating		Applied								
Ref. Symbol	Part Number	Applicable Specification	Nominal	at 60°C	Duty Cycle%	Circuit Usage	Stress Ratio	T_N	Failure Rate Source	Base F.R. x 10^6	K_E	K_S	Application Failure Rate x 10^6
Q15	TX2N930	MIL-S-19500/253	300 mw 45 BV_{CEO}	230 mw 45 V		1.2 mw 12 V	.005 .367	.24	MIL-HDBK-217A	.240	1.5	0.1	.03255
Q16	JAN2N2605	MIL-S-19500/354	360 mw 70 BV_{CBO}	288 mw 70 V		.14 mw 12V	<.001 .171	.2	MIL-HDBK-217A	.470	1.5	0.1	.0705
Q18	TX2N2222A	MIL-S-19500/255	500 mw 50 BV_{ECO}	383 mw 50 V		50 μw 5 V	<.001 .1	.2	MIL-HDBK-217A	0.195	1.5	0.1	0.02925
Q19	TX2M2222A	MIL-S-19500/255	500 mw 50 BV_{ECO}	383 mw 50 V		6 mw 12 V	.016 .24	.2	MIL-HDBK-217A	0.195	1.5	0.1	0.02925
Q20	JAN2N2605	MIL-S-19500/354	360 mw 70 BV_{CEO}	288 mw 70 V		13.2 mw 12 V	.046	.234	MIL-HDBK-217A	.531	1.5	0.1	.0795
Q21	TX2N2222A	MIL-S-19500/255	500 mw 50 BV ECO	383 mw 50 V		1.2 mw 12 V	.003 .24	.2	MIL-HDBK-217A	0.195	1.5	0.1	0.02925

TABLE 20

CONVERTER CHARGER SUBSYSTEM TELEMETRY AMPLIFIER

PART IDENTIFICATION			STRESS						PREDICTION				
			Device Rating		Applied								
Ref. Symbol	Part Number	Applicable Specification	Nominal	at 60°C	Duty Cycle %	Circuit Usage	Stress Ratio	T_N	Failure Rate Source	Base F.R. x 10^6	K_E	K_S	Application Failure Rate x 10^6
R1	RCR05G104JS	MIL-R-39008/4	125mw	125mw		< 1mw	.008		MIL-STD-199(301.2)	.000225			.000225
R2	RCR05G105JS	MIL-R-39008/4	125mw	125mw		< 1mw	.008		MIL-STD-199(301.2)	.000225			.000225
R3	RCR05G511JS	MIL-R-39008/4	125mw	125mw		60mw	.48		MIL-STD-199(301.2)	.000600			.00600
R4	RCR05G474JS	MIL-R-39008/4	125mw	125mw		< 1mw	.003		MIL-STD-199(301.2)	.000225			.000225
R5	RCR05G103JS	MIL-R-39008/4	125mw	125mw		.33mw	.264		MIL-STD-199(301.2)	.000280			.000280
R6	RCR05G511JS	MIL-R-39008/4	125mw	125mw		< 1mw	.008		MIL-STD-199(301.2)	.000225			.000225
C1	CKR06BX103KR	MIL-C-39014/2	200V	200V		6V	.03		MIL-STD-198(1001.2)	.000050			.000050
D2	TX1N752A	MIL-S-19500/127	400mw	368mw		5.6mw	.015	.096	MIL-HDBK-217A	.415000	1.0	.1	.041500
Q1	JAN2N2605	MIL-S-19500/354	360mw 70BV_{CBO}	288mw		60uw 12 V_{CE}	<.001 .172	.20	MIL-HDBK-217A	.470000	1.5	.1	.070500
Q2	TX2N930	MIL-S-19500/253	300mw 45BV_{CEO}	230mw		.36mw 12 V_{CE}	.001 .468	.234	MIL-HDBK-217A	.213000	1.5	.1	.031950
Q3	JAN2N2605	MIL-S-19500/354	360mw 70BV_{CBO}	288mw		.6mw 12 V_{CE}	.002 .172	.20	MIL-HDBK-217A	.470000	1.5	.1	.070500
									Total Telemetry Amplifier				.216280
									4 Telemetry Amplifiers				.865120

TABLE 20

CONVERTER CHARGER SUBSYSTEM DELAY TIME GENERATOR

PART IDENTIFICATION			STRESS						PREDICTION				
			Device Rating		Applied								
Ref. Symbol	Part Number	Applicable Specification	Nominal	at 60°C	Duty Cycle%	Circuit Usage	Stress Ratio	T_N	Failure Rate Source	Base F.R. x 10^6	K_E	K_S	Application Failure Rate x 10^6
R1	RCR05G473JS	MIL-R-39008/4	125mw	125mw		< 1mw	<.008		MIL-STD-199 (301.2)	.000225			.000225
R2	RCR05G224JS	MIL-R-39008/4	125mw	125mw		< 1mw	<.008		MIL-STD-199 (301.2)	.000225			.000225
R3	RCR05G511JS	MIL-R-39008/4	125mw	125mw		< 1mw	<.008		MIL-STD-199 (301.2)	.000225			.000225
R4	RNR55C4532JS	MIL-R-55182/1	100mw	100mw		< 1mw	<.01		MIL-STD-199 (302.2)	.00210			.002100
R5	RNR55C6982FS	MIL-R-55182/1	100mw	100mw		< 1mw	<.01		MIL-STD-199 (302.2)	.0021			.002100
R6	RNR55C6982FS	MIL-R-55182/1	100mw	100mw		< 1mw	<.01		MIL-STD-199 (302.2)	.0021			.002100
R7	RNR55C4532JS	MIL-R-55182/1	100mw	100mw		< 1mw	<.01		MIL-STD-199 (302.2)	.0021			.002100
R8	RCR05G511JS	MIL-R-39008/4	125mw	125mw		< 1mw	<.008		MIL-STD-199 (301.2)	.000225			.000225
R9	RNR60C2213FS	MIL-R-55182/3	125mw	125mw		< 1mw	<.008		MIL-STD-199 (302.2)	.0021			.002100
R10	RNR60C4423FS	MIL-R-55182/3	125mw	125mw		< 1mw	<.008		MIL-STD-199 (302.2)	.0021			.002100
R11	RCR05G473JS	MIL-R-39008/4	125mw	125mw		< 3mw	.024		MIL-STD-199 (301.2)	.000225			.000225
R12	RCR05513JS	MIL-R-39008/4	125mw	125mw		< 1mw	<.008		MIL-STD-199 (301.2)	.000225			.000225
R13	RNR60C1783FS	MIL-R-55182/3	125mw	125mw		< 1mw	<.008		MIL-STD-199 (302.2)	.0021			.002100
R14	RNR55C1003FS	MIL-R-55182/1	100mw	100mw		< 1mw	<.008		MIL-STD-199 (302.2)	.0021			.002100
R15	RCR05G105JS	MIL-R-39008/4	125mw	125mw		< 1mw	<.008		MIL-STD-199 (301.2)	.000225			.000225
R16	RCR05G334JS	MIL-R-39008/4	125mw	125mw		< 1mw	<.008		MIL-STD-199 (301.2)	.000225			.000225
R17	RCR05G155JS	MIL-R-39008/4	125mw	125mw		< 1mw	<.008		MIL-STD-199 (301.2)	.000225			.000225
R19	RCR05G514JS	MIL-R-39008/4	125mw	125mw		< 1mw	<.008		MIL-STD-199 (301.2)	.000225			.000225
R20	RCR05G334JS	MIL-R-39008/4	125mw	125mw		< 1mw	<.008		MIL-STD-199 (301.2)	.000225			.000225
R21	RCR05G155JS	MIL-R-39008/4	125mw	125mw		< 1mw	<.008		MIL-STD-199 (301.2)	.000225			.000225
R22	RCR05G474JS	MIL-R-39008/4	125mw	125mw		< 1mw	<.008		MIL-STD-199 (301.2)	.000225			.000225
R26	RNR55C4532FS	MIL-R-55182/1	100mw	100mw		< 1mw	<.01		MIL-STD-199 (302.2)	.0021			.0021
R27	RNR55C6982FS	MIL-R-55182/1	100mw	100mw		< 1mw	<.01		MIL-STD-199 (302.2)	.0021			.0021
R28	RNR60C1503FS	MIL-R-55182/3	125mw	125mw		< 1mw	<.008		MIL-STD-199 (302.2)	.0021			.0021

TABLE 20

CONVERTER CHARGER SUBSYSTEM COMPARATOR - REGULATOR (continued)

PART IDENTIFICATION			STRESS						PREDICTION				
			Device Rating		Applied								
Ref. Symbol	Part Number	Applicable Specification	Nominal	at 60°C	Duty Cycle %	Circuit Usage	Stress Ratio	T_N	Failure Rate Source	Base F. R. x 10^6	K_E	K_S	Application Failure Rate x 10^6
C1	CKR06BX104 KR	MIL-C-39014/2	100 V	100 V		12 V	.12		MIL-STD-198 (1001.2)	.00005			.00005
C2	CKR05BX680 KR	MIL-C-39014/1	100 V	100 V		7 V	.07		MIL-STD-198 (1001.2)	.00005			.00005
C3	CKR06BX122 KR	MIL-C-39014/2	100 V	100 V		12 V	.12		MIL-STD-198 (1001.2)	.00005			.00005

TABLE 20

CONVERTER CHARGER SUBSYSTEM
ENABLE SWITCH

PART IDENTIFICATION			STRESS						PREDICTION				
			Device Rating		Applied								
Ref. Symbol	Part Number	Applicable Specification	Nominal	at 60°C	Duty Cycle %	Circuit Usage	Stress Ratio	T_N	Failure Rate Source	Base F.R. x 10^6	K_E	K_S	Application Failure Rate x 10^6
R1	RCR05G621JS	MIL-R-39008-4	125 mw	125 mw		< 1 mw	.008		MIL-STD-199 (301.2)	.000225			.000225
R2	RCR05G622JS	MIL-R-39008/4	125 mw	125 mw		< 1 mw	.008		MIL-STD-199 (301.2)	.000225			.000225
R3	RCR05G303JS	MIL-R-39008/4	125 mw	125 mw		30 mw	.24		MIL-STD-199 (301.2)	.000250			.000250
R4	RCR05G105JS	MIL-R-39008/4	125 mw	125 mw		< 1 mw	.008		MIL-STD-199 (301.2)	.000225			.000225
R5	RCR05G204JS	MIL-R-39008/4	125 mw	125 mw		< 1 mw	.008		MIL-STD-199 (301.2)	.000225			.000225
D1,2	TX1N4148	MIL-S-19500/116	75 mw	58 mw		21 μw	<.001		MIL-HDBK-217A	.195000	1.5	.1	.058500
Q1	TX2N2905A	MIL-S-19500/290	600 mw 60 BV_{CEO}	480 mw 60 V		105 mw 30 V	.219 .5	.377	MIL-HDBK-217A	1.700000	1.5	.1	.255000
Q2	TX2N2907A	MIL-S-19500/291	400 mw 60 BV_{CEO}	320 mw 60 V		1.5 mw 30 V	.005 .5	.20	MIL-HDBK-217A	.470000	1.5	.1	.070500
Q3	TX2N2222A	MIL-S-19500/255	500 mw 50 BV_{CEO}	383 mw 50 V		.2 mw 30 V	<.001 .6	.20	MIL-HDBK-217A	.195000	1.5	.1	.029250
									Total Converter-Charger Subsystem				5.737845

g) A series reliability model is assumed, i.e., the failure of any part is defined as a system failure.

Based upon the foregoing assumptions and conditions, the SMS microthruster reliability may be computed as follows:

$$R = \exp\left(-\sum_{i=1}^{n} \lambda_i t\right)$$

where λ_i is the application failure rate of the ith part shown in the last column of Table 20, and t is the thruster operating time during the five year mission. Thus, the thruster reliability, $R_T = \exp - (27.66465 \times 10^{-6})\ (3030) = \exp - .083824 = .916176$. Similarly the reliability of the thruster less the main energy storage capacitors, $R_E = \exp - (6.74465 \times 10^{-6})\ (3030) = \exp - .020436 = .979564$.

3.7.4 Summary and Conclusions

The reliability study of the SMS pulsed plasma microthruster shows that:

a) The predicted reliability of a single Fairchild Republic microthruster for a five year mission is .92.

b) Predicted microthruster reliability less the main energy storage capacitors is .98.

c) An overwhelming percentage of microthruster system electronic parts have been selected from the flight category of GSFC-PPL-11, Preferred Parts List.

d) The SMS microthruster derating criteria set forth in Appendix A has been satisfied.

e) The results of the quantitative reliability prediction are conservative since the computation is based upon worst case operating conditions. Reliability may be expected to increase if the severity of the parts usage thermal environment is reduced.

The numerical failure rates used in the analysis are slightly pessimistic. In the case of RCR and RNR resistors, the applied operating stresses were often considerably below the minimum values listed in the failure rate derivations source. Extrapolation of the failure rate curves was not permitted and the lowest tabulated stresses were used.

3.7.5 Derating Criteria for the SMS Microthruster

The following tables present the derating criteria imposed on the electrical components in the design analysis.

TABLE 21 -Derating Criteria Tables

Table 21a. Derating Outline For Capacitors

Dielectric Class	Derate To	Remarks
Ceramic	50% of rated voltage	All capacitors: Except as noted below, capacitors shall not be used at ambient temperatures exceeding 85°C. The design shall also provide proper derating of capacitors operated under AC, pulse or transient voltages specified in applicable specifications.
Mica (Dipped)	60% of rated voltage	
Mica (Molded)	40% of rated voltage	
Paper	50% of rated voltage	
Mylar	75% of rated voltage	
Glass or Porcelain	50% of rated voltage	
Tantalum (Solid electrolytic) 3 ohm/volt surge limiting resistor	60% of rated voltage	
0.1 ohm/volt surge limiting resistor	40% of rated voltage	Ambient temperature shall not exceed 50°C.
Tantalum (Wet electrolytic)	70% of rated voltage	Ambient temperature shall not exceed 70°C.
Tantalum (Foil)	70% of rated voltage	

Table 21b DERATING OUTLINE OF CONNECTORS

Number of Contacts Used in Connector	Contact Size	Maximum Current per contact[1/] (Amperes)					Remarks
		Wire Size (AWG)					
		16	18	20	22	24	
1 to 4	16	13.0	9.2	6.5			All connectors: Maximum allowable operating voltage shall be 25% of the dielectric withstanding voltage rating for the anticipated environment.
1 to 4	20			6.0	4.5	3.3	
5 to 14	16	9.0	7.0	5.0			
5 to 14	20			5.0	3.5	2.7	
15 or more	16	6.5	5.0	3.7			
15 or more	20			3.7	2.5	2.0	

1/ Maximum current may be carried by only 10% of the contacts at one time. At such time, other contacts should be limited to 100 mA.

Table 21c DERATING OUTLINE OF EMI FILTERS

Class	Derate To	Remarks
All Filters	50% rated feed thru current and 50% rated DC working voltage	Ambient temperature shall not exceed 85 C.

DERATING OUTLINE OF FUSES

Table 21d (e. g., Littelfuse "Picofuse" & Bussmann "Tron")

Fuse Current Rating (Amperes)	Derate to the Following (%) of Rated Amperes 1/	Remarks
5	50%	Derating of fuses allows for possible loss of pressure, which lowers the blow current rating and allows for a decrease of current capability with time.
2	50%	
1	45%	
1/2	40%	
3/8	35%	
1/4	30%	

1/ Derating factors are based on data from fuses mounted on printed circuit boards and conformally coated.

Table 21e. DERATING OUTLINE OF INDUCTORS AND TRANSFORMERS

Inductor Class per MIL-C-15305	Transformer Class per MIL-T-27	Maximum Operating 1/ Temperature (Ambient plus temp. rise)	Remarks
0	Q	65°C	Derate maximum winding voltage of all inductors and transformers to 50% of the manufacturers rated voltage.
A	R	85°C	
B	S	105°C	

1/ a) Maximum operating temperature equals ambien temperature + temperature rise + 10°C hot spot temperature
Temperature rise = $\frac{R-r}{r}(T+234.5)$ — R, is the resistance of winding under load;
r, is the resistance of winding without load at a nbient temperature, T

b) The insulation classes of MIL style inductive parts have maximum operating temperature ratings which are generally based upon a life expectancy of at leart 10,000 hrs. The maximum operating temperatures in this table are selected to extend the life expectancy by a factor of 5 beyond the MIL rating

c) Custom made inductive parts should be evaluated on a materials basis and stressed at levels which give maximum operating temperatures well below the rated maximums of the materials used. These should be commensurate with the deratings shown above for standard devices.

Table 21f DERATING OUTLINE OF RELAYS

Class	Derate To	Remarks
All Relays	50% of rated contact current	Users should be cautioned not to reduce coil current or voltage below that required for reliable operation.

Table 21g DERATING OUTLINE OF RESISTORS

Class	Derate To	Remarks
Carbon Composition (RCR)	50% of rated power	All resistors:
Film, General Purpose (RLR)	50% of rated power	a) Maximum voltage shall not exceed 80% of the maximum rated voltage on any resistor.
Film, High Stability (RNR)	50% of rated power	b) When two or more resistors are mounted so closely that heat from one resistor influences ambient conditions of another, they should be derated by an additional factor of 0.5.
Wirewound Accurate 1% Tolerance	50% of rated power	c) Resistors with weldable nickel leads shall be derated by an additional factor of 0.5.
0.5% Tolerance	35% of rated power	
0.1% Tolerance	25% of rated power	
Wirewound Power, chassis mount	30% of rated power	
Wirewound Power, (RWR)	50% of rated power	
Variable Trimmers	50% of rated power	

Table 21h. DERATING OUTLINE OF DIODES

Class	Derate To*	Remarks
General Purpose	50% of rated power	All diodes:
Rectifier.	20% of rated power	a) Derating factors are based on a 25°C ambient temperature.
	50% of rated forward current	*b) Junction temperature shall not exceed 65% of $T_{j\ (max)}$
	50% of PIV	c) Peak inverse voltage or transients shall not exceed 80% of manufacturers rated value unless otherwise stated.
Reference Diode	20% of rated power	
Switching Diode	20% of rated power	
Silicon Controlled Rectifier	20% of rated power	
	50% of rated forward current	
Zener	50% of rated power	

Table 21i DERATING OUTLINE OF SILICON TRANSISTORS

Class	Derate To*	Remarks
Low Power NPN	20% of rated power	*Junction temperature shall not exceed 125°C for all applications. In the event of a conflict between this and the power derating factors, the 125°C limit shall govern. Breakdown voltage for all devices should be derated to 75% BV_{ECO}, 75% BV_{EBO} and 75% BV_{CBO}.
Low Power PNP	20% of rated power	
High Power NPN	15% of rated power	
Switching NPN	20% of rated power	
Switching PNP	20% of rated power	
Unijunction	20% of rated power	

Table 21j DERATING OUTLINE OF FIELD EFFECT TRANSISTORS (FET)

Class	Derate To*	Remarks
General Purpose	40% of rated power	*Junction temperature shall not exceed 125°C for all applications. Breakdown voltage for all devices should be derated to 75% BV_{DSO}, 75% BV_{DGO} and 75% BV_{SGO}.
High Speed Switch	40% of rated power	
Medium Power	30% of rated power	
High Power	30% of rated power	

Table 21k. DERATING OUTLINE OF INTEGRATED CIRCUITS

Class	Derate To	Remarks
Digital		
1. AC and DC Fan-Outs	60% of Manufacturer max rating	The Manufacturer's suggested bias voltages shall not be derated unless precautions are taken to assure that such action does not cause possible malfunction.
2. Combination of AC and DC Fan-Outs		
a) Load limits of AC levels	60% of Manufacturer max rating	
b) Load limits of DC levels	40% of Manufacturer max rating	

Table 21l. DERATING OUTLINE OF THERMISTORS
(Temperature Sensitive Resistor)

Class	Derate To	Remarks
All Thermistors	50% of rated power	

TABLE 12. DERATING OUTLINE OF TRANSFORMERS
(See Table 05. Inductors and Transformers)

Table 21m. DERATING OUTLINE OF WIRE AND CABLE

	Derate to - Amps. max.		
Wire Size	Bundle or Cable	Single	Remarks
26	1.4	2.5	1. Current ratings for bundles or cables are based on bundles of 15 or more wires at 70°C in a hard vacuum. In smaller bundles the allowable current may be increased as the bundle approaches a single wire.
24	2.0	3.3	
22	2.5	4.5	
20	3.7	6.5	
18	5.0	9.2	
16	6.5	13.0	2. Ratings are based on Teflon insulated wire (Type TFE)
14	8.5	19.0	
12	11.5	25.0	
10	16.5	33.0	
8	23.0	44.0	

Table 21n. DERATING OUTLINE OF QUARTZ CRYSTALS

Class	Derate To	Remarks
All Crystals	50% of rated drive level	

3.8 CONVERTER-CHARGER SUBSYSTEM

3.8.1 General Description (Refer to Figures 1 and 2)

The power conditioner (see Figures 37 and 38) accepts input power at 29.4 volts. This is routed through an input filter directly to the high voltage power converter and indirectly through an enable switch to the auxiliary power supply. When the unit receives an enable signal, the auxiliary power supply will produce the following outputs: 620 V out to the 2 microfarad ignition capacitor, 29.4 V and 12 V out to the portion of the control logic which is external to the power conditioner, ± 12.5 V power for the internal low level electronics, and the drive signal to the H.V. power converter. The H.V. power converter charges the 8 microfarad thruster capacitor to 1450 V and the "hold time" (the time elapsing between the time the 8-microfarad capacitor reaches 1450 V and the time it is actually fired) is sensed by the delay time generator. The delay time generator begins generating larger delays if the sensed hold time is too long and vice versa. This operates to delay the point in time in the operating cycle that the H.V. power converter is energized such that, whatever the spin rate of the satellite, full-charge hold times of between 5 and 50 milliseconds are generated. During the hold time, the 1450 volt output is held precisely to that predetermined maximum voltage by action of the comparator-regulator.

3.8.2 Description of Main Subcircuits

3.8.2.1 Power Conversion Circuitry

a. H.V. Power Converter: (Refer to Figure 39)

This circuit accepts input power at 29.4 volts and converts it into energy delivered at a near constant rate to charge two 4.0 microfarad capacitors in the thruster from 0 to 1450 volts in 0.5 seconds. Power switch transistor Q1 is turned on for the first 50 microseconds of each cycle, during which time current builds up in primary N1 of energy-storage transformer T2. During the next 100 microseconds, Q1 is turned off and the stored energy is delivered to the load capacitor via N2 of T2 and high voltage rectifier D8. Turns ratio N2:N1 is 50:1.

T1 is the base drive transformer. Current feedback is employed with N2:N3 equal to 10:1 such that Q1's base-to-collector current ratio equals 1:10. This insures adequate but not excess base current for Q1 under all

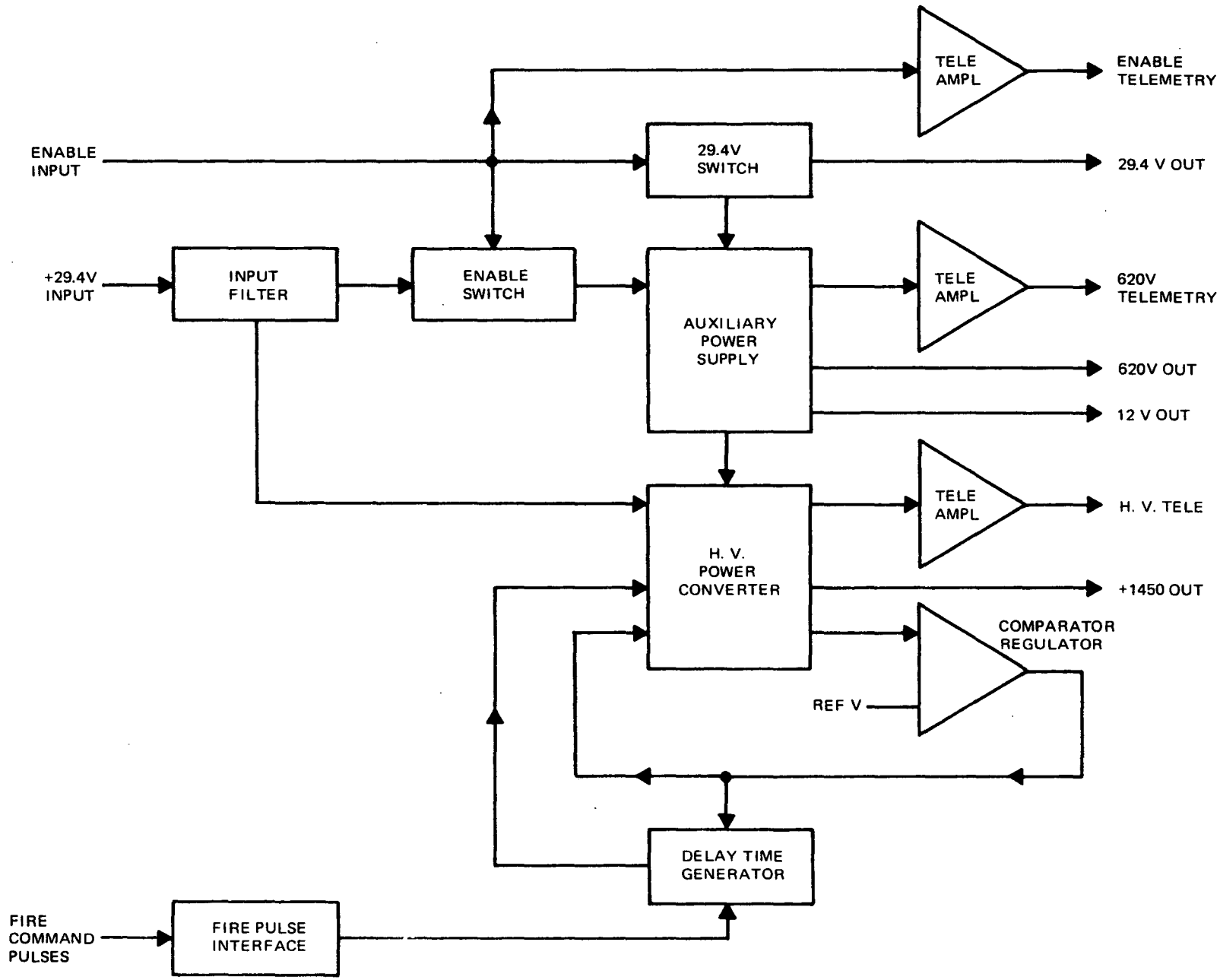

Figure 37. Power Conditioner Functional Block Diagram

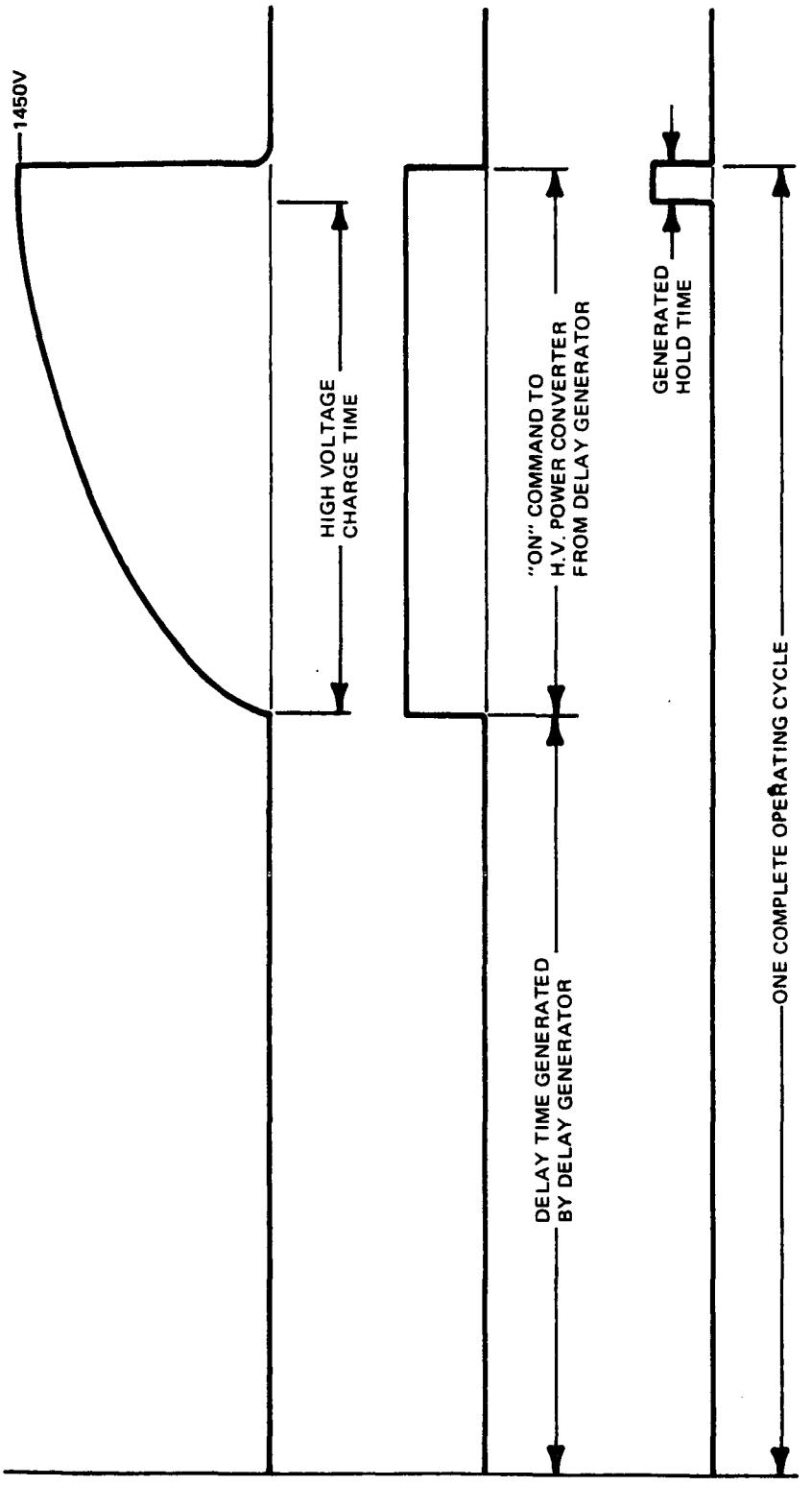

Figure 38. Timing Diagram

FOLDOUT FRAME I

FOLDOUT FRAME II

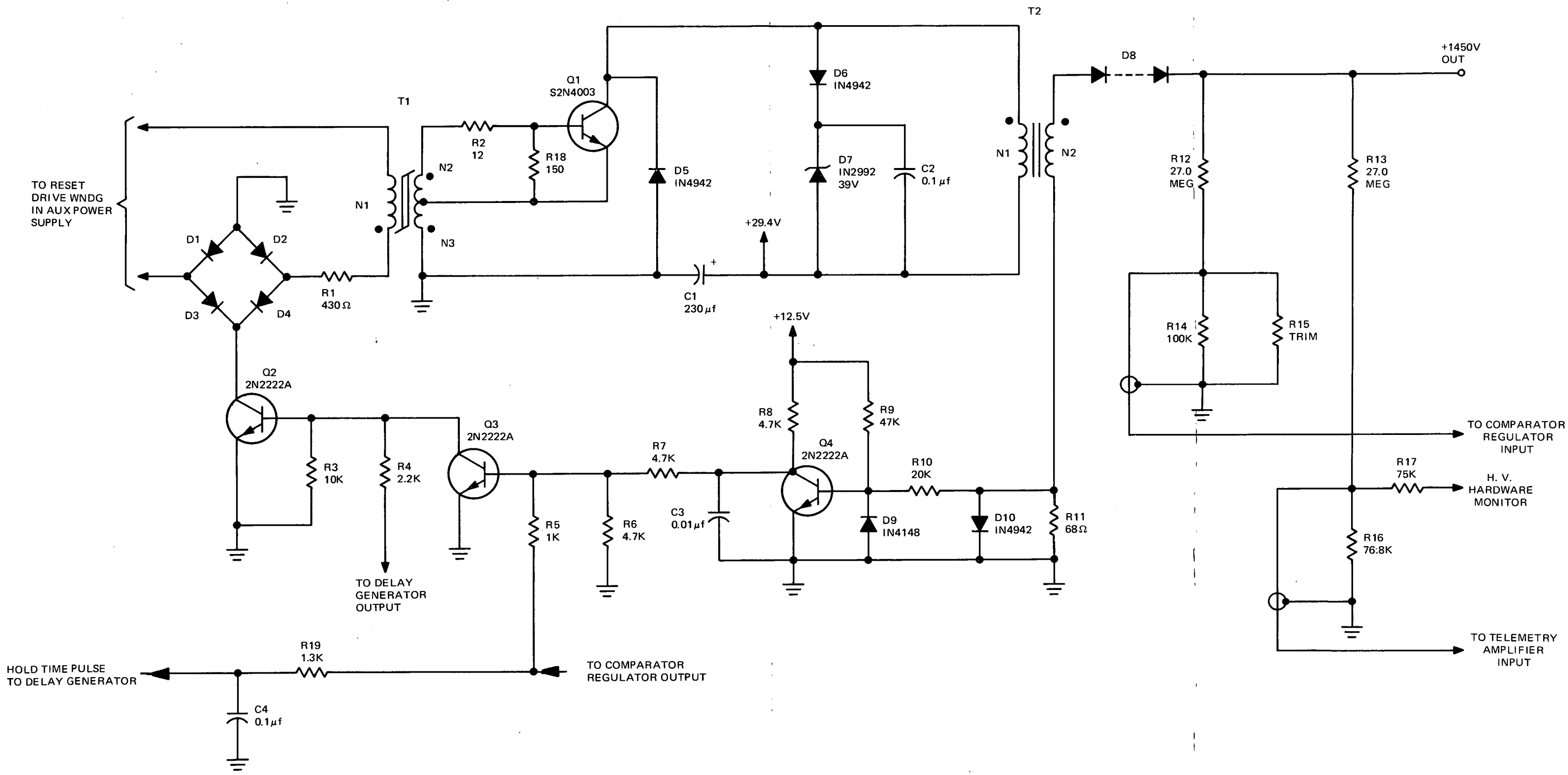

Figure 39. H.V. Power Converter Schematic (Wilmore Schematic 16B0113)

transient and steady-state conditions and results in efficient, saturated switching. Winding N1 of T1 receives a 12-volt square drive signal at 6.7 KC from the auxiliary power supply when the control switch transistor Q2 is turned on. Transistor Q2 is controlled by the output of the delay generator which turns on the H.V. power converter at a point in time which will allow the output capacitor to reach full charge just shortly before it is fired, thus minimizing the time the energy-storage capacitor is at high voltage.

Transistor Q3 serves a control function, that of inhibiting Q2 action; it is controlled from the comparator-regulator which limits the output at 1450 volts. Q4 and associated circuitry serves to inhibit Q2 action and thereby current limit the converter under short circuit conditions.

b. Auxiliary Power Supply (Refer to Figure 40)

This circuit is a physically-simple oscillator which takes input power from the 29.4 V source and through appropriate windings on transformer T1 and associated rectifiers, generates the 620 V power for charging the 2 microfarad ignition capacitor in the thruster, the 12 V and 29.4 V outputs to the control logic, the ± 12.5 V power for the power conditioners' own internal low level circuit needs, and the square-wave drive signal for the H.V. power converter stage.

The 620 volts is obtained from T1, N6 and the voltage doubler D5, D6, C3, and C4. Resistors R5 and R6 limit the current during the charging interval and during short circuit conditions. This circuit will charge a 2.0 microfarad capacitor from 0 to 620 V in 0.5 seconds or less. It will, of course, recharge the 2.0 microfarad capacitor after a discharge pulse regardless of whether or not the discharge of the 620-volt output is accompanied by a discharge of the 1450-volt output.

Internal ± 12 V power is obtained from windings N7 and N8 on T1 and through D7, D8, D9, D10, C5, and C6. Part of the + 12.5 V power is routed through the current limiter Q3, Q4, Q5 and Q6 to provide the 12 V, at not greater than 25 MA required by the control logic external to the power conditioner. Current limiting takes place above 30 MA to provide short circuit and overload protection for this output.

FOLDOUT FRAME 1

FOLDOUT FRAME 11

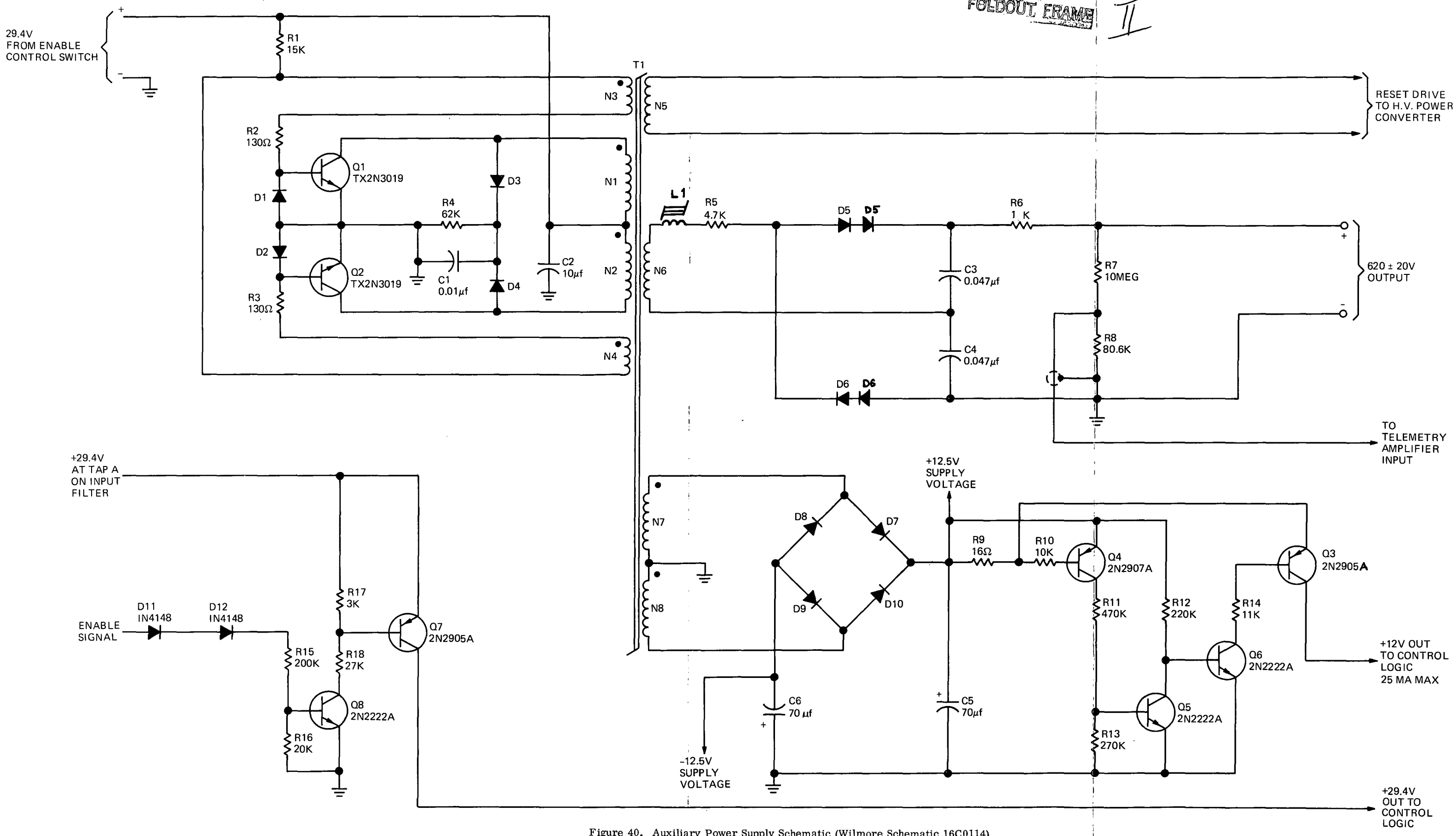

Figure 40. Auxiliary Power Supply Schematic (Wilmore Schematic 16C0114)

Transistor Q7, Q8, and associated circuitry comprise a controlled switch to furnish 29V output to the control logic external to the power conditioner when the power conditioner is enabled.

3.8.2.2 Spin-Rate Dependent Control Circuitry

a. Overall Operation

The power conditioner receives fire command pulses which vary from 0.833 pulses/sec. to 1.833 pulses/sec. The power conditioner has a special control loop to sense, indirectly, this pulse rate. It then provides a delay so that the H.V. power converter begins recharging the 8 microfarad energy-storage capacitor at a time such that its peak charge of 1450V (prior to the next discharge) will be held between 5 and 50 milliseconds. That is, the "hold time" will be automatically regulated to within the 5-to-50 ms range regardless of pulse rate.

The above is accomplished by sensing a "hold-time" signal generated by the comparator-regulator and comparing this against an internal time reference. An error signal proportional to this difference is generated. This error signal is used to control a delay generator which turns on the 1450V charger at such a time that after 1450V is reached in 0.5 seconds, the 8 microfarad capacitor is held at 1450V for only the desired short "hold-time" before the capacitor is fired again. The overall circuit is capable of operation at any pulse rate in the SMS range, and upon experiencing a change in pulse rate from one extreme of the range to the other, will adjust to again produce operation with proper hold times within approximately 30 seconds.

b. Delay Generator (Refer to Figure 41)

The delay generator receives, as on input, a "hold-time" pulse which is derived from the output of the 1450V comparator-regulator. This pulse begins when the output reaches 1450V and ends when the 1450-volt capacitor is discharged.

Q1 is a switch activated by the hold-time pulse which, working in conjunction with current source Q2 and current sink Q3, generates a ramp across C4 which rises linearly for the duration of the hold time. When this ramp reaches

FOLDOUT FRAME I

FOLDOUT FRAME II

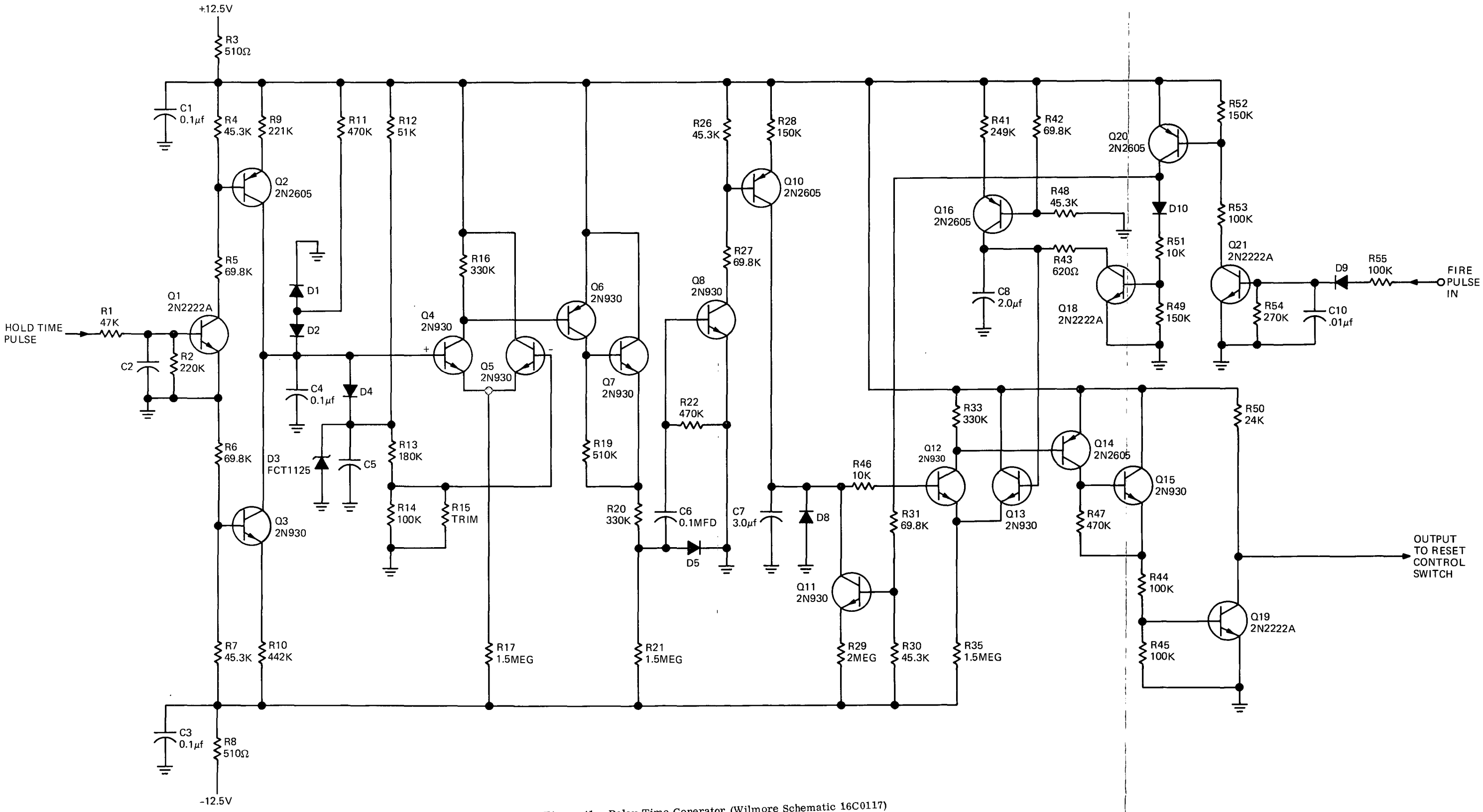

Figure 41. Delay Time Generator (Wilmore Schematic 16C0117)

a voltage equal to that at the junction of R13, R14, the voltage comparator Q4, Q5, Q6, and Q7 delivers a positive step to the base of Q8. Because of C6, transistor Q8 can activate current source Q10 for a time of either 30 milliseconds or for the duration of the "on time" of Q7, whichever is less. Transistor Q10 "pumps" C7, such that as long as hold times are too long, C7's voltage is being raised by a definite small increment each operating cycle. The current source Q16, discharge switch Q18, and C8 comprise a ramp generator whose linearly rising voltage is discharged to zero once each operating cycle at the time of the fire command pulse (and by it). At the same time, current sink Q11 is also "keyed" by the fire command pulse such that in the absence of any other currents, the voltage on C7 would be lowered by a definite small amount once each operating cycle. When the voltage ramp on C8 rises to a value equal to that stored on C7, voltage comparators Q12, Q13, Q14, and Q15 turn off Q19. This causes a positive output signal from the delay time generator, which turns on the 1450 V charger circuit. It is by this process of adding a small voltage to C7 equal to the voltage subtracted each operating cycle that the loop is able to "lock in" to produce a stable and accurate hold time, cycle after cycle. Because of the action of C6 and Q8, the entire loop is adaptive, in that it has a coarse mode of control to rapidly "track" gross changes in pulse rate and has a fine mode of control which comes into play once the hold time is changed to nearly the correct value.

3.8.2.3 Telemetering (Refer to Figure 42)

Four points in the power conditioner are being monitored and buffered by isolation amplifiers whose outputs are fed outside the package. For all four of these a scale factor is obtained by use of a voltage divider such that +5 volts out of a telemetry amplifier represent 1.2 times the normal value of the function.

The amplifiers as shown have an output impedance less than 1000 ohms and a very high input impedance such that no significant inaccuracy is caused by amplifier input loading.

The value of R1 shown is chosen to represent relative size only. In each individual amplifier, R1 will be tailored such that R1 plus the output resistance of the point being monitored will break with C1 to produce a deliverate corner at 150 Hz above which the response will fall at 6db/octave.

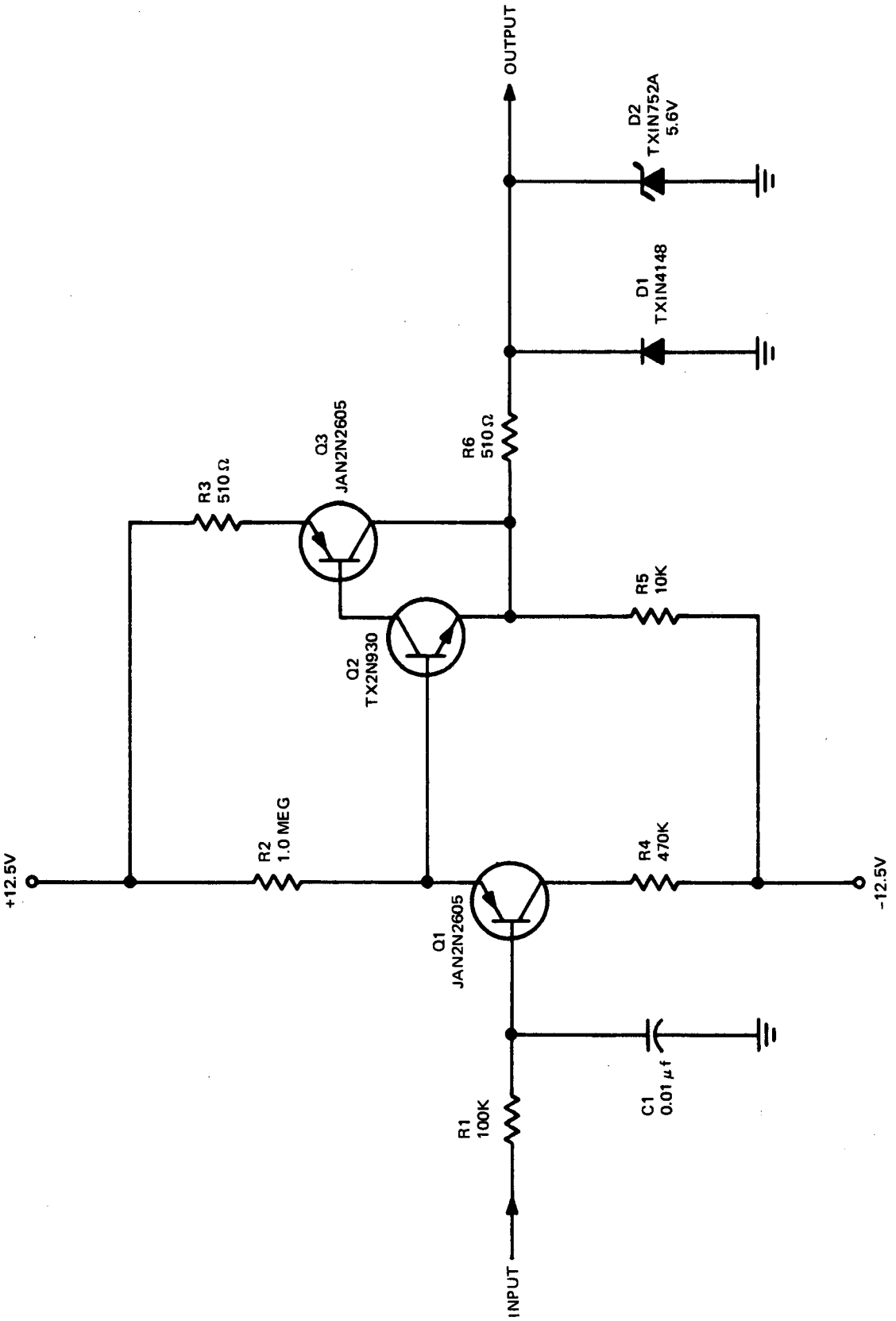

Figure 42. Telemetry Amplifier (Wilmore Schematic 16A0116)

R6, D1, and D2 serve to protect the amplifier output and to limit output excursions between -0.7 and + 5.5 volts.

3.8.2.4 Implementation of Principles

All of the subcircuits have been breadboarded and independently tested for proper functional operation at room temperature. The subcircuits which must interface properly for entire closed loop operation, have been integrated and tested for proper individual and system operation over the intended operating temperature range. This system test included the enable switch, auxiliary power supply, H.V. power converter, comparator-regulator, and delay generator.

The enable switch schematic and the comparator-regulator schematic are presented as Figures 43 and 44, respectively.

3.9 PROGRAM FOR NEXT REPORTING PERIOD

The results of this report will be incorporated in the final engineering drawings of the complete system. The next reporting period will cover Task II, "Flight Prototype Model Design," and Task III, "Model Specification" and will generate the finalized design.

3.10 CONCLUSIONS

The detailed design analysis performed during the Task I reporting period and presented herein, has shown that no problems are expected in meeting the reliability and structural requirements. The system electronics reliability have been calculated to be 0.92 for a five year life. The study also indicates that the original weight estimates are essentially correct. Only by using alternate, as yet unproven energy storage capacitors and extensively using Beryllium as a structural potential, will it be possible to notably reduce the estimated weight. Since either of these latter two approaches represent higher risk approaches, neither will be incorporated into the final design.

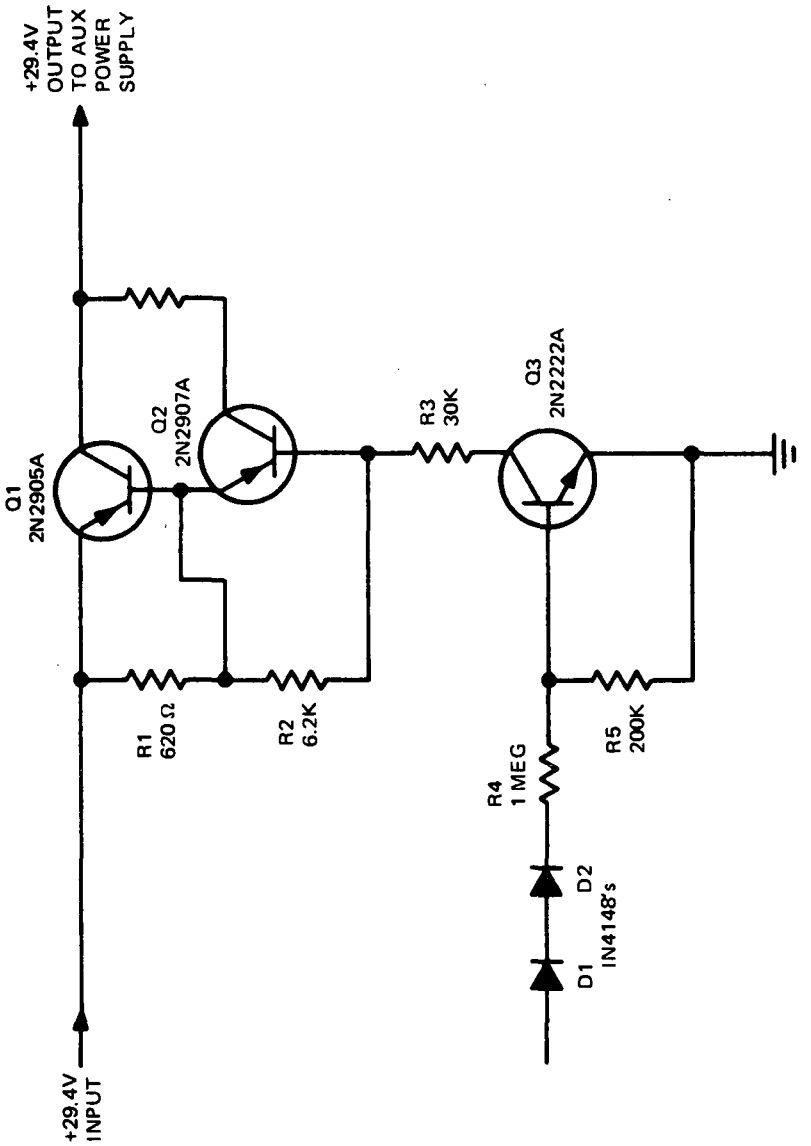

Figure 43. Enable Switch Schematic (Wilmore Schematic 16A0118)

FOLDOUT FRAME I

FOLDOUT FRAME II

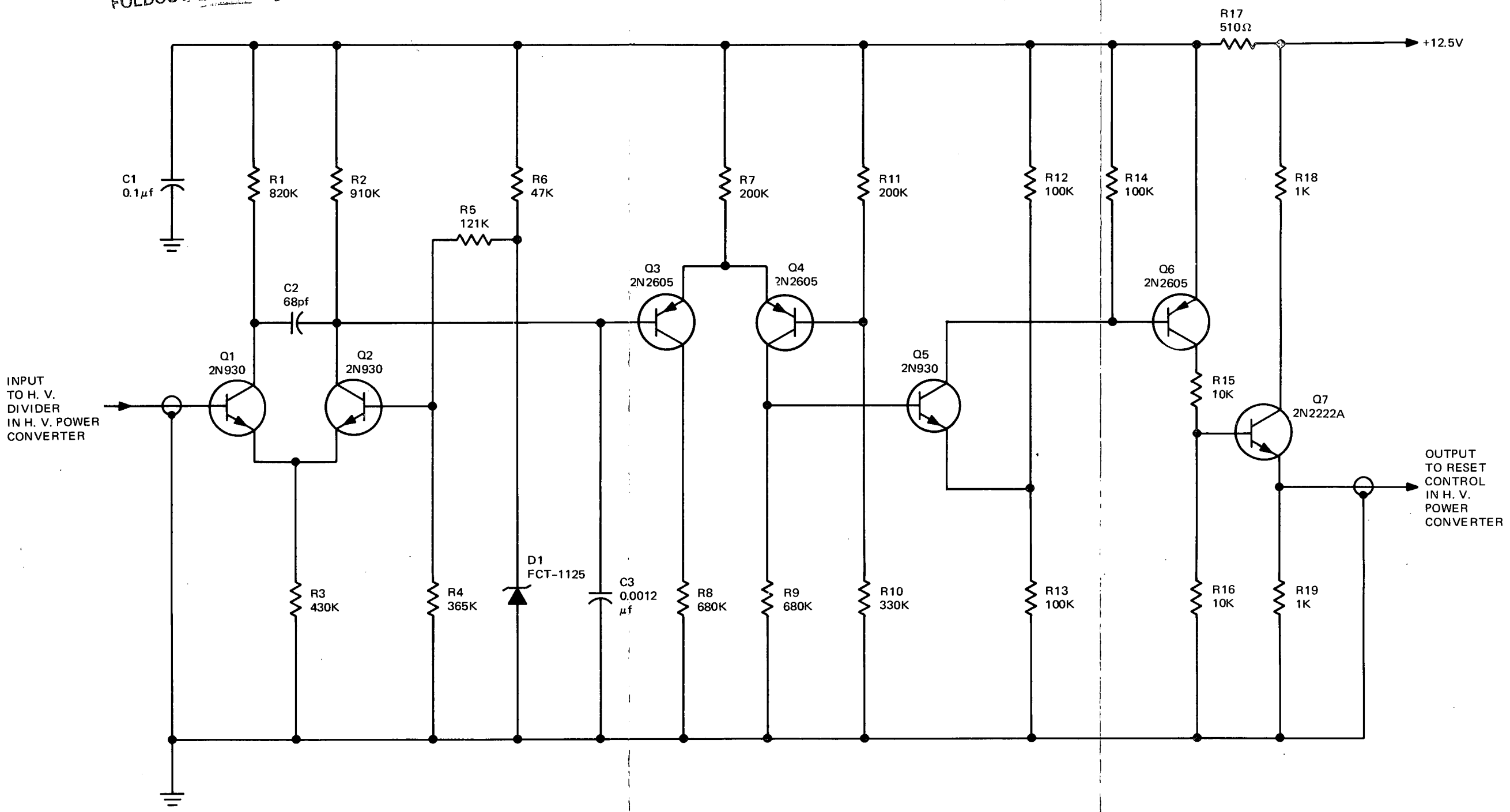

Figure 44. Comparator-Regulator Schematic (Wilmore Schematic 16B0115)

3.11 REFERENCES

1. Guman, W., Nathanson, D. M., Pulsed Plasma Microthruster Propulsion System for Synchronous Orbit Satellite, AIAA Paper 69-298, March 3-5, 1969 Vol. 7, No. 4, April 1970, page 409, J. Spacecraft & Rockets.

2. Braga-Illa, A., The Future of Self-Contained Control of Synchronous Orbits, AIAA Paper 70-479,, April, 1970.

3. Guman, W., Vondra, R., Thomassen, K., Pulsed Plasma Propulsion System Studies, AIAA Paper 70-1148, September, 1970.

4. Gorowitz, B., Karras, T., Life Tests on Capacitors for Pulsed Plasma Engine Application, General Electric Report R65SD26. Available as AD616771, June 29, 1965.

5. Moore, E. T., Wilson, T. G., and McIntire, J. N., Lightweight Power Conditioning System for Ion Engines Using Energy Storage Transformers for Conversion, Nondissipative Regulation and Protection, IEEE Transactions on Aerospace and Electronic Systems, Vol. AES-2, No. 4, pages 151-159, July, 1966.

6. Cox, D. M., McIntire, N. J., Bemis, A. R., and Moore, E. T., Power Conditioning for Pulsed Load Applications Requiring Repetitive Capacitor Charging, Suppl. to IEEE Transactions on Aerospace and Electronic Systems, Vol. AES-3, No. 6, November, 1967.

7. Guman, W., Pulsed Plasma Technology in Microthruster, AFAPL-TR-68-132, Air Force Aero Propulsion Laboratory, Dayton, Ohio, November, 1968.

8. Guman, W., Studies of a Solid Propellant Pulsed Plasma Thruster AFOSR 6th Symposium on Advanced Propulsion Concepts, Bell Aerospace Company, Niagara Falls, New York, May, 1971.

9. Hoshi, Yuji, A New Polyvinylidene Fluoride, Modern Plastics, Jan, 1971, page 110-114.

10. Philco Ford Company, Spec. No. WDL-SH-212002, page 18.